Functions of Vti1a and Vti1b in the Development of the Mouse Nervous System: Evidence from Double Knockout Mice

Dissertation
zur Erlangung des Doktorgrades

der Mathematisch-Naturwissenschaftlichen Fakultäten

der Georg-August-Universität zu Göttingen

by

Ajaya Jang Kunwar

from Morang, Nepal

Goettingen, 2008

D 7

Referent: Prof. Dr. Ernst A Wimmer

Korreferent: Prof. Dr. Thomas Pieler

Tag der mündlichen Prüfung: March 2008

Dedicated to

My Parents

and

Sisters

Acknowledgment

I wish to express my sincere gratitude to my supervisor **Prof. Dr. Kerstin Krieglstein** (head of the Neuroanatomy department, faculty of medicine) for her excellent guidance and many insightful conversations during the development of the ideas in this thesis work. I am honored to have such a great personality as my mentor and I thank her for helpful comments, continuous support, fruitful scientific discussion/ suggestions during my whole PhD period. I truly worship her for providing me an opportunity to learn and practice science in her lab. Her input in the early stages of my scientific career has helped me a lot to enhance my knowledge in neuroscience.

My sincere thanks go to **Dr. M. Rickmann** for his generous support and useful guidance during my PhD work and critical reading of the thesis. I am really impressed on his knowledge about electron microscopy and neuroanatomy which also helped me to learn many things in those aspects.

My deepest sincere thanks are presented to the members of the thesis committee, **Prof. Dr. Ernst Wimmer** for his helpful discussion during my PhD study and critical reading of my dissertation; **Prof. Dr. Thomas Pieler**, **Prof. Dr. Ralf Heinrich, Prof. Dr. Reinhard Jahn** and **Prof. Dr. Ralf Ficner** for their critical reading of my dissertation.

Similarly, my special thanks goes to **Prof. Gabi Fischer Von Mollard**, Dept. of Chemistry/Biochemistry, Uni. Bielefeld for the creation of *vti1a* and *vti1b* double knockout mice and for continuous support from her and her group members Bianca and Sasha.. Special thanks goes to **Dr. Victor Tarabykin**, MPI experimental medicine for allowing me to work in his lab and providing valuable suggestions during cortical project.

I am blissful to have great support from my parents and sisters during entire PhD period. They were my back bones who continuously fed me emotional support and pushed me to achieve this prestigious crown.

Publications:

Paper

1) Kunwar AJ, Rickmann M, Backofen B, Sorensen J, Von Mollard GF, Krieglstein K. SNAREs (vti1a and vti1b) double knockout mice show severe phenotype in central and peripheral nervous system. *Manuscript in preparation.*

Posters

1) Developmental deficits in central and peripheral mouse nervous system after knockout of membrane fusion proteins.
Kunwar AJ, Rickmann M, Bianca Backofen, Fischer von Mollard G, Krieglstein K.
37th Annual Meeting of the Society for Neuroscience, 3-7 Nov 2007, San Diego, USA.

2) Developmental deficits in central and peripheral nervous system in SNARE vti1a and vti1b knockout mice. Poster Session No: 567
Kunwar AJ, Rickmann M, Fischer von Mollard G, Krieglstein K
7th Meeting of the German Neuroscience Society (31st Goettingen Neurobiology Meeting), 29 Mar-01 Apr 2007, Goettingen, Germany.

3) Developmental deficits in central and peripheral mouse nervous system after knockout of SNARE vti1a and vti1b. Poster No. (47)

Kunwar AJ, Rickmann M, Fischer von Mollard G, Krieglstein K
Anatomische Gesellschaft. 27-29 Sep 06, Wurzburg, Germany.

Table of contents

1. Abbreviations:

AC : Anterior commisure

AP : Adaptor protein

Blbp : Brain lipid binding protein

BDNF : Brain derived neurotrophic factor

BMPs : Bone morphogenic proteins

Brn1 : Brain-specific homeobox/POU domain protein 1

BSA : Bovine serum albumin

Con or Ctrl : Control

CC : Corpus callosum

CCVs : Clathrin coated vesicles

CTIP2 : Chicken ovalbumin upstream promoter transcription factor-
interacting protein 2

CFA : Corticofugal axons

CNS : Central nervous system

DA : Dopamine

DAB : Diaminobenzidine

DAPI : 4',6-diamidino-2-phenylindole

DiI : 1,1'-dioctadecyl-3,3,3',3'- tetramethylindocarbocyanine perchlorate

DOPA : Dihydroxyphenylalanine

DRG : Dorsal root ganglion

DCVs : Dense core vesicles

DV : Dorso-ventral

E : Embryonic day

EDTA : Ethylenediaminetetra acetic acid

EE : Early endosome

EC cells : Enterochromaffin cells

ECM : Extracellular matrix

ER : Endoplasmic reticulum

ERAD	: ER-associated degradation pathway
EM	: Electron microscopy
Fezl	: Forebrain embryonic zinc-finger-like protein
GAP-43	: Growth associated protein-43
GFAP	: Glial fibrilary acidic protein
HC	: Hippocampal commisure
HE	: Haematoxylin-eosin
KO	: Knockout (double knockout)
LAMP	: Limbic associated membrane protein
LAMP-1	: Lysosomal associated membrane protein-1
LAMP-2	: Lysosomal associated membrane protein-2
LC	: Locus coeruleus
LE	: Late endosome
L2	: Lumbar vertebra level 2
MAPK	: Mitogen-activated protein kinase
MN	: Motoneurons
MTOC	: Micro tubule organization centre
MVBs	: Multi vesicular bodies
NaCl	: Sodium chloride
NA	: Noradrenaline
NF	: Neurofilament
NGF	: Nerve growth factor
Nod+Pet	: Nodose-Petrosal ganglia
NPCs	: Neural progenitor cells
NT3	: Neurotrophin 3
PAP	: Peroxidase anti peroxidase
PBS	: Phosphate buffered saline
PCD	: Programmed cell death
PCNA	: Proliferative cell nuclear antigen
PCR	: Polymerase chain reaction
PFA	: Paraformaldehyde solution

PI3K   : Phosphatidylinositol 3-kinase

PNMT   : Phenylethanolamine-N-methyltransferase

PNS   : Peripheral nervous system

PSPB   : Pallio-subpallial border

RE   : Recycling endosome

RT-PCR   : Reverse transcriptase polymerase chain reaction

SATb2   : Special AT-rich sequence binding protein 2

SCG   : Superior cervical ganglion

SG   : Secretory granule

SDS   : Sodium dodecyl sulfate

Sema   : Semaphorin

SNARE   : Soluble N-ethyl-maleimide-sensitive fusion protein
                attachment protein receptor

SN   : Substantia nigra

SV   : Synaptic vesicle

TAE   : Tris acetate buffer

Tbr1   : T-box brain gene 1

TG   : Trigeminal ganglion

TH   : Tyrosine Hydroxylase

TrkA   : Tyrosine kinase A

TUNNEL   : Terminal deoxynucleotidyl transferase mediated dUTP nick end
                labeling

TCA   : Thalamocortical axons

TGN   : Trans Golgi network

VAMP   : Vesicle associated membrane protein

VTA   : Ventral tegmental area

VZ   : Ventricular zone

5-HT'   : 5-hydroxytryptamine (serotonin)

2. Introduction:

Some of the distinguishing features of all eukaryotic cells are that they are subdivided into numerous compartments which have distinct functions and are separated by protein-lipid membranes. Proteins and other material are transported between these compartments to support vital processes like nutrient uptake and growth. These compartments are essential to ensure that various specialized cellular processes happen concurrently. The transport is essential for maintaining different physiological process ranging from expansion of plasma membrane, growth cone formation, synaptic vesicle trafficking, endocytosis, mobilization of signaling cascades to secretion and delivery of proteins and other molecules within or outside of cells.

Many organelles namely plasma membrane, early endosomes, late endosomes, recycling endosomes, lysosomes, Golgi apparatus and endoplasmatic reticulum communicate through membrane enclosed vesicles containing membrane impermeable cargo molecules. This is achieved by multiple vesicles that are constantly circulating in the cell, budding off from one membrane and fusing with another. Since these vesicles are in a constant flow, these processes need to be tightly regulated side by side maintaining its own identity. They undergo a series of different coordinated fusion or fission steps and transport between these organelles usually involves specialized trafficking vesicles. It buds and fuses, transferring cargo from one cellular compartment to another. Therefore, vesicular structures do not only link different intracellular organelles, but also provide a mechanism by which the cell delivers newly synthesized proteins to the plasma membrane [Alberts *et al*., 1994]. Among a number of molecules identified in trafficking events so far, SNARE (Soluble NSF attachment protein receptor where NSF stands for N-ethyl-maleimide-sensitive fusion protein) plays a central role in intracellular membrane trafficking events of secretory pathway [Chen and Scheller, 2001].

2.1: Trafficking at endoplasmic reticulum and Golgi:

Each organelle has a defined localization and function that has a specific membrane composition of lipids and proteins. During trafficking, a carrier vesicle that pinches off from the donor compartment, is transported to and finally fuses with its acceptor compartment. A prerequisite for correct targeting is for the donor and acceptor membranes to recognize each other (tethering and docking) before the lipid bilayers fuse. All these processes are mediated by specific soluble and membrane resident proteins and are subject to high degrees of regulation.

Proteins which are required within the cytosol and membrane proteins of the plasma membrane leave via the secretory pathway. The secretory vesicles originate from the endoplasmic reticulum (ER). During their synthesis on ribosomes, these proteins are translocated into the ER where they are subjected to go through glycosylation and subsequently pass to the Golgi apparatus. Within the Golgi, proteins travel through different compartments from cis, medial to trans Golgi network (TGN), where they undergo further glycosylation. Henceforth, sorting occurs in the TGN, which means they can be packaged for regulated secretion into secretory granules (SG) or into constitutive secretory vesicles (SV) (Fig. 2.1).
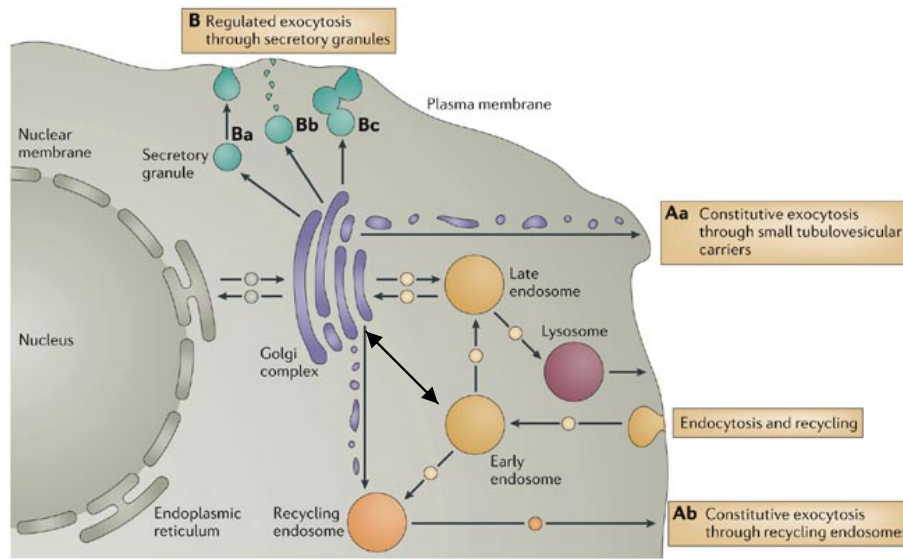
Fig. 2.1: Multiple steps of intracellular membrane trafficking. Eukaryotic cells have complex pathways for the transport of proteins and membranes between cell organelles, and to and from the cell surface. Proteins are formed in endoplasmic reticulum (ER), pass through Golgi for further processing and reach to their final destination. The transport takes place via membrane bound vesicles by retro- and anterograde trafficking. Principally, the endosomal system carries the proteins from the Golgi either to the lysosomes for degradation or to the outside of the cell for secretion. Vesicles can also directly bud off from the trans Golgi network (TGN) and fuse to the plasma membrane to secrete their contents outside the cells. Substances entering into the cells are also carried to their respective destinations or recycled back to the plasma membrane via the endosomal compartments. [Adopted from Stow et al., 2006].

Another important function of the ER is to prevent misfolded proteins from entering the secretory pathway. In this so called ER quality control, the chaperones Bip, calnexin and calreticulin have a central role in retaining the misfolded proteins or unassembled subunits in the ER [Hammond and Helenius, 1995]. Misfolded proteins are degraded by an ER-associated degradation (ERAD) pathway [McCracken and Brodsky, 1996].

Alternatively, lysosomal proteins are recognized at the TGN and transported via late endosomes to lysosomes. The mannose 6-phosphate receptor MPR46 binds soluble lysosomal enzymes in the TGN and transports them to endosomes. Due to the low endosomal pH, MPR46 receptors dissociate from the enzymes and return to the TGN for next round of transport. MPR46 is mainly localized to the TGN and endosomes [Kornfeld

and Mellman, 1989]. Some lysosomal proteins fail to be transported to late endosomes. In this case, they go through the secretory pathway to the plasma membrane, then are recaptured by another kind of mannose-6-phosphate receptor, MPR-300 and reach lysosomes via endocytosis.

On the other hand, extracellular material reaches the lysosomes through endocytosis via early endosomes (EE) and late endosomes (LE). Some of this material has to be returned back to the cell surface after being endocytosed. This takes place either directly from early endosomes or from recycling endosomes (RE). The best characterized endocytic pathway involves clathrin, which forms coated membrane invaginations on the plasma membrane that recruit cell-surface receptors and then, through a series of highly regulated steps, pinch off to form clathrin-coated vesicles [Kirchhausen, 2000; Mukherjee et al., 1997]. Examples of receptor-mediated endocytic pathways are epidermal growth factor (EGF) uptake mediated by its receptor EGF-R. Clathrin coated pit formation is facilitated by adaptor complexes (APs). Similarly, Rab11 and Rab6a have been shown to mediate early endosome-to-TGN trafficking of Shiga toxin and the TGN marker protein TGN38 [Mallard et al., 2002].

2.2: Different compartments of the endosomal system:

Endocytosis is a process whereby cells absorb material (molecules such as proteins) from the outside by engulfing it with their cell membrane. Endocytosis can occur either via clathrin, caveolae, and pincher mediated process or by alterations of the cytoskeleton (phagocytosis). Among them, clathrin coated vesicles (CCVs) are the most common means of receptor mediated endocytosis. The CCVs rapidly lose their coat proteins and undergo fusion with the early /sorting endosomes (EE).

2.2.1: Early or sorting endosomes: The early endosomes are a complex compartment with tubulo-vesicular morphology. They are slightly acidic (pH 6.0 - 6.8) and are mainly responsible for dissociation of the ligand-receptor complex [Kornfeld and Mellman, 1989]. Acidic nature of the early endosomes lessens the risk of damaging the receptors which are supposed to be recycled again [Mellman, 1996]. In addition, there exists a

bidirectional vesicular traffic between the TGN and the early endosomes. Furthermore, the early endosomes can undergo homotypic fusion with other endosomal vesicles and tubules.

2.2.2: Recycling endosomes (REs): The tubular extensions of the EEs give rise to the recycling endosomes, which are responsible for recycling of receptors. These recycling receptors are freely available after endocytosis. Some endosomes fuse to the plasma membrane while others translocate to the perinuclear cytoplasm and accumulate near the micro tubule organization centre (MTOC) [Hopkins, 1983; Yamashiro et al., 1984]. REs are morphologically distinct than the sorting endosomes [Dunn et al., 1989; Ghosh et al., 1994; Marsh et al., 1995; Mayor et al., 1993] and maintain a distinct pH environment. Additionally, the perinuclear recycling vesicles act as an intracellular pool of recycling receptors.

2.2.3: Late endosomes and lysosomes: The early endosomal vesicles carrying the ligand /cargo pass through the cytoplasm along microtubules and fuse with the late endosomes (LEs) which eventually give rise to lysosomes. The pH drops to 4.5-5.0 and a pool of degradative enzymes leads to degradation of the ligands in the lysosomes. The lysosomes appear as electron dense organelle called 'dense body' surrounded by a single membrane in electron microscopy. The recycling from lysosomes is very slow. This explains why cells are able to accumulate large amount of internalized materials and also the dense appearance of the lysosomes [Mellman, 1996]. While the transport from EE, LE to lysosome remains unclear, two hypotheses have been proposed. Firstly vesicle shuttle model, where the EEs are regarded as stable structures and the cargo is pinched off from EEs into small transport vesicles that would eventually fuse with the LEs. Secondly, the maturation model which has been widely accepted recently, suggests that the entire EE moves as a unit and is converted into the late endosomes [Lodish *et al.*, 2001].

2.2.4: Multivesicular bodies: The LEs when seen electron microscopically contain a number of internal vesicles and have been termed as *multi vesicular bodies* (MVB) or *multi vesicular endosomes* (MVE). These are formed by inward invagination of the

limiting endosomal membrane [van Deurs et al., 1993]. The MVBs are proposed to play a role in the down regulation of signal transduction by sequestering the receptors [Di Fiore and Gill, 1999; Katzmann et al., 2002]. Several receptors including the EGF-R have been localized to the internal membranes of the MVBs [Felder et al., 1990].

2.2.5: Secretory lysosomes: Usually lysosomes are regarded as the last station of endocytic pathways. However, there is increasing evidence that there is an existence of specialized lysosomes that can act as storage compartments and can exocytose the contents in a regulated fashion. Secretory lysosomes have been studied in specific cell types such as the cytotoxic T lymphocytes which secrete lytic granules [Burkhardt et al., 1990; Griffiths, 2002] and melanocytes that secrete melanosomes responsible for pigmentation of skin, eyes and hair [Griffiths, 2002].

2.2.6: Secretory vesicles and dense core secretory granules: These vesicles carry the proteins to be exported to the exterior of the cells. The proteins to be exported are thought to be sorted into these vesicles under specific signals at the TGN. These vesicles bud from the TGN, become mature and are exocytosed either via the constitutive way in secretory vesicles (SVs) or in a regulated manner in secretory granules (SG) [Blott and Griffiths, 2002; Bright et al., 1997; Chidgey, 1993].

2.3: SNARE superfamily:

SNARE superfamily consists of 25 member proteins in *Sacchaaromyces cerevisiae*, 36 in human and 54 in *Arabidopsis thaliana* [Jahn and Scheller, 2006]. Among all, the SNARE complex functioning in neuronal exocytosis were first SNAREs to be identified and best characterized. They include the synaptic vesicle protein syntaxin [Bennett et al., 1992], SNAP-25 [Oyler et al., 1989], VAMP (also called synaptobrevin) [Trimble et al., 1988]. Typically four SNAREs make a SNARE core complex that governs a fusion reaction. They are conserved in evolution and possess a common domain structure (Fig.2.2). Once a core complex is formed, the extremely stable structure is resistant to SDS denaturation, protease digestion, clostridial neurotoxin cleavage [Hayashi et al., 1994] and is heat stable up to 90 ºC [Yang et al., 1999].

With an increasing number of members, SNARE proteins can be divided into several small protein families. Although similarities between distant members of these protein families are rather limited, it is thought that they all operate by means of a common mechanism.

2.4: SNARE classification:

Sutton, Fasshauer, Jahn, Brunner (1998)
Nature 395, 347-353
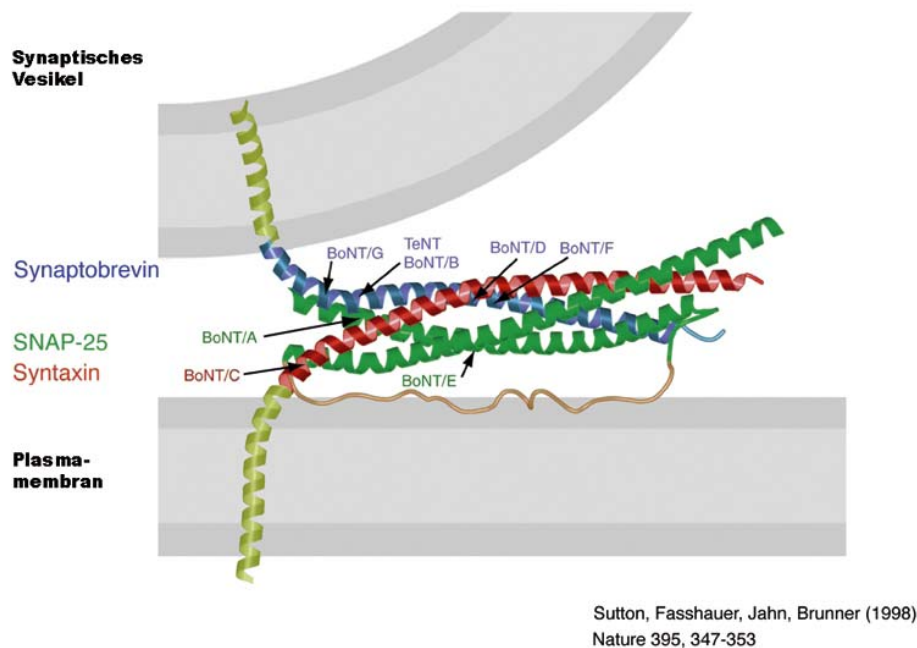
Fig. 2.2: SNARE complex containing v-SNARE and t-SNARE. V-SNAREs synaptobrevin 1 or synaptobrevin 2 (blue) found on synaptic vesicles and t-SNAREs syntaxin 1 (red) and SNAP-25 (green) localized in the plasma membrane form a SNARE complex that governs a fusion reaction. [Adopted from Sutton et al., 1998].

SNAREs have been traditionally divided into two broad families such as v-SNARE (associated with vesicle) and t-SNARE (associated with target membrane). However this terminology has been reclassified as it was not sufficient in describing isotypic vesicle SNAREs (e.g. early or late endosomes) and also certain SNAREs function in several transport steps with varying partners. For example Sec22, a SNARE found in *S. cerevisiae* functions in both anterograde and retrograde traffic between the endoplasmic reticulum and the Golgi apparatus. To avoid confusion, they have been reclassified into Q-SNARE (glutamine containing SNARE) and R-SNARE (arginine

containing SNARE). Q-SNARE can be further divided into Q-a, Q-b and Q-c SNAREs based on their localization in highly conserved SNARE complex. Since the nomenclature Q-SNARE and R-SNARE originated on the basis of structural configuration, they will be explained in more detail under the title "SNARE structure".

2.5: SNARE hypothesis:

The SNARE hypothesis was proposed in 1993 and it states that each type of transport vesicle has a distinct v-SNARE that makes pair with a unique cognate t-SNARE (a trans SNARE complex) at appropriate target membrane and this specific interaction docks the vesicle at the correct membrane, with the subsequent dissociation of the SNARE complex by soluble complex containing ubiquitous cytoplasmic ATPase, NSF and α-SNAP [Chen and Scheller, 2001; Hohl et al., 1998]. Although the biochemical activity of α-SNAP and NSF, which helps to dissociate the SNARE complex, has not been disputed, its specific roles have been revised [Mayer et al., 1996]. The current view however says that instead of directly driving fusion, NSF acts as a chaperone to reactivate SNAREs after one round of fusion.

SNAREs role in docking, as proposed by SNARE hypothesis, has also been questioned by the finding that SNARE cleaving neurotoxin do not affect vesicle docking at the synapse [Hunt et al., 1994] and it was further supported by experiment showing SNARE deficient drosophila have an increased but not decreased number of docked vesicles [Broadie et al., 1995; Schulze et al., 1995]. Small GTPases of the Rab family have been suggested to be important in the early stage of vesicle targeting and tethering [Zerial and McBride, 2001]. Therefore, it is possible that SNARE mediated fusion specificity is overlaid on Rab-mediated docking specificity to make the system even more reliable [Chen and Scheller, 2001].

2.6: SNARE structure:

The SNARE complex consists of four helix bundle structure. They have an evolutionarily conserved central coiled coil stretch of 60-70 amino acids, also known as SNARE motif. SNARE motifs are arranged in heptad repeats and are pivotal to the function of these proteins. Towards the C-terminal end, most SNAREs have a single hydrophobic transmembrane domain which is connected to SNARE motif by a short linker. Many

SNAREs have independently folded domains that are positioned N-terminal to the SNARE motif and that vary between the subgroups of SNAREs [Fasshauer, 2003]. However there are some exceptions such as a subset of SNAREs (e.g. evolutionary younger brevins) [Rossi et al., 2004] lacks the N-terminal domain (Fig. 2.3). Another subset lacks transmembrane domains, but most of these SNAREs contain hydrophobic post-translational modifications that mediate membrane anchorage. These SNAREs include a small group, that is represented by neuronal SNARE SNAP-25 (25-kDa synaptosome associated protein), which contain two different SNARE motifs that are joined by flexible linker that is palmitoylated (Fig. 2.3a, Qbc zigzag lines).

Copyright © 2006 Nature Publishing Group
Nature Reviews | Molecular Cell Biology
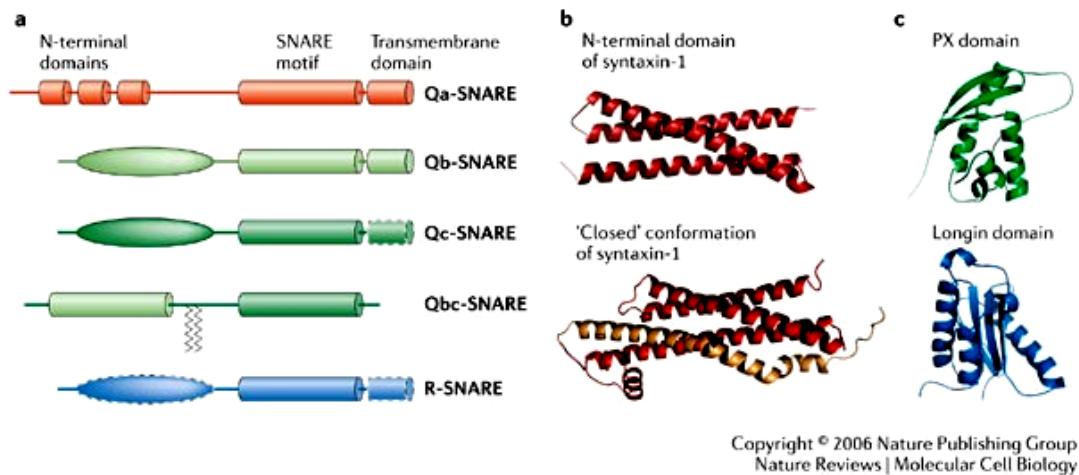
Fig. 2.3: Linear and three-dimensional structures of SNAREs. a Qa-SNAREs consist N-terminal antiparallel three-helix bundles. Oval shape represents N-terminal domains of Qb-, Qc- and R-SNAREs. Qbc-SNAREs which lack transmembrane domain make a small subfamily of SNAREs, the SNAP-25. **b** three-dimensional structure of the isolated N-terminal domain of syntaxin-1 (Upper panel). 'closed' conformation of syntaxin-1(lower panel), where the N-terminal domain of syntaxin-1 (red, as in the upper panel) is associated with part of its own SNARE motif (beige structure; absent in the upper panel). **c** Three-dimensional structures of the N-terminal domains of other SNAREs, showing structural diversities. Color scheme: (Qa-SNARE, red; Qb-SNARE, light green; Qc-SNARE, dark green; and R-SNARE, blue). [Adopted from Jahn and Scheller, 2006].

SNARE families are further divided into subfamilies according to their sequences of the SNARE motifs. To date, crystal structures of only two SNARE complexes have been resolved. A well known example is the neuronal SNARE-complex, which mediates fusion reaction between synaptic vesicles and the plasma membrane. It consists of the v-

SNAREs synaptobrevin 1 or synaptobrevin 2, which are found on synaptic vesicles and t-SNAREs syntaxin 1 and SNAP-25 localized in the plasma membrane [Sutton et al., 1998]. The crystal structure was obtained from recombinant SNARE motifs without transmembrane domains and corresponds probably to the stage after fusion (cis-SNARE-complex).
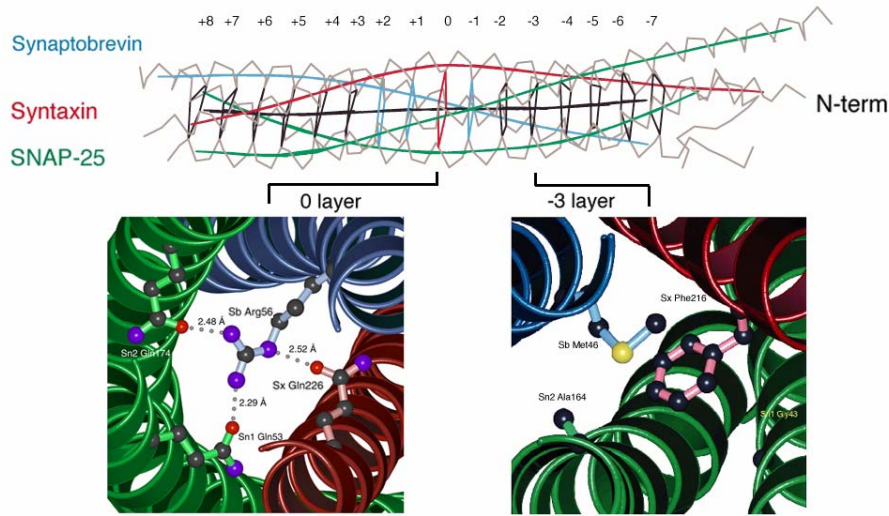
Sutton, Fasshauer, Jahn, Brunger (1998) Nature 395, 347-353

Fig. 2.4: A SNARE complex showing 'O' layer. Crystal structure of neuronal SNARE complex which consists of synaptobrevin, syntaxin, and SNAP-25. Zero (0) layer showing three glutamine (Gln) and one arginine (Arg) residues which interact with each other in the centre. [Adopted from Sutton et al., 1998].

Sixteen layers can be identified in the SNARE complex in which amino acid residues from all four helices are oriented in such a way that they face each other into the inside of the bundle and interact with each other. Most amino acids are hydrophobic and that are perpendicular to the axis of the helix bundle. However, in the middle of the bundle an unusual hydrophilic layer was discovered that consists of three glutamine (Q) contributed by Syntaxin 1, SNAP-25 and one arginine (R) contributed by synaptobrevin 2 (Fig. 2.4). The surface of the synaptic fusion complex is highly grooved and possesses distinct hydrophilic, hydrophobic and charged regions. These characteristics may be important for membrane fusion and for the binding of regulatory factors affecting neurotransmission [Sutton et al., 1998].

2.7: Mechanism of SNARE mediated lipid fusion:

In the aqueous environment of cytosol, the fusion of two lipid membranes is energetically unfavourable because of the repulsive electrostatic forces between the two membranes [Zimmerberg et al., 1993]. It was suggested that 'bridging' proteins can act as scaffolds to bring the two membranes close together [Monck and Fernandez, 1996]. The formation of the SNARE complex is believed to begin from the amino- to the carboxy-terminal end (zipping), a process which may provide the energy necessary to overcome the repulsion of the opposing membranes, thus resulting in membrane fusion. During fusion, opposing members that are in contact proceed via a series of intermediates. When distance between the two layers is sufficiently reduced, 'hemifusion' occurs which is followed by the distal leaflet membrane breakdown resulting in the opening of 'fusion pore'. Eventually, fusion pore expands resulting full content mixing and membrane relaxation (Fig. 2.5). The model of fusion pore was supported by both freeze fracture electron microscopy [Chandler and Heuser, 1980] and patch clamp techniques [Breckenridge and Almers, 1987]. At the end, the SNAREs resume a cis complex (all SNAREs in one membrane) and need to be disassembled and recycled for a new round of fusion. After disassembling of SNARE complexes by NSF and α-SNAP, they are sorted to their appropriate membranes and are ready for subsequent rounds of fusion.
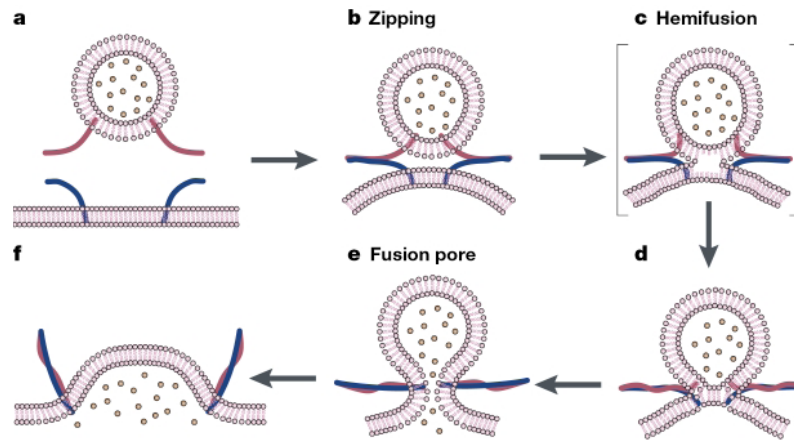
Fig. 2.5: Model showing SNARE-mediated lipid fusion. a Initially the two membranes come close to each other but the SNAREs are not yet in contact. **b** Zipping begins from amino-terminal end, drawing the two membranes further towards each other. **c** subsequently causing increased curvature and lateral tension of the membranes, exposing the bilayer interior. As the separation is sufficiently reduced, spontaneous hemifusion occurs. **d** the highly hostile void space at the membrane junction in (**c**) causes the beginning of contacts between the distal membrane leaflets. **e** The lateral tension in the trans bilayer contact area induces membrane breakdown, resulting a fusion pore. **f** Membrane relaxes after fusion pore expands. [Adopted from Chen and Scheller, 2001].

SNARE assembly exerts pressure in such a way that the linkers between transmembrane domain and the helical bundle of SNARE motif are stiff. Therefore, straining these linkers transmits energy onto membranes bending them or disturbing the hydrophilic-hydrophobic boundary. As a result, opposing membranes are not only pressed against each other, they are also deformed which facilitates the fusion stalks [Jahn and Scheller, 2006]. After membrane attachment, fusion is initiated by the concerted action of SNARE and SM proteins (Sec1/Munc18-like proteins). SM proteins are soluble proteins often associated with syntaxin-like SNAREs. During or after fusion, Rab proteins are inactivated by GTPase-activating proteins (GAPs), and dissociate from the respective membranes to initiate a new cycle of fusion.

2.8: Subcellular distribution of SNAREs:

Almost all intracellular compartments contain SNARE proteins. SNAREs are constantly moved from donor to acceptor compartment on the surface of transport vesicles. After membrane fusion, a SNARE protein should be recycled back to the donor compartment.

Therefore localization of a SNARE is not sufficient to predict its function [Jahn and Sudhof, 1999].

Immunofluorescence microscopic study showed that vti1a, a Qb-SNARE, is localized to the Golgi and the TGN [Kreykenbohm et al., 2002; Xu et al., 1998] whereas brain specific splice variant vti1a-β is enriched in synaptic vesicles [Antonin et al., 2000c]. Vti1b has been shown to be overlapped with markers for Golgi and TGN, endosomes, vesicles and tubules in the TGN [Advani et al., 1998; Kreykenbohm et al., 2002] which is in line with the *in vitro* study carried out by Antonin et al., 2000a, showing late endosomal fusion events and solving of the crystal structure of the endosomal SNARE complex (endobrevin /syntaxin 7/syntaxin 8/ Vti1b). Endobrevin (VAMP 8) is localized to early and late endosomes [Antonin et al., 2000b]. Syntaxin 8 is preferentially associated with early endosomes, indicated by its co-labeling with Rab5 [Subramaniam et al., 2000] and with the TGN [Prekeris et al., 1999]. Functional studies and electronic microscopy data show syntaxin 7 localization to late endosomes [Mullock et al., 2000] as well as to early endosomes [Prekeris et al., 1999]

Numerous studies have been carried out to find the localization of SNAREs and its function during membrane fusion and the mechanisms of sorting of SNARE proteins to certain compartments are still unknown. It is likely that adaptor complexes play a role. Although, most SNAREs lack the known adaptor-binding trafficking motifs, only VAMP-4 and VAMP-7 contain recognizable di-leucine motifs, suggesting that alternative or additional motifs may regulate adaptor binding to SNARE or cargo molecules. VAMP-4 mislocalizes when di-leucine motif is removed, which suggests that AP-1 and VAMP-4 interaction is required for proper sorting of VAMP-4 [Peden et al., 2001].
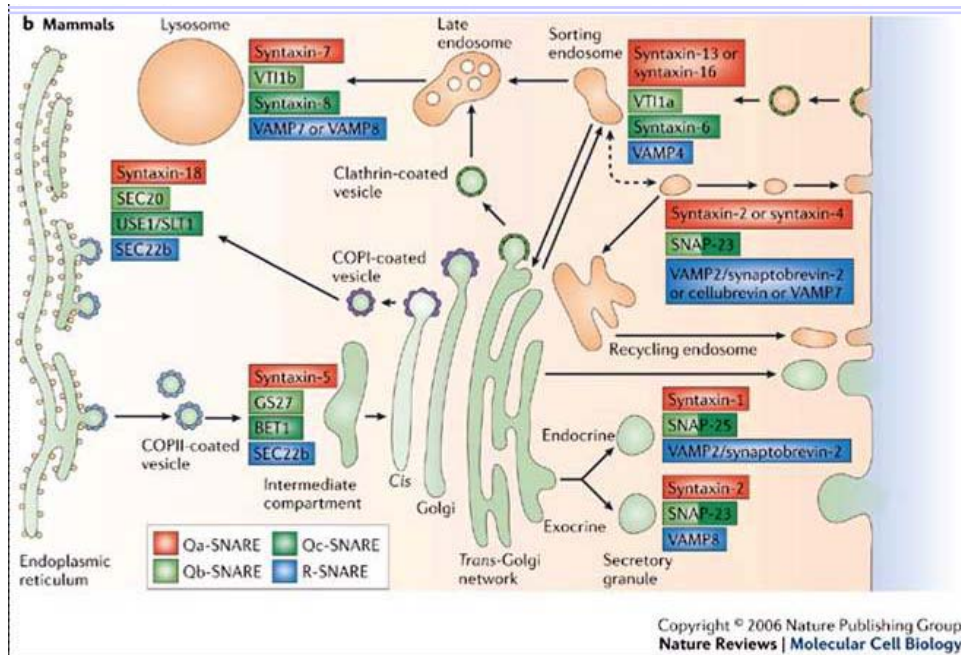
Fig. 2.6: SNAREs involved in different intracellular fusion steps in a mammalian cell. In endosomal fusion events, Syntaxin13 or Syntaxin 16, Vti1a, Syntaxin-6, VAMP-4 forms a complex and are responsible for early endosomal fusion plus recycling after endocytosis whereas Syntaxin-7, Vti1b, Syntaxin-8 and VAMP-7 or VAMP8 are responsible for late endosomal fusion and lysosomal degradation. Other SNARE complexes are also depicted in the picture. [Adopted from Jahn and Scheller, 2006].

2.9: Candidates for the early and late endosomal SNARE complexes:

At least two types of isotypic fusion events have been documented in endosomal system: one early endosomal and another late endosomal fusion [Gruenberg and Howell, 1989]. It has been reported that syntaxin 13 (Qa) and syntaxin 6 (Qc) are potential members of the SNARE complex involved in early endosomal fusion [Bock et al., 1997; Mills et al., 2001; Prekeris et al., 1998]. Antibody against vti1a was found to inhibit fusion of early endosomes [Antonin et al., 2000a].

Co-immunoprecipitation study has shown a SNARE complex containing syntaxin 16 (Qa), vti1a (Qb), syntaxin 6 (Qc) and VAMP4 (R) [Kreykenbohm et al., 2002] suggesting this complex might mediate early endosomal fusion. Similarly using recombinant SNAREs as competitive inhibitors, endobrevin and vti1a was also reported in early

endosomal fusion [Antonin et al., 2000a]. In contrast, one study suggested an involvement of the neuronal SNAREs SNAP-25 and synaptobrevin, which were found in a complex with syntaxin 13 [Sun et al., 2003] (Fig. 2.6). Based on their intracellular localization, potential R-SNAREs of the early endosomal complex could be endobrevin [Antonin et al., 2000b], Ti-VAMP (also known as VAMP7) [Advani et al., 1999] and VAMP4 [Steegmaier et al., 1999] which are all found to be associated with early endosomes. Since endobrevin is absent in brain, VAMP4, which is ubiquitously expressed could replace endobrevin as R-SNARE, but both R-SNAREs could co-exist in parallel complexes in other tissues [Antonin et al., 2000b].

The Q-SNAREs syntaxin 6 [Simonsen et al., 1999], syntaxin 7, syntaxin 8 [Prekeris et al., 1999], syntaxin 10 [Tang et al., 1998], syntaxin 11 [Valdez et al., 1999], syntaxin 13 [Prekeris et al., 1998] and vti1a [Antonin et al., 2000b] were also found on endosomal compartments suggesting they might be potential members of the early endosomal complex. Very recently, Brandhorst et al., 2006 demonstrated that early endosomal fusion is largely mediated by a complex formed by syntaxin 13, syntaxin 6, vti1a, and VAMP4, whereas the exocytic and late endosomal SNAREs play little or no role in the reaction. In addition, proteoliposomes reconstituted with early endosomal SNAREs promiscuously found to be fused with liposomes containing exocytotic or late endosomal SNAREs suggesting specificity of SNARE pairing is not sufficient to determine the specificity of organelle fusion. Apparently, most likely candidates as reported in co-immunoprecipitation and *in vivo* studies are syntaxin 13 or syntaxin 16 (Qa), vti1a (Qb), syntaxin 6 (Qc) and VAMP4 (R) [Jahn and Scheller, 2006].

Regarding the late endosomal compartment, several SNAREs have been identified in the fusion reactions which include R-SNAREs VAMP-7 [Advani et al., 1999; Ward et al., 2000] and Q-SNAREs Syntaxin 7 [Mullock et al., 2000; Nakamura et al., 2000; Prekeris et al., 1999] and Syntaxin 13 [McBride et al., 1999]. More specifically Syntaxin 7, Syntaxin 8, and vti1b and endobrevin/VAMP-8 have been found to be responsible for fusion of late endosomes and they have similar structural properties as the neuronal SNARE complex. When antibodies specific for these proteins were used, homotypic

fusion of late endosomes was inhibited and delivery of epidermal growth factor to lysosomes was also retarded [Antonin et al., 2000b].

Despite having varying data, identifying the function of SNAREs can have several difficulties. First, some SNAREs are involved in more than one fusion step and interact with different sets of SNARE partners [von Mollard et al., 1997]. On the other hand, stable complexes that form among SNAREs *in vitro* do not interact *in vivo* [Fasshauer et al., 1999; Yang et al., 1999]. It can also be possible that several SNARE complexes operate in parallel in an individual reaction, resulting functional redundancy. Therefore, more accurate and precise functional data must be achieved in order to identify the function of SNAREs that mediate a certain fusion step. An involvement of local regulatory factors that coordinate SNARE activity in certain fusion steps cannot be excluded.

2.10: Functions of vti1a and vti1b:

Unlike in yeast where a Qb-SNARE, Vti1p is utilized throughout the endosomal system as a part of four different SNARE complexes, *Caenorhabditis elegans*, *Arabidopsis thaliana*, *Drosophila* and mammals express two proteins vti1a and vti1b. The two mammalian proteins share 30% of their amino acid sequences with each other and also with yeast vti1p [Advani et al., 1998; Fischer von Mollard and Stevens, 1998; Lupashin et al., 1997]. They have overlapping localization but form distinct SNARE complexes.Vti1a forms complex with R-SNARE VAMP-4, syntaxin 16 or syntaxin 13 (Qa), syntaxin 6 (Qc). Vti1b forms complex with VAMP-7 [Jahn and Scheller, 2006; Zwilling et al., 2007] or VAMP-8, syntaxin -7 (Qa) and syntaxin 8 (Qc) [Kreykenbohm et al., 2002; Mallard et al., 2002]. Affinity purified antibodies raised against the cytoplasmic region of vti1a specifically detect a 29-kilo dalton integral membrane protein enriched in the Golgi membrane [Xu et al., 1998].

Vti1a was also co-immunoprecipitated with syntaxin 5 and syntaxin 6, but syntaxin 5 and syntaxin 6 were not part of the same complex, showing that vti1a might be a member of two distinct SNARE complexes [Xu et al., 1998]. Moreover, microinjection of antibodies specific for vti1a (also called vti-rp2) into Vero cells prevents VSV G-protein transport to

the cell surface and accumulates in peri-nulear area [Xu et al., 1998] and brain specific splice variant vti1a-β was found in synaptic vesicles [Antonin et al., 2000c]. Vti1a, syntaxin 6, syntaxin 16 in a t-SNARE complex interacted with VAMP-4 or VAMP-3 in two different quaternary SNARE complexes [Mallard et al., 2002]. Using a novel permeabilized cell system, it has been suggested that these complexes have a role in transport from early endosomes/recycling endosomes to the TGN.

Vti1a- β has seven additional amino acids (LIKLREE) directly N-terminal before the SNARE motif that can possibly play an important role for cellular distribution of that protein [Antonin et al., 2000c]. Ultrathin cryosections obtained from mossy fiber synapse showed abundant presence of both vti1a and vti1a-β at nerve terminals. Similarly, VAMP-4, syntaxin 6 and syntaxin 16 were also found to be enriched in small synaptic vesicles suggesting role of this complex for biogenesis of synaptic vesicles [Kreykenbohm et al., 2002].

Vti1b on the other hand has 233 amino acid residues. A recent study showed that vti1b is localized in the peri-nuclear area with extension of the staining further into the periphery of the cell [Kreykenbohm et al., 2002]. Vti1b is a member of a SNARE complex mediating fusion of late endosomes *in vitro*. In addition to vti1b, the complex consists of syntaxin 7, syntaxin 8, and endobrevin/VAMP-8 which have been crystallized and showed four helix-bundle structures. This complex was very similar to the neuronal SNARE complex [Antonin et al., 2002] where vti1b takes the position of the N-terminal helix of SNAP-25 and syntaxin 8 is equivalent to the C-terminal helix of SNAP-25.

Both vti1a and vti1b are expressed in almost all tissues e.g. adrenal gland, brain, pancreas, kidney, spleen, thymus, heart and skeletal muscles as confirmed by western blot method. Vti1a is localized to the cell body as well as to nerve terminals whereas vti1b is found more towards the cell body of hippocampal neurons [Antonin et al., 2000c].

2.11: Vti1b single knockout phenotype:

Previous reports have shown that vti1b deficient mice are viable and fertile and do not show serious defects; however, they have reduced amounts of syntaxin 8 [Atlashkin et al., 2003]. This was due to degradation of the syntaxin 8 protein, while the amounts of its other SNARE partners, syntaxin 7 and endobrevin did not change suggesting that vti1b is specifically required for the stability of a single SNARE partner. Most vti1b-deficient mice were indistinguishable from wild-type mice and did not display defects in transport to the lysosome. However, 20% of the vti1b-deficient mice were smaller than other normal sized vti1b knockout mice. In addition, lysosomal degradation of an endocytosed protein was slightly delayed in hepatocytes derived from these smaller mice. Similarly, multivesicular bodies and autophagic vacuoles accumulated in hepatocytes of some smaller vti1b-deficient mice. Liver cysts were also found in aged normal-size vti1b-deficient mice. Eight out of 23 vti1b-deficient mice between 15 and 21 months old had multiple liver cysts. These cysts were filled with a clear fluid containing a yellow liquid. The data from single vti1b knockout mouse suggested that SNAREs can compensate for the reduction in syntaxin 8 as well as for the loss of vti1b in most mice even though vti1b shows only 30% amino acid identity with its closest relative vti1a [Atlashkin et al., 2003].

2.12: Role of other SNARE proteins *in vivo*:

Studying knockout animal to investigate the role of certain genes *in vivo* has a range of advantages over experiments designed for *in vitro* studies. Gene ablation is one way to study gene function in its physiological context. While large pool of data suggesting the role of SNARE proteins in different intracellular events *in vitro*, very little is known about its role *in vivo*. SNARE knockout mice die early or they do not show severe phenotype suggesting other SNARE's role in gaining functional redundancy. VAMP-2 and SNAP-25 homozygous mice, for example, die perinatally while heterozygous littermates do not show apparent phenotype [Schoch et al., 2001; Washbourne et al., 2001]. SNAP-25 KO mice when analysed between embryonic days 17.5 and 19, show normal growth kinetics and fasciculation patterns in thalamocortical fibre [Molnar et al., 2002]. It has also been suggested that SNAP-25 is not required for nerve growth or spontaneous neurotransmitter release, but is crucial for evoked synaptic transmission at

neuromuscular junctions and central synapses [Washbourne et al., 2001]. Similarly, synaptobrevin-2 (VAMP-2) knockout study shows that it is required for fast calcium-triggered synaptic-vesicle exocytosis as well as for fast synaptic-vesicle endocytosis [Deak et al., 2004]. VAMP-8 knockout mice, on the other hand, show heterogeneity in their function. VAMP8 homozygous mice seem normal at birth, but one third of animals die after 10-12 days showing disruption of thymus morphology and maturational defect in thymocytes. These one third mice showed loss of weight at postnatal day 8-9 which was termed as "small not sick" and after 2-3 consecutive days of weight loss, they died. However those survived became healthy adults but were lighter than littermates [Namita Kanwar, PhD thesis 2006].

2.13: Predicted role of vti1a/1b in development of different cellular events in vivo:

Endocytic machinery is a vital process in many important intracellular events. It is required to maintain polarity in epithelial cells. For example, syntaxin 3, SNAP-23, and α-SNAP have been shown their role in apical membrane fusion of MDCK cells [Low et al., 1998]. VAMP8 is localized in apical endosomal membranes of nephric tubule epithelium and in MDCK cells. This asymmetric localization and cycling behavior suggested its role in apical (but not basolateral plasma membrane) endosomal trafficking in polarized epithelium cells [Steegmaier et al., 2000]. Similarly, α-SNAP has also been shown to play a role in determining symmetric versus asymmetric cell division in development of cortical neurons. In hyh (hydrocephalus with hop gait) mice where α-SNAP gene is mutated, ventricular epithelial cells (neural progenitor cells) withdraw prematurely from cell cycle, causing alteration in cortical layering pattern [Chae et al., 2004].

Endocytic machinery could also be required for growth cone development during dendritic and axonal outgrowth process. Uninterrupted vesicular movement is required during these activities which possibly involves endosomal fusion and recycling events. This would ultimately result in addition of plasma membrane and helpful for axonal extension. A role in development of neurite outgrowth for Syntaxin 13, a developmentally regulated SNARE protein, has been documented [Hirling et al., 2000].

Alternatively, peripheral ganglia neurons which exhibit a unique architecture, has severe physical limitations on the possible mechanisms for signal transduction. They depend almost entirely upon target-derived soluble trophic factors for their survival. During development of peripheral ganglia, neurons are generated in excess number and only few neurons who can make connection with target organ can survive. The neurons which can not make contact will eventually die. According to neurotrophic factor hypothesis, those surviving neurons require target-derived soluble factors for their survival and the target derived neurotrophic factor induces signals in the presynaptic terminal of axons which involves endosomal fusion and recycling events. This finally propagates surviving signal to the cell body.

Chromaffin cells in adrenal gland have abundant amount of vesicles and require continuous vesicular activities to produce a number of hormones like epinephrine and norepinephrine. This makes chromaffin cells as an elegant model for measuring vesicular activities. Therefore chromaffin cells or enterochromaffin cells in gut could be few other important tissues where vti1a/1b function can be analyzed. Similarly, synaptic vesicles (SVs) may be another organelle of interest for investigation. SVs are storehouse for neurotransmitters and after action potential stimulation; they undergo Ca^{2+}-dependent exocytosis. Exocytosis is followed by immediate retrieval of SVs via clathrin dependent endocytosis and is locally recycled to regenerate exocytosis-competent vesicles. Moreover despite having debate about intermediate steps in the recycling pathway, it is almost clear that nerve terminals contain endosomes and that the SV cycle may involve endosomal intermediates, although not necessarily during each recycling event [Sudhof, 2004].

Therefore, keeping in mind that the role of vti1a in early endosomal fusion and recycling after endocytosis events and vti1b's role in late endosomal fusion/lysosomal degradation events, it would be interesting to investigate their role in vti1a/1b double mutant mice especially in above mentioned cells/tissues. This would lead a better understanding about roles of vti1a/1b in different developmental cellular process *in vivo*.

3. Aims and Objectives:

Vti1a and vti1b are SNARE proteins specifically localized at the early and late endosome going along with their proposed function to contribute to early and late endosome fusion. However, mutant mice for each gene did not show any severe phenotype suggesting that vti1a and vti1b, sharing 30 % similarity in amino acid sequences, can potentially compensate for one another.

The aim of this project was to characterize the biological consequences of defective endosomal SNARE protein function by analyzing vti1a/vti1b double deficient mice. The focus of the analysis was the development of the central and peripheral nervous system. Potentially defective cell biological events may include:

(a) Asymmetric cell division, leading to impaired neural stem cell development.

(b) Retrograde transport of guidance cues or growth factors leading to impaired migration of progenitor cells, to impaired axon growth and impaired projections.

(c) Defective endocytosis within the exocytosis cycle, possibly leading to impaired neuronal activity.

4. Materials and Methods:

4.1: Animals:

Since single knockouts $Vti1a^{-/-}$ and $Vti1b^{-/-}$ as well as triallelics $Vti1a^{+/-}$, $Vti1b^{-/-}$ and Vti1a $^{-/-}$, Vti1b$^{+/-}$ were viable, fertile and survived to full term without any difficulty, double knockouts were generated by mating between male ($vti1a^{+/-}$, $vti1b^{-/-}$) with female ($vti1a^{-/-}$, $vti1b^{+/-}$) or other way around. Mouse knockouts were created by our collaborators Prof. Gabi Fischer von Mollard, University of Bielefeld, Biochemie II, Bielefeld, Germany [Atlashkin et al., 2003, Vadim Atlachkine PhD thesis, 2002]. The morning of the day at which a vaginal plug was detected in females, was designated gestation day 0.5. Experiments were performed according to the National Health and ethical regulations. Animals were kept in a regulated environment (23°C ± 1°C, 50 % ± 5 % humidity) on a 12-hr light:12-hr dark cycle, with food and water ad libitum.

4.2: DNA extraction:

Total genomic DNA was isolated from the limbs and the tail of the embryos using standard protocol. In brief, tails or limbs were cut and incubated with 400µl of lysis buffer from 6 hours to overnight at 55 ˚C under vigorous shaking. Hair and other insoluble material were removed by centrifuging at 13000 rpm for 10 min. Supernatant was separated into a new eppendorf tube and equal amount of isopropanol (400 µl) was added. DNA was precipitated after vigorous shaking and the resulting pellet was washed with absolute ethanol. Thereafter, pellet was air dried and re-dissolved in autoclaved distilled water (20-100 µl depending upon pellet size). Finally the solution was kept under 37 ˚C with gentle shaking condition for 2hr. During the first 20 min, the lid was kept open for complete ethanol evaporation. DNA was stored at 4˚C until further experiment.

4.3: Genotyping:

To identify the genotypes of the animals, genotyping was carried out by polymerase chain reaction, PCR, [Mullis and Faloona, 1987], a common method of creating copies of specific DNA fragments. The reaction starts with the denaturation of two strands of

DNA. After separating the DNA strands, the temperature is lowered so that primers can attach themselves to the single DNA strands (annealing). Finally, DNA-polymerase has to fill in the missing strands. It starts at the annealed primer (the free 3´-OH group) and works its way along the DNA strand (elongation). Repeating the previous steps (denaturation, annealing and elongation) for 35 cycles will exponentially enrich the reaction with the primer-flanked DNA sequence.

The PCR reaction was carried out in a 30μl reaction volume with the following constituents: genomic DNA, primers (Invitrogen), dNTPs (Cat. No: 1969046; Roche), 10X PCR Buffer $(NH_4)_2SO_4$ (Invitrogen, part no: Y02028), *Taq* DNA polymerase recombinant (Invitrogen, cat. No: 10342-020), MgCl2 (Invitrogen, part no:Y02016) .

4.3.1: Mastermix preparation:

To prepare a final reaction volume of 50 μl, the following volumes and concentrations was used:

19.3	μl	H_2O
3	μl	Buffer $(NH_4)_2SO_4$ 10x
3	μl	$MgCl_2$ 25mM
0.6	μl	dNTPs 10mM
1.5	μl	Primer forward 10mM
1.5	μl	Primer Reverse 10mM
1.0	μl	Template (genomic DNA)
0.1	μl	Taq Polymerase

4.3.2: Primer sequences (Invitrogen):

4.3.3: PCR programs:

The amplification reaction was done in a PCR thermocycler (Mastercycler, Eppendorf) using the following programs:

For vti1a +/+, vti1a -/- and vti1b +/+, vti1b -/- PCR:

- Initial denaturation   4 minutes   95 °C
- Denaturation   1 min   93 °C ⎫
- Annealing   40 sec   51.5 °C ⎬ 35 x Cycle
- Elongation   40 sec   72 °C ⎭
- Final elongation   5 minutes   72 °C
- Hold   10 °C

4.4: Laser dissection of trigeminal and vestibular ganglia:

To see the expression of vti1a and vti1b in mRNA level, wild type trigeminal and vestibular ganglia cells were dissected from E18.5 mice using laser dissecting microscope (Arcturus, Pix Cell IIe). First of all, fresh and unfixed wild type E18.5 head was embedded in Jung tissue freezing medium (Leica) and 10 μm thick sections, containing trigeminal or vestibular ganglia were cut on a cryostat machine (Microm international). Sections were picked up on superfrost®-plus microscopic slides (Menzel GmbH and Co) and were briefly air dried. To identify the tissue, they were shortly stained in clean Haematoxylin and Eosin (1 minute each) and processed for laser dissection or stored at -80˚C until needed.

4.5: RNA extraction from trigeminal and vestibular ganglia:

Total mRNA was isolated from laser dissected trigeminal and vestibular ganglia using PicoPure^{TM} RNA isolation kit provided by company (Arcturus). Preparation was done according to manufactured protocol. Briefly, Cells were captured and collected by CapSure HS Cap with the ExtraSure Extraction Device. The CapSure ExtraSure assembly was placed in a CapSure HS alignment tray and 10 μl of extraction buffer was added. A new 0.5 ml centrifuge tube was placed onto the Capsure-Extrasure assembly and covered with incubation block (Fig. 4). Thereafter the whole block was incubated for 30 min at 42 ˚C. The microcentrifuge tube with the CapSure Extrasure assembly was centrifuged at a speed of 800 x g for two minutes and the cell extract was collected accordingly.
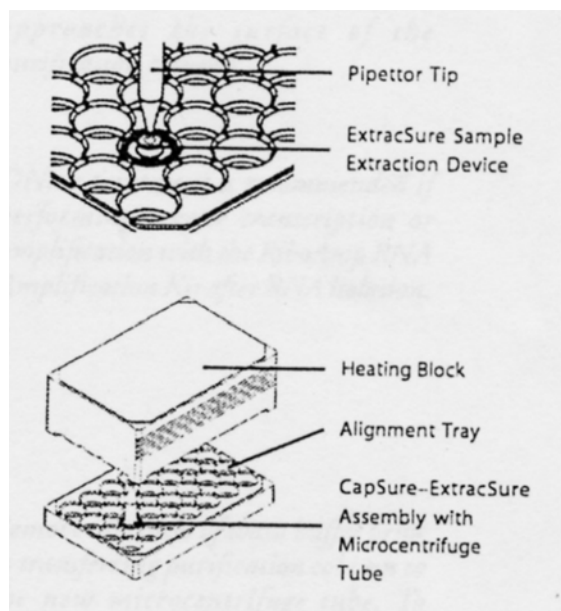
Fig.4: PicoPure^{TM} RNA extraction process. RNA was extracted from TG and vestibular ganglia by standard protocol. Capsure-Extrasure assembly was fitted with 0.5ml microcentrifuge tube as shown above and incubated for 30 min at 42 ˚C.

4.5.1: RNA isolation:

Before proceeding to RNA isolation, the RNA purification column was preconditioned with 250 µl of condition buffer for 5 min. at room temperature and centrifuged with 16000 x g for one min. Then 10µl of 70% ethanol was pipetted into cell extract and mixed well by pipetting up and down. The mixture was pipetted into preconditioned purification column and centrifuged at 100 x g for 2 minutes initially to allow binding RNA to the column followed by 16000 x g for 30 sec. to remove flowthrough. Then column was washed twice with washing buffer 1 and 2 (W1 and W2 provided), centrifuged at 8000 x g, again washed with W2 and centrifuged at 16000 x g for 2 min. Finally, RNA was eluted with elution buffer and collected in new 0.5ml microcentrifuge tube. The recommended total volume of eluted RNA was 11 µl.

4.5.2: RT reaction:

Before performing RT reaction RNA concentration was checked with photometer. The total volume of eluted RNA was heated to 70˚C for 10 min. and then quenched on ice.

RT reaction was set up by following protocol

- 10 µl heat denatured RNA (600 ng)
- 4µl 10x PCR buffer with MgCl$_2$
- 2 µl 10 mM dNTPs
- 1 µl random primers
- 1 µl Superscript II reverse transcriptase
- 0.5 µl RNA inhibitor
- 1.5 µl water

Samples were then left at 42˚C for 1 hr and thereafter for 10 min at 72˚C. Then RT-PCR was set up as follows.

- 2 µl cDNA product
- 3 µl 10x PCR
- 0.5 µl Taq polymerase
- 2 µl primer forward
- 2 µl primer reverse
- 1 µl dNTPs
- 19.5 µl water

The following PCR program was used to amplify the cDNA product.

For vti1a +/+, vti1a -/- and vti1b +/+, vti1b -/- PCR:

- Initial denaturation   3 minutes   95 °C
- Denaturation   30 sec   93 °C
- Annealing   30 sec   51.5 °C   40 x Cycle
- Elongation   30 sec   72 °C
- Final elongation   2 minutes   72 °C
- Hold   10 °C

Primer	Sequence (5′→3′)
Vti1a*for*	CAAGAAATGGGGAAACTGGA
Vti1a*rev*	AACATCTCTTGGCCGATTTG
Vti1b*for*	CGATATGCACCCCTGACTTT
Vti1b*rev*	GGCTTTCAGTGCCTTGTAGG
Gapdh*for*	ATGACTCTACCCACGGCAAG
Gapdh*rev*	GATCTCGCTCCTGGAAGATG

Size of vti1a mRNA = 215bp

Size of vti1b mRNA = 217bp

Size of GAPDH mRNA = 100bp

4.6: Agarose gel electrophoresis:

PCR products were analyzed on 1.5 % agarose gels (Cat. No: 2267.3, Roth, Germany). Agarose was heated in TAE buffer for about 6 minutes. The solidified gel was kept inside the running chamber which was filled with 1x TAE. PCR products were mixed with 5X loading buffer and loaded into the wells. Then the gels were run at 120 V for about 60 min. The gels were then soaked in ethidium bromide bath for 30 minutes and finally, the amplified PCR products were visualized by UV light and photographs taken.

4.7: Embryo preparation:

Pregnant mothers were killed by cervical dislocation and then embryos were removed from the mother, washed with saline (0.09 % NaCl) and photographed to document any obvious phenotypic changes.

4.7.1: Fixation:

At embryonic day (E) 18.5, embryos were transcardially perfused with 4% paraformaldehyde (PFA) whereas younger than E18.5 embryos were fixed directly by immersion in 4% PFA or Bouin's fixative. If not perfused, skin and brain coverings (duramater and arachnoid matter) were cut and the brain was exposed to allow easy access of fixative to brain tissue. Brains, bodies, skulls and adrenal glands were post fixed in Bouin's fixative (75% picric acid, 25% formaldehyde, and 5% glacial acetic

acid) for 5-6 hours, washed with 70% ethanol 3-4 times before leaving it overnight or in 4% PFA for varying time (3hr to overnight) depending upon age of animals.

4.7.2: Dehydration:

After fixation, tissues were processed in an automated embedding station (LEICA ASP 200) through ascending series of ethanol for dehydration and cleaning (70% - I & II - 1 ½ hr each, 80% 1hr, 90% 1hr, absolute Ethanol 1hr, xylene I&II, 1hr each, liquid paraffin I&II – 1hr each). Finally, tissues were embedded in fresh paraffin with proper orientation.

4.7.3: Sectioning:

Serial sections (8 μm for E12.5 and 10μm for other stages) were obtained using microtome (Techno-med GmbH, Bielefeld, Germany), mounted on glycerin-coated slides. Sections were then dried at 37 to 40 °C in hot plate and kept in oven for at least one day at 37 °C.

4.8: Controls:

Mice with genotype Vti1a (+/-), Vti1b (+/-) and triallelics 1a (+/-), 1b (-/-) or 1a (-/-), 1b (+/-) were fertile and survived well. Therefore to get maximum number of knockouts, we crossed triallelic mice regardless of male and female genotypes. The genotype closest to wildtype in the same litter was Vti1a (+/-), Vti1b (+/-). Therefore, in almost all cases they were used as controls unless otherwise stated.

4.9: Morphological studies:

4.9.1: Deparaffinisation:

Paraffin sections were deparaffinized first through xylene I to IV, 5 min. each and then rehydrated through a series of descending concentrations of isopropanol, namely 100% X 2 times, followed by 96% X 2, 80%, 70%, 50% for 5 minute each. Finally, they were briefly washed in distilled water before proceeding into further steps. Isopropanol was used instead of ethyl alcohol to ensure minimum shrinkage of tissue. All experiments involving deparaffinisation of paraffin embedded tissue were carried out by above mentioned process unless otherwise indicated.

4.9.2: Nissl-staining:

Paraffin sections of transgenic and wild-type mice were deparaffinized, briefly dipped into distilled water and afterwards transferred to 1.5% cresylviolet solution for 5-10 minutes. After this, sections were rinsed in distilled water, and differentiated in a solution containing distilled water and few drops of glacial acetic acid to remove excess staining. Sections were then transferred to an ascending series of ethyl alcohol (50, 70, 90, 96, 100 % x 2), and finally to xylene (x 4), before they were mounted using entellan (Merck, Germany) and cover slipped.

4.9.3 Haematoxylin-eosin (HE) staining:

Paraffin sections (10 μm) were deparaffinized, rehydrated to distilled water and transferred to Mayers hemalaum solution (cat no: T865.2; Roth, Germany) for 4-8 minutes. After this, sections were rinsed in distilled water and washed in running tap water for blueing cell nuclei for 10 minutes. Then sections were incubated with 0.1 % eosin solution (cat. No: 45380; Merck, Germany) for 10-15 minutes to color cytoplasmic content and rinsed with distilled water. Afterward, sections were transferred to an ascending alcohol-series (50%, 70%, 90%, 96%, 2-3 min each and 100 % ethanol I & II, 5 min each) followed by xylene I, II, III (5 min each) and mounted using entellan (Merck, Germany) and coverslipped.

4.10: DiI labeling:

There was an impairment in internal capsule fibers in vti1a/1b double knockouts when labeled immunohistochemically by anti neurofilament antibody. Since it was undetermined whether these fibers were thalamocortical and corticofugal axons, DiI labeling was used to selectively label the incoming and outgoing fibers to and from cortex. For thalamocortical axons, E16.5 heads were fixed in 4% PFA overnight after exposing skull. Next day brain was removed from skull and fixed for another day to improve fixation. Then, DiI paste (Molecular probes) was applied carefully on both side of dorsal thalamus after making a small vertical slit on either side. Drops of 2% agarose gel was put over the applied area to fix the DiI paste and left in fresh PFA for 3 weeks to allow for diffusion along the axons. After 3 weeks, brains were immersed in 30% saccharose solution overnight and cut on a vibrotome into 100 - 120μm thick sections.

Sections were picked up onto superfrost® plus microscope slides and coverslipped in DAKO fluorescence mounting medium. Similarly DiI paste was applied to most parts of frontal and parietal cortex to label the corticofugal axons. Pictures were taken with a Nikon microscope with attached Axiocam camera and software and further processed by "Image J" program for better quality in some cases.

4.11: Electron microscopy:

E18.5 brains and adrenal glands of E16.5 and E18.5 were fixed using standard protocol. Briefly, brain and adrenal glands were removed from embryos and immediately dropped into fixatives containing (3% Glutaraldedyde, 2% PFA, 1% Acrolein and 2.5% DMSO in 0.1M phosphate buffer) and left for overnight. Acrolein was added just before starting experiment. Next day tissue were washed with buffer (0.1M phosphate buffer), post fixed in osmium tetroxide, washed and dehydrated through ascending series of ethanol (30%, 50%, 70%, 90% and 100%) and then propyleneoxide 2x. After dehydration tissues were infiltrated with spur, epoxy medium (composition = 10g Vinylcyclohexene dioxide + 6g DER + 26g Nonenylsuccinic anhydride pure + 0.4 Dimetylaminoethanol) embedded and polymerized at 70 ˚C overnight. First semithin sections of 2μm were obtained and stained with Richardson stains to reach the desired tissue level, then ultrathin sections were cut at approximately 50nm and picked up on formvar coated copper grid. Ultrathin sections were then stained with uranyl acetate and lead citrate [Hayat, 1970].

4.12: Immunohistochemistry:

4.12.1: Growth Associated Protein-43 staining:

Growth Associated Protein-43 (GAP-43) is a protein which is specifically expressed in axonal growth cones. Rabbit anti GAP-43 antibody (Chemicon) was used at a concentration of 1:400 on E14 and E18.5 cortex to label the newly formed axonal growth cones and growing axons. Briefly, tissue sections were deparaffinized, rehydrated to distilled water and heated for 5 min in citrate buffer (0.1M, pH = 6) in a microwave oven at 550 W for antigen retrieval. The hot slides in citrate buffer were brought to room temperature (20 min) and unspecific binding sites were blocked by 10% normal goat serum (NGS) in phosphate buffer saline (PBS) containing 0.1% triton X-100 for 1 hour. Then sections were incubated in a solution containing 5% NGS, 0.1% Triton-X in PBS,

and polyclonal rabbit anti - GAP-43 antibody (Chemicon) at 4 C° overnight. After washing with PBS 3 times (5min. each), sections were incubated with goat anti rabbit secondary antibody labeled with FITC (GaR, Molecular probes, 1:500) for one hour at room temperature. Sections were washed again with PBS 3 times (5 min.), cell nuclei were stained with DAPI (DAKO, 1:800 in PBS 5-10 min), washed again with PBS and finally mounted and coverslipped in DAKO fluorescent mounting medium.

4.12.2: Glial fibrilary acidic protein (GFAP) staining:

GFAP protein is a member of the intermediate filament protein family that provides support and strength to cells. GFAP polymerizes to form the main intermediate filament found in astroglial cells. Rabbit polyclonal anti-GFAP antibody (DAKO) was used to label astrocytes in forebrain sections. Primary antibody was diluted 1:200 and goat anti rabbit secondary antibody (G α Rab-FITC) was used at 1:500 concentration. Subsequent steps were same as for the GAP-43 staining.

4.12.3: Synaptophysin and synapsin staining:

The synapsins are a family of proteins that have long been implicated in the regulation of neurotransmitter release at synapses. Specifically, they are thought to be involved in regulating the number of synaptic vesicles available for release through exocytosis at a time. Synapsins are encoded by three different genes, synapsin I, II and III, and different neuron terminals will have different amounts of these. Polyclonal rabbit anti-synapsin antibody (Synaptic systems, Germany) was used to label all synapsins in E18.5 cortex. The primary antibody concentration was used at 1:50 and goat anti rabbit secondary antibody was used (GαR-FITC) at 1:500. Overall procedure was same as above.

4.12.4: Tyrosine Hydroxylase (TH) staining:

Tyrosine hydroxylase (TH) catalyzes the rate-determining initial step in the biosynthesis of catecholamines such as dopamine, noradrenaline and adrenaline. Therefore antibodies against TH are used as a marker for dopaminergic and adrenergic neurons. Paraffin sections were deparaffinized, rehydrated to distilled water and heated for 5 min in citrate buffer (0.1M, pH = 6) in a microwave oven at 550 W for antigen retrieval. Endogenous peroxidase activity was quenched by pre-incubation in 3% H_2O_2 (Merck) for 10 min. Thereafter subsequent steps were followed same as described above until incubation with

monoclonal mouse TH anti-serum (MAB5280, Chemicon, 1:200) overnight (See GAP-43 staining). After rinsing with PBS, sections were incubated in goat anti mouse antibody (GαM; 1:50; Nordic) for one hour at room temperature, rinsed in PBS and incubated with mouse peroxidase anti peroxidase (PaP-M; 1:800; Nordic) for one hour at room temperature. Visualization of the immune complex was achieved by incubation with Nickel intensified diaminobenzidine (DAB; Sigma) reaction according to Adam's method [Adams, 1977]. The sections were dehydrated, cleared in ethanol and xylene and mounted using entellan. For controls, in all cases PBS was substituted for the primary antisera in order to test for nonspecific labeling. No specific cellular staining was observed when primary antiserum was omitted.

4.12.5: Neurofilament staining:

Neurofilaments are intermediate filaments that support neuronal and axonal cytoplasm. Rabbit polyclonal anti-neurofilament (NF) antibody (AB1981, Chemicon) was used as neuronal marker; it stains axons as well as neuronal cell body of the central and peripheral nervous system. Therefore, thalamocortical, spinotrigeminal axons in central nervous system and neuroendocrine cells in gut were identified by incubating with anti-NF antibody (1:1500) at 4 °C overnight. After that GaR (1:50) and PaP-R (1:800) were used in subsequent steps. The reaction was then visualized with Ni-intensified DAB. All other techniques were the same as for anti-TH antibody described above.

4.12.6: 5-hydroxytryptamine (5-HT') staining:

Serotonin (5-hydroxytryptamine, 5-HT') was used as a marker for hindbrain serotonergic neurons. Sections were processed as above and were incubated with rabbit anti-5HT' antibody (S-5545, Sigma) at a concentration of 1:1000 at 4 C° overnight. Subsequent methods were the same as for neurofilament staining.

4.12.7: Vti1a staining:

The expression of vti1a proteins in different tissue in different embryonic periods of wild type mice were seen by using either mouse monoclonal (BD biosciences. 1:800) or rabbit polyclonal (1:200, kindly gifted by our collaborators, Gabi F. Von Mollard, Bielefeld, Germany) anti-Vti1a antibodies. The secondary antibodies goat anti-mouse labeled FITC (GαM-FITC) or goat anti-rabbit (Cye-3) were used at 1:500 concentration. Rest of the

method was followed same as GAP-43 staining. PAP immunolabeling was followed by GαRab (1:50), PAP-Rab (1:800) and visualized with DAB as described earlier.

4.12.8: Vti1b staining:

The expression of vti1b proteins in different tissue at different embryonic age of wild type mice was visualized using either mouse monoclonal (BD biosciences, 1:500)) or rabbit polyclonal (1:200, kindly gifted by our collaborators, Gabi F Von Mollard, Bielefeld, Germany) anti-Vti1b antibody. The secondary antibodies goat anti-mouse labeled with FITC (GαM-FITC) or goat anti-rabbit (Cye-3) were used at a concentration of 1:500. For detection steps see GAP-43 and TH staining above.

4.12.9: Chromaffin cells staining:

For specific staining of chromaffin cells, paraffin sections of adrenal gland were immunostained using a rabbit anti-tyrosine hydroxylase (anti-TH) antibody (Chemicon). Similarly, immunostaing for PNMT (Phenylethanolamine-N-methyltransferase) was performed using a polyclonal rabbit anti-PNMT antibody (Chemicon) specifically detecting differentiated chromaffin cells. Anti-TH antibody (1:200) or anti-PNMT (1:500) antibodies were applied at 4 C° overnight. Cells were visualized either by fluorescence or PAP- DAB staining method as mentioned earlier. In case of PAP-DAB techniques, after DAB step, sections were washed thrice with PBS and directly embedded in DAKO fluorescent mounting medium. Dehydration and xylene steps were avoided to ensure minimum shrinkage of chromaffin cells.

4.12.10: Labeling of neuroendocrine cells of gut

Chromogranin A and B are members of the chromogranin/secretogranin (granins) family of neuroendocrine secretory proteins, i.e. they are located in secretory vesicles of neurons and endocrine cells. The dual efficacy of chromogranin A and B makes it a potent marker for peptide hormone producing cells which are found in cells of the adrenal medulla, enterochromaffin-like cells in gut and beta cells of the pancreas. Rabbit polyclonal anti-chromogranin A+B (Monosan) antibody was used to label these cells in gut of E18.5 control and vti1a/1b dKO mice. Primary antibody concentration was used at 1:50 concentration and secondary antibody (GαR-FITC) at 1:500. For detection see GAP-43 staining protocol above.

4.12.11: Labeling for cortical neurons
4.12.11.1: SATB2/CTIP2 staining:

Antibody against special AT-rich sequence binding protein 2 (SATB2) and chicken ovalbumin upstream promoter transcription factor-interacting protein 2 (CTIP2) were used to label the upper layers (2-4) and layer 5th neurons at E18.5 cortex. Very briefly, sections were deparaffinized and rehydrated with decreasing grades of alcohol as mentioned earlier. To enhance antigen retrieval, sections were treated in antigen unmasking solution (Vector laboratories, 4.8ml in 500ml of H20), heated in microwave (900W) for 4 min, cooled under ice and again heated for 2 minutes. After bringing to room temperature, unspecific binding sites were blocked by treating in 1% BSA (Sigma) with 0.1% tween-20 or triton X-100 for 1hour at room temperature. Sections were then incubated in mixture of two primary antibodies, one against SATB2 (Rabbit polyclonal, 1:1000 in 1% BSA, kindly provided by Dr. Victor Tarabykin, Max Plank Exp. Medicine, Goettingen, Germany) and other against CTIP2 (rat monoclonal, Abcam, 1:200) and kept overnight at 4˚C. After washing with PBS, sections were treated in secondary antibodies directed against Donkey anti-Rabbit IgG-Alexa 488-green (1:500, Invitrogen) and Goat anti-Rat IgG-Alexa 568-red (1:500, Invitrogen) for 1 hour, washed again and then nuclei were labeled with diluted DAPI solution for 5 min. (DAKO, 1:600 in PBS). Finally sections were mounted in DAKO fluorescent mounting media.

4.12.11.2: Tbr1/CTIP2 staining:

Deep layer of cortical markers T-box brain gene 1 (Tbr1, Chemicon) and CTIP2 (Abcam) antibodies were used to label 6th and 5th layer neurons. Briefly brain sections were treated with primary antibodies rabbit anti-Tbr1 (1:400) concentrations and rat anti-CTIP2 (1:200). Secondary antibodies (Donkey anti-Rabbit green) and (Goat anti-Rat-red) were used at 1:500 concentration and subsequent steps were same as SATB2/CTIP2 staining.

4.12.12.3: Reelin staining:

Cajal Retzius cells, which are the principal cells in layer one of cortex, were labeled by antibody against Reelin (Calbiochem). Mouse monoclonal reelin antibody was used as 1:100 concentrations for overnight incubation whereas Chicken anti mouse IgG-Alexa 594-red (1:500, Invitrogen) was used as secondary antibody. Rest of methods was applied as mention above in SATB2/CTIP2 staining.

4.12.12.4: Blbp/Nestin staining:

Radial glial cells were labeled by using two antibodies one against brain lipid binding protein (Blbp) and other against nestin. Mixture of two antibodies *i.e.* Rabbit polyclonal Blbp (Chemicon, 1:1000) and mouse monoclonal Nestin (Chemicon, 1:100) were able to label radial glia cells in same brain section at E18.5. Secondary antibodies were treated as 1:500 concentrations (Goat anti rabbit IgG, conjugated with Alexa 594 red and Goat anti mouse IgG, conjugated with Alexa 488-green) for one hour. Besides fluorescence techniques, nestin antibody (Hybridoma bank, 1:2 concentration) was also used for PAP immunolabeling at E14 .5 and E18.5 stages (See detail procedure in TH staining).

4.12.12.5: Proliferative cell nuclear antigen (PCNA) staining:

To detect cells which are still proliferating, a mouse monoclonal antibody directed PCNA was used (Novokastra). In brief, sections were deparaffinized, rehydrated to distilled water and heated in citrate buffer in a microwave oven to improve antigen retrieval as described above. Sections were treated with 3% H_2O_2 in PBS to block endogenous peroxidase activity. Non-specific binding was blocked by pre-incubation in 10% normal goat serum (NGS; Sigma) containing 0.1% Triton for two hours. Sections were incubated with anti-PCNA antibody (1:100) at 4 °C overnight. After rinsing with PBS, sections were incubated in goat anti mouse (GaM) antibody, rinsed in PBS and incubated with mouse peroxidase anti peroxidase (PaP-M) and visualized with Ni-intensified DAB as described above.

4.13: Counting procedure:

The total number of cells of interest *e.g.* number of peripheral ganglia and TH-positive cells in ventral tegmental area and substantia nigra were counted by counting every fifth serial section (10 µm) of different tissues to avoid double counting and later the total numbers were multiplied by factor 5. Cells which had both noticeable cytoplasm and clearly visible nuclei were only counted. Data represent means of minimum n = 3 ± SEM.

4.14: Solutions:

4.14.1: Phosphate buffer (PB) solution:

27.69 grams (g) $NaH_2PO_4.H_2O$ (**A**) was dissolved in 1000 ml distilled water

35.69 g $Na_2HPO_4.2H_2O$ (**B**) was dissolved in 1000 ml distilled water

190 ml of "**A**" was mixed with 810 ml of "**B**" to prepare 1L PB (0.2M; pH = 7.4)

4.14.2: Phosphate buffered saline solution (PBS):

9.0 g NaCl and 100 ml PB 0.1M were added to 900 ml distilled water to prepare 1L PBS (pH = 7.2).

4.14.3: Paraformaldehyde solution (4%PFA):

40 g of PFA (Merck, Germany) were dissolved in 500 ml distilled water, heated to 60 ˚C. Aldehyde formation occurred upon addition of few drops of NaoH (1M). Then the solution was cooled to room temperature, filtered and mixed with 500 ml of 0.2M PB to prepare 1 litter of 4% PFA (pH = 7.4).

4.14.4: Citrate buffer:

21.01 g $C_6H_8O_7.H_2O$ (A) was dissolved in 1000 ml distilled water

29.40 g $C_6H_5Na_3O_7.2H_2O$ (B) was dissolved in 1000 ml distilled water

190 ml of A was mixed with 810 ml of B to prepare 1L citrate buffer (0.1M; pH = 6.0)

4.14.5: Tris acetate buffer (TAE, 50X, pH = 7.9, 1L):

242 g Tris

57.1 ml glacial acetic acid

18.61 g EDTA (0.5M, pH = 8.0)

4.14.6: Lysis buffer:

100 mM Tris pH 8.0

200 mM NaCl

5 mM EDTA

0.2% SDS

20 μl/ml Proteinase K

4.17: List of chemicals and their companies:

Acetic acid (CH3COOH) (Carl Roth GmbH, Art. No. 3738.1)

Acrolein 90% (Sigma Aldrich, USA, Lot no. S35243-266, Cat: 11, 022-1), stored at 0-5 ºC.

Agarose (Carl Roth GmbH, Art. No. 2267-3)

Ammonium Nickel Sulphate (Fluka-Garantic Analy. No. 212800-1182)

Antigen unmasking solution (Vector laboratories Inc. Burlin game, Catl .No. H-3300)

Bovine serum albumin (BSA) (Sigma, cat/lot n. A3294)

Buffer $(NH_4)_2SO_4$ (Invitrogen, part no: Y02028)

Citric acid monohydrate (Merck, K91554344 211)

Cobalt II chloride (Merck, Art. 25339, No. 2306380, MW 237.93g)

Creslyviolet (Merck, K2198335-947)

DAKO cytomation fluorescent mounting medium (Lot. No. 00006582, Ref.-S3023)

DEPC (Carl Roth, No 2165428)

DER (Serva, Lot no. 22030)

dNTPs (Cat. No: 1969046; Roche)

DMAE (Dimetylaminoethanol, $C_4H_{11}NO$) Lot. 070341, Serva electrophoresis, GmbH, Germany, stored at +15 to +30 ºC.

EDTA (Ethyleneamine tetraacetic acid) (Carl Roth, Art. No. 8043.2)

Eiweiss- Glycerin (Carl Roth GmbH, Art. No. P049.1)

Ethanol 99.8% (Carl Roth GmbH, Art. No. 9065.4)

Entellan (Merck, Germany, HX 624397)

Eosin (Merck, Ci. No. 45380, S. No. 881)

Formaldehyde (Merck, K35277505-546)

Haematoxylin (Merck, Germany, Lot no. 645 - K660838, Art. 4305)

Hydrochloric acid (HCl) (Carl Roth GmbH, Art. No. 4625.1)

Hydrogen Peroxide (H_2O_2), (Roth, Art No. 9681.1)

2-Propanol (Carl Roth GmbH, Art. No. P049.1)

$MgCl_2$ (Invitrogen, part no:Y02016)

NeuroTrace Multicolour Tissue-Labelling Kit (Molecular Probes, USA), (Lot. No. 50E1-1)

NSA (Nonenylsuccinic anhydride pure (C13H20O3 (Lot: 12727) stored at +15 to +30 ºC.

PFA (Paraformaldehyde, Merck, Germany, Lot. No. K35277505-546)

Picric Acid (Sigma, Batch # 013K6053)

Propylene oxide (C_3H_6O), Serva, Lot no. 060272

Taq DNA polymerase (Invitrogen, cat. No: 10342-020)

TRIS (Roth, Art. No. 3580.1)

Trisodium citrate di-hydrate (Roth, Art. No. 3580.1)

VCD (Vinylcyclohexene dioxide), Fluka, Sigma-Aldrich, USA, stored at RT. (Lot. No. 1294848)

Xylol 98% (Carl Roth GmbH, Art No. 9713.3)

4.18: List of instruments and their companies:

Confocal laser microscope (Leica, ASP200)

Dissecting Microscope (Zeiss, Stemi DV4)

Electron microscope (LEO, 906E)

Fluorescence microscope (Nicon microscope attached with Axiocam MRC software, Zeiss)

Frigomobil (Reichert Jung, Germany)

Laser dissecting microscope (Arcturus)

Light microscope (Nicon)

Microtome (Light microscopy), (Techno-med GmbH, Bielefeld, Germany)

Microtome (cryostat) (Microm international, HM560, GmbH, Germany)

Paraffin embedding machine (Leica EG 1150C)

Paraffin processing automated machine (Leica, ASP 200)

PCR mastercycler (Eppendorf)

5. Results:

Vti1a and vti1b double knockout (KO) mice die shortly before birth. Double KO embryos appear inactive when taken out at embryonic day 18.5 (E18.5). During perfusion they act and showed normal heartbeat as compared to controls. This means, the KOs die between E18.5 and birth. Single knockouts of vti1a and vti1b mice were viable and fertile showing very mild phenotype. Triallelic mice for example *vti1a (+/-), vti1b (-/-)* and *vti1a (-/-), vti1b (+/-)* also survive and are fertile. To generate double KO, we crossed either male (+/-,-/-) and female (-/-, +/-) or vice versa. Littermates closest to wild type could be obtained from above mating (+/-, +/-). Unless otherwise mentioned, vti1a (+/-), 1b (+/-) served as controls (Ctrl).

5.1: General phenotype seen in central nervous system (CNS):

Most double knockout mice (KO) were little smaller than controls in body size. However, body size was not a reliable criterion for distinguishing between controls and knockouts. Although controls vti1a (+/-), vti1b (+/-) and triallelic vti1a (+/-), vti1b (-/-) or vti1a (-/-), vti1b (+/-) could be distinguished from KO (-/-, -/-) by dissecting trigeminal ganglion which showed severe neurodegeneration at late embryonic stages, heterozygous and triallelic animals could not be distinguished from each other by above criteria. To be sure to get (+/-, +/-) as control, embryos were genotyped using PCR with appropriate primers.

In general, KO brain was also relatively smaller and showed wide ventricles, e.g. lateral ventricles (Fig. 5.1$_a$B, asterisk) as compared to control (Fig. 5.1$_a$A, asterisk). Lateral ventricles are wide cavities present on either side within the cortical hemisphere containing cerebrospinal fluid. Major projection tracts as well as commissural fibres were either absent or highly reduced in size. For example anterior commisure, a bundle of axonal fibres which runs transversely to connect ventral and anterior parts of cortical hemispheres, was completely absent in E18.5 KO (Fig. 5.1$_a$B, yellow arrow). Similarly, hippocampal commisure which joins the two hippocampi was also absent in E18.5 KO (Fig. 5.1$_a$B, black arrow) when compared to control (Fig. 5.1$_a$A, black arrow).
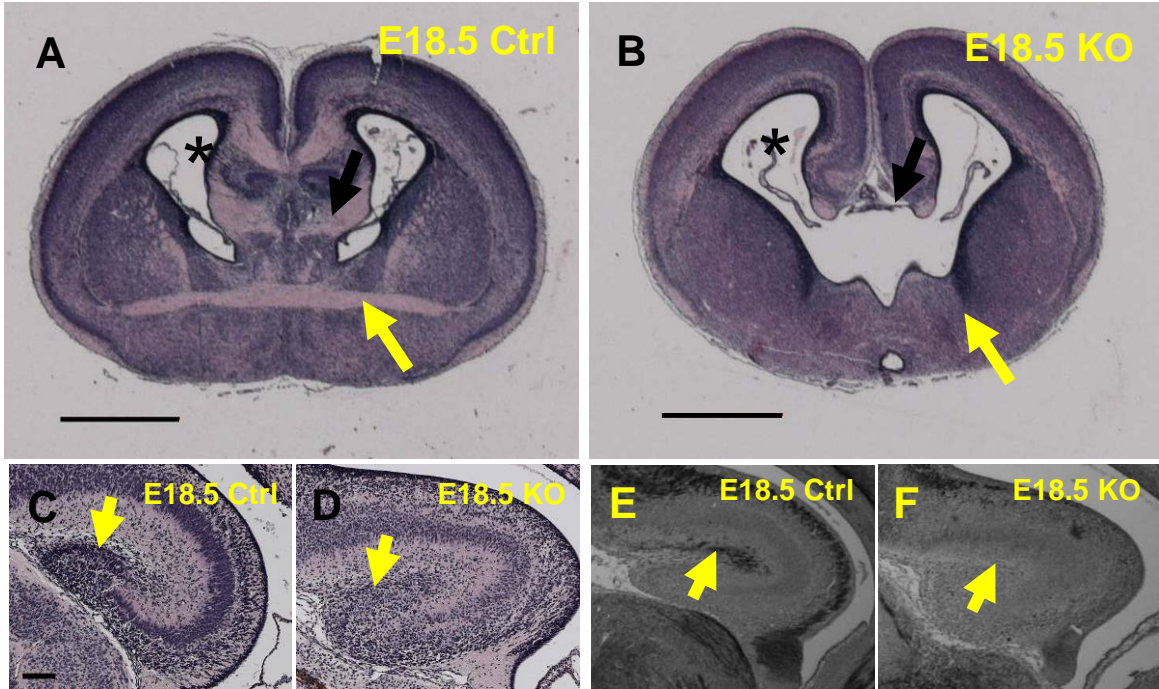
Fig. 5.1$_a$: General phenotype of vti1a/1b double knockout mice in forebrain at E18.5. At E18.5, overall size of KO brain is reduced, lateral ventricles are enlarged (B, asterisk), hippocampal commisure is absent (B, black arrow) and anterior commisure is also missing in knockout (B, yellow arrow) as seen in haematoxylin and eosin (HE) stained brain tissue. Similarly, dentate gyrus of hippocampus is also deformed (D, arrow), neurofilament positive fibers are absent in hippocampal proper (F, arrow) as compared to control (C, arrow) and (E, arrow). Neurofilament staining in E, F is dark PAP- immunohistochemistry. Scale bar: 1000μm (A, B), 100μm (C-F).

On the other hand, the antero posterior length of corpus callosum was decreased as shown in HE stained E18.5 brain sections (Fig. 5.1$_b$B, bracket). When seen in coronal view at rostral level, the thickness of corpus callosum was comparable (Fig. 5.1$_b$C and 5.1$_b$D) but its thickness was greatly reduced in the middle (Fig. 5.1$_b$H). Absence of anterior commisure in KO was confirmed in saggittal view (Fig. 5.1$_b$B, arrow). A striking phenotype was seen in E18.5 KO hippocampus. KO hippocampus had thickened dentate gyrus showing higher number of cells (Fig. 5.1$_a$D) as compared to control (Fig. 5.1$_a$C) and hippocampal proper lacked neurofilament positive fibers as shown by neurofilament immunohistochemistry (Fig. 5.1$_a$F. arrow). The fibers of fornix, which runs below the corpus callosum, were also missing in E18.5 KO (Fig. 5.1$_b$H, black arrow) as compared to control (Fig. 5.1$_b$G, black arrow).
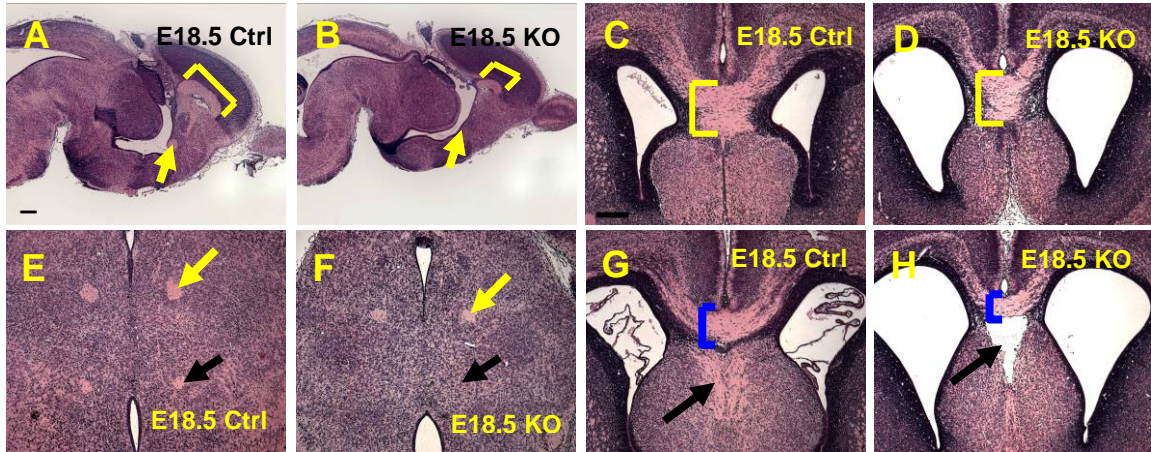
Fig. 5.1_b: General phenotype of vti1a/1b double knockout mice at E18.5. HE staining at E18.5 shows that the antero-posterior extent of corpus callosum is reduced in KO (B, bracket, saggittal view). In coronal view, rostrally, the thickness of corpus callosum differs minimally (C and D, yellow bracket) whereas in middle, its thickness is clearly reduced (H, blue bracket) as compared to control (G). Note fibers of fornix are also missing in KO (H, arrow) leaving a huge gap. In diencephalon, fasciculus retroflexus are present in both control and KO (E, F, upper two round bundles, yellow arrow) whereas mammilothalamic tracts are missing in KO (F, black arrow). Absence of anterior commisure can also be seen in saggittal view (B, arrow). Scale bar: 250µm in A, B; 100 µm in C-H.

In diencephalon, KO thalamus lacked mammilo-thalamic tract, a longitudinal bundle of fibers which runs antero posteriorly (rostro-caually) on either side of third ventricle (Fig. 5.1_bF, black arrow). Instead, fasciculus retroflexus were present in both control and KO (Fig. 5.1_bE, 5.1_bF, yellow arrow).

5.2: Absence of pontine nuclei in KO mice:

Pontine nuclei, which lie in ventral most part of pons, were completely absent in KO as seen in both E16.5 saggittal (Fig.5.2B, 5.2D, black arrows) and E18.5 coronal view (Fig. 5.2F). Pons is the part of brainstem between medulla oblongata and midbrain which contains neurons relaying the connection between cerebrum and the cerebellum, as well as ascending and descending tracts. Corticopontine fibers carry information from the primary motor cortex to the ipsilateral pontine nucleus in the ventral pons, and the pontocerebellar projection then carries that information to the contralateral cerebellum via the middle cerebellar peduncle.
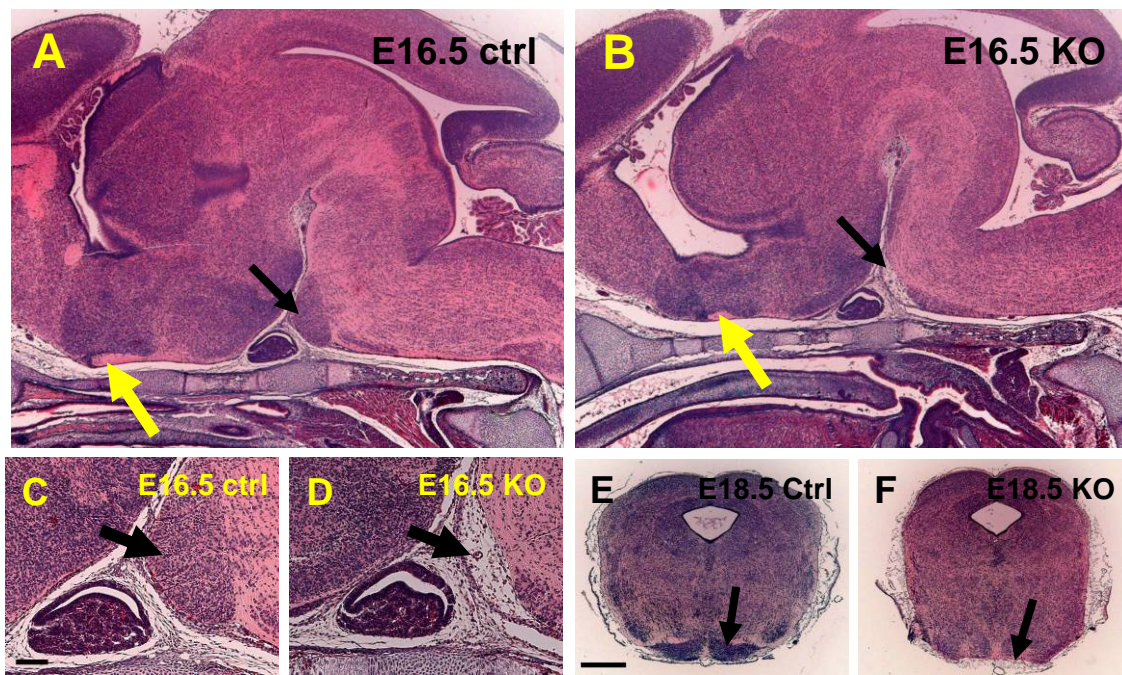
Fig. 5.2: Absence of pontine nuclei in KO. In saggittal view, E16.5 KO mice completely lack pontine nuclei (B, black arrow), higher magnification (D, arrow) which were normal in corresponding controls (A and C, black arrow). Lack of pontine nuclei can also be seen at E18.5 in coronal view (F, arrow). Note optic chiasma was also thin in KO (B, yellow arrow) as compared to control (A, Yellow arrow) Scale bar 100μm (C, D) and 500μm (A, B, E, F).

5.3: Huge gap in lateral part of cerebrum in KO mice:

E18.5 KO forebrain brain showed a conspicuous gap on either side of cerebrum (Fig. 5.2A, arrow). These gaps were seen at the region where external capsule normally resides. The external capsule is bundle of fibres which divides cortex with subcortical structures. The external capsule was labelled with nestin antibody which clearly showed absence of nestin immunoreactive fibres in lateral part of KO cortex (Fig. 5.3B, arrows) as compared to control (Fig. 5.3A).
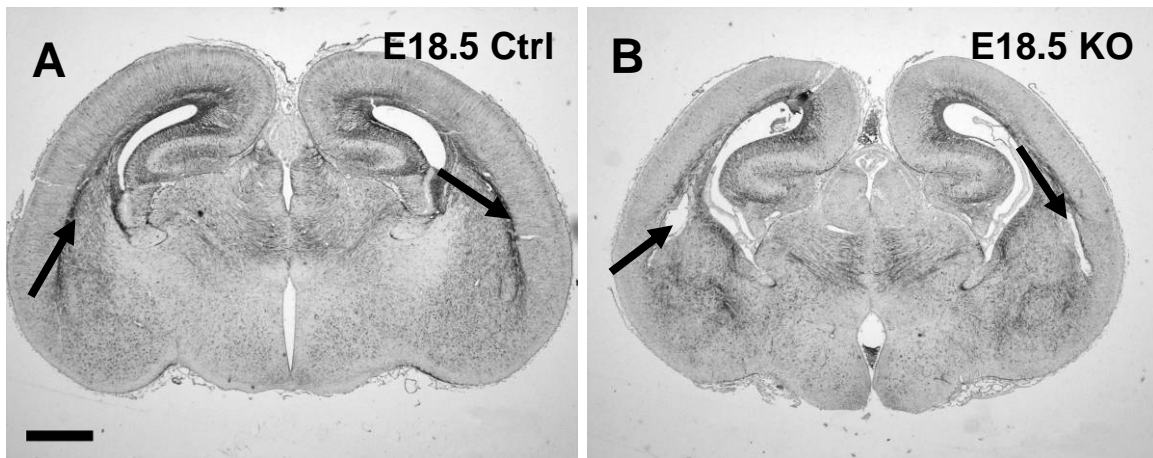
Fig. 5.3: Huge gap on lateral side of cerebrum in KO mice. There was a huge gap present at the lateral side of E18.5 KO cerebrum (B, arrows). Nestin immunoreactive fibres are missing in KO (B, arrows) compared to control (A, arrows). Scale bar 250μm (A, B)

5.4: Unusual fibre bundle in lateral part of striatum:

Striatum, which is a part of ventral pallium is found at rostral levels and lies medial to the cortex. A major fibber tract runs through striatum, the internal capsule, which is formed by corticofugal and thalamocortical fibers. In addition smaller axon bundles traverse the striatum. These bundles (blue arrows in Fig. 5.4A, 5.4B) were greatly reduced in E18.5 KO (blue arrows in Fig. 5.4E, 5.4F). Instead, there was an accumulation of axons lying lateral to striatum (yellow arrows in Fig. 5.4E, 5.4F), which was not seen in controls (Fig. 5.4A, 5.4B, yellow arrows). Those unusual fibers were neurofilament positive (Fig. 5.4F, yellow arrows) and nestin negative (Fig. 5.4G, yellow arrows) as shown by immunohistochemistry. Substantial amount of fibers in striatum originate from ipsilateral thalamus and from ipsilateral cortex and to lesser extent from contralateral cortex as well. A fluorescent dye, DiI, was used to find the origin of the unusual fibers. DiI paste when

applied to both sides of cortex, confirmed that those unusual fibers were indeed derived from cortex. On the other hand, DiI applied at both side of thalamus showed no positive fibers in knockout (Fig. 5.4J, yellow arrows). Majority of fibers which normally resides medial part of striatum in E18.5 control (Fig. 5.4A, blue arrows) were also missing in KO (Fig. 5.4E, blue arrows) as shown in HE stained tissue. This was further confirmed by labelling with neurofilament (Fig. 5.4F, blue arrows) and DiI (Fig. 5.4H, 5.4J, blue arrows), corresponding controls are (Fig. 5.4B, blue arrows) and (Fig. 5.4D, 5.4I, blue arrows).

DiI at thalamus
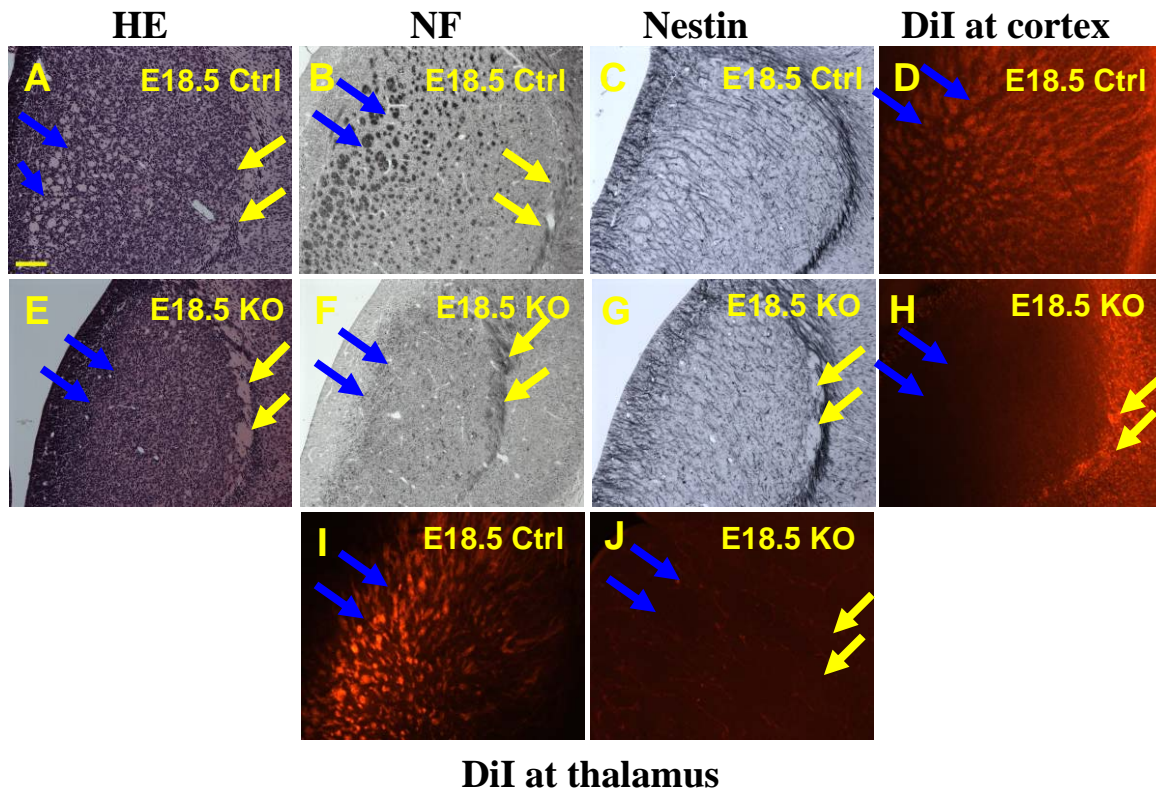
Fig. 5.4: Unusual bundle of fibers in KO striatum. A bundle of unusual fibers were seen on lateral side of striatum as shown in HE stained tissue (E, yellow arrows) which was not seen in control (A, yellow arrows). Those fibers were neurofilament positive (F, yellow arrows) and nestin negative (G, yellow arrows). DiI labelling was used to trace the source of those fibers. They can either predominantly come from cortex, ipsilateral thalamus or some fibers from contralateral cortex. Tracing experiment after DiI paste applied at cortex, confirms that those unusual fibers were coming from cortex (H, yellow arrows) because DiI labelling when applied at thalamus did not show any of these fibers in striatum (J, yellow arrow). Note, the majority of fibers which are normally found in medial part of striatum in control (A, blue arrows) were completely absent in KO (E, blue arrows) as shown in HE stained tissue, which was also confirmed by neurofilament immunohistochemistry (F, blue arrows) and DiI labelling (H, J, blue arrows). Scale bar 100µm (A-J).

5.5: Impairment of thalamocortical axons and corticofugal axons in KO mice:

A spectacular phenotype of major projection fibres in KO was found in thalamocortical axons (TCA). TCA are the fibres, which connect thalamus and cortex. Basically in principle, TCA convey all the sensory information from different parts of the body to the cortical area where they are represented in topographical manner. In addition, TCA feed back motor information to motor cortical areas. By E14.5, neurofilament labelled thalamocortical axons have just reached cortex in control (Fig. 5.5A, arrow) whereas in KO they can't cross pallio-subpallial (PSPB) border (Fig. 5.5B, arrow). Some times the pallio sub-pallial border is called cortico-striatal border. By E18.5, TCA have grown further and reached most of cortex (Fig. 5.5C, arrow), whereas in KO, they stop half way and stay within internal capsule region (Fig. 5.5D).
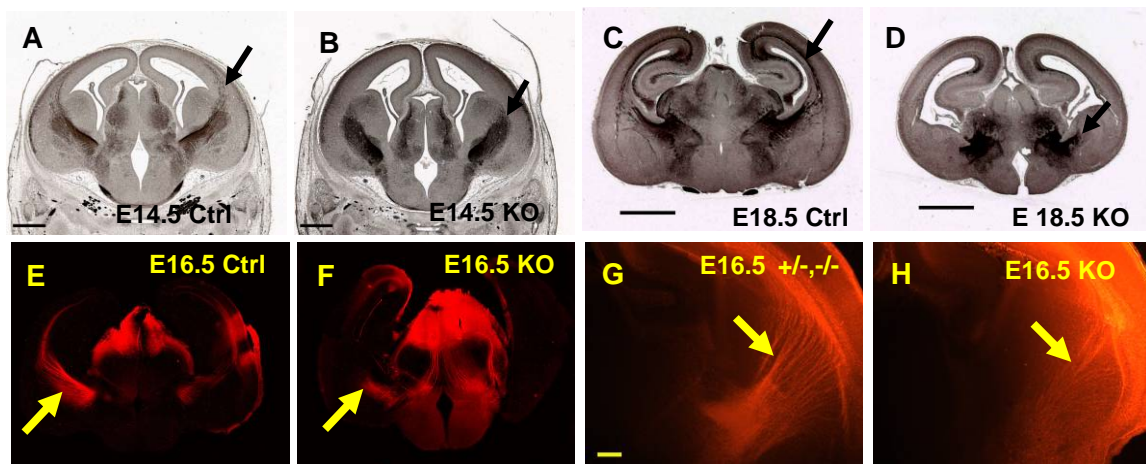
Fig. 5.5: Impairment in major cortical projection fibres in KO. At E14.5, neurofilament labelled thalamocortical axons (TCA) can not cross pallio subpallial border (arrow in B) as compared to control (A). TCA start to degenerate thereafter and at E18.5, they lie with in half of their way in KO (D), instead in control they reach to cortex normally. This was also confirmed by applying DiI to thalamus at E16.5 (arrow in F) as compared to control (E). On the other hand, DiI labelled corticofugal fibres were significantly diminished in E16.5 KO (arrow in H) as compared to (+/-, -/-) mice which was considered here as control (G). Scale bar 500µm (A, B), 1000µm (C, D, E, F) and 200µm (G, H).

Since neurofilament immunohistochemistry can not differentiate between thalamocortical axons and corticofugal axons which also pass through the internal capsule. We used the tracer DiI to selectively label the thalamocortical and corticofugal axons separately. Corticofugal axons here refer to all fibers leaving cortex. When applied to thalamus, DiI labelled knockout thalamocortical axons showed that they can not reach cortex, instead they stop in the middle of their way (Fig. 5.5F) confirming earlier results with neurofilament immunohistochemistry. DiI paste applied to cortex, labels all the corticofugal axons running through striatum except for the primary olfactory pathway. DiI paste was applied to most of the cortex to label all the corticofugal axons comprising corticothalamic, corticopontine, corticospinal fibers. DiI labelling demonstrated that only few fibers from cortex can leave the cortex in E16.5 KO (Fig. 5.5H, arrow) unlike in control in which thick bundle of fibers was labelled (Fig. 5.5G, arrow).

5.6: Loss of pyramidal tract and/or corticospinal fibers in KO:

The pyramidal tract or corticospinal tract is a massive collection of axons that travel between the cerebral cortex of the brain and the spinal cord. The corticospinal tract mostly contains motor axons. It can consist of two separate tracts in the spinal cord, the lateral corticospinal tract and the medial one. Additionally, corticobulbar tract is considered to be a pyramidal tract. Corticobulbar tract carries signals that control motor neurons located in cranial nerve nuclei rather than motor neurons located in the spinal cord. Together corticospinal and corticobulbar tracts form the pyramidal tract. HE stained brain section at the region of medulla in coronal view shows that pyramidal tracts are absent in both E14.5 KO (Fig. 5.6H, arrow), and E18.5 (Fig. 5.6J, arrow) when compared to controls (Fig. 5.6G and 5.6I, arrow). Further rostrally, the pyramidal tract can be seen as part of the cerebral peduncle which passes on either of ventral thalamus. HE stained sections at E18.5 KO showed clearly reduced cerebral peduncles (Fig. 5.6D, arrow) when compared to corresponding control (Fig. 5.6A, arrow). This was also shown by neurofilament immunohistochemistry (Fig. 5.6F, 5.6C and yellow boxed inserts). In contrast, when DiI was applied to cortex, it did not label the cerebral peduncle suggesting that it contained no fibers from cortex (Fig. 5.6E, arrow). Therefore, the remnants of cerebral peduncle in KO must contain fibers not related to cortex.
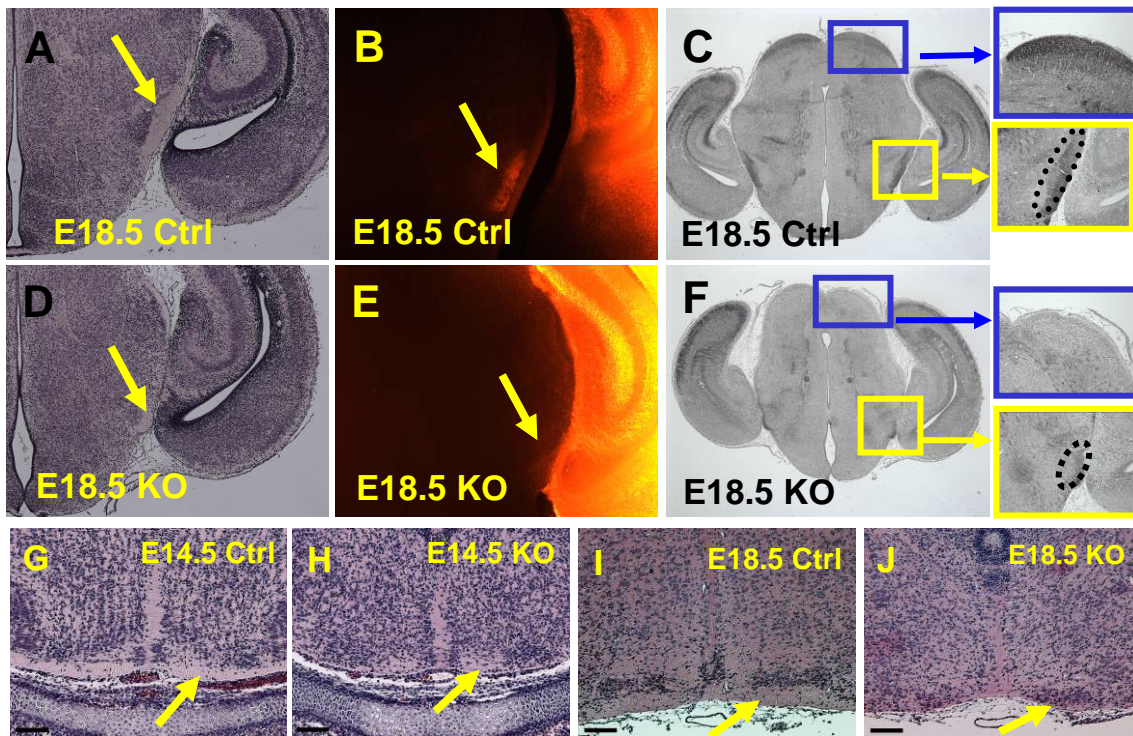
Fig. 5.6: Loss of corticospinal and pyramidal tracts in KO. Cerebral peduncle was almost absent in KO. It was hardly seen in E18.5 KO HE stained section (D, arrow) and in neurofilament labelled tissue (F, yellow box, also seen in higher magnification) compared to controls (A and C) but was completely absent in DiI labelled tissue when applied at cortex (E, arrow). This suggests that no fibers from cortex reach there to form cerebral peduncle. This was also confirmed when seen at the level of medulla. The pyramidal tract at medulla, which is formed by fibers from cortex via cerebral peduncle, was completely absent at both E14.5 and E18.5 KO (H, J, arrows) when compared to controls (G, I). Scale bar 100 µm (A, B, D, E, G-J), and 200µm   (C, F).

5.7: Other affected tracts:

Neurofilament positive fibers in superior colliculus were missing in E18.5 KO (Fig. 5.6F, also in higher magnification, blue boxes) as compared to corresponding control (Fig. 5.6C, blue boxes). The superior layers of superior colliculus receive input from retina as well as from visual cortex. In KO mice, cortical neurons were also affected and could not give subcerebral tracts. Thus it seems possible that a portion of optic axons which comes from visual cortex to the mesencephelon was missing in KO. The other mildly affected

tracts were optic tract and optic chiasma which were thinner in KO (Fig. 5.2B, yellow arrow) as compared to control (Fig. 5.2A, yellow arrow).

The other affected tracts were related to degeneration of peripheral sensory ganglia. Neurofilament positive spino-trigeminal tract axons were absent in E16.5 KO (Fig. 5.7D, yellow arrow) as shown in saggittal view. Already at E14.5, tracts of Lissauer were absent from KO spinal cord (Fig. 5.7B, yellow arrow) as seen in nissl-stained sections. Tracts of Lissauer (dorsolateral tract) contain axons of nociceptive dorsal root ganglion cells. These axons ascend 1-2 segments before they form synapses in substantia gelatinosa.
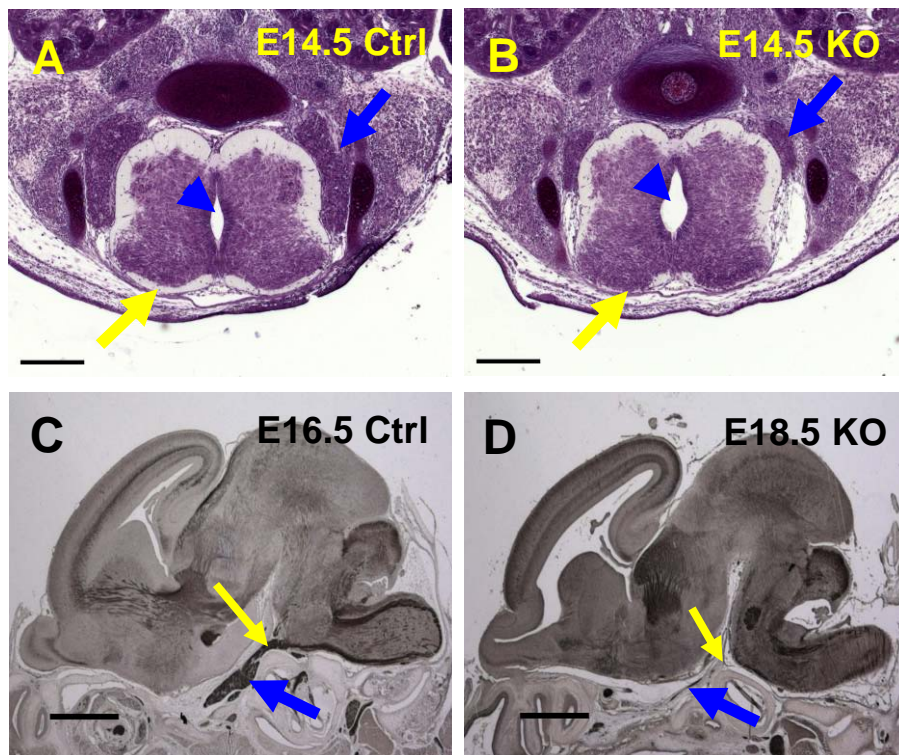
Fig. 5.7: Absence of tracts of Lissauer and spinotrigeminal tract in KO. Nissl stained tissue of E14.5 shows at the level of L3 that tracts of Lissauer are absent in KO spinal cord (B, yellow arrow). Tracts of Lissauer are formed by fibers coming from dorsal root ganglion (DRG) neurons which show severe neurodegeneration (B, blue arrow). Spinotrigeminal tract, which is related to trigeminal ganglion showing similar neurodegeneration (D, blue arrow), was also missing in E16.5 KO (D, yellow arrow). Note spinal canal was also dilated in KO (B, arrow head). Scale bar 200µm (A, B) and 500 µm (C, D).

Both dorsal root ganglia and trigeminal ganglia, which are associated with above mentioned tracts, are reduced by 80% in E14.5 and 98% in E18.5 KO mice compared to corresponding controls. (See details in results section – "5.11 Neurodegeneration at peripheral ganglia").

5.8: Loss of neurites and decrease in dopaminergic neuronal cell count:

Tyrosine hydroxylase is an enzyme responsible for catalyzing the conversion of the amino acid L-tyrosine to dihydroxyphenylalanine (DOPA). Dopaminergic neurons in substantia nigra and ventral tegmental area were labelled by anti- tyrosine hydroxylase (TH) antibody and total numbers of TH positive cells were counted at E14.5 and E18.5 in ventral tegmental area (VTA) and substantia nigra (SN) collectively. In E14.5 KO, total numbers of TH positive neurons were reduced by 14.30% (Fig. 5.8K, graph, see also in table 5.1) and at E18.5 KO, total numbers were reduced by 52.40% (Fig. 5.8L, graph, see also in table 5.1). When looking at neurite outgrowth, TH positive neurons were appeared similar in E14.5 control and KO (Fig. 5.8E, 5.8F). In contrast, SN and VTA at E18.5 KO completely lacked TH-positive neurites (Fig. 5.8H, arrow) unlike control, which showed well defined neurites (Fig. 5.8G). Likewise, E16.5 KO saggittal brain section showed that the TH positive nigro-striatal fibers do not reach to the striatum. Instead they divert slightly dorsal at the thalamo-striatal border (Fig. 5.8J), which was not in case of control (Fig. 5.8I).

Besides dopaminergic neurons in midbrain, TH positive noradrenergic neurons were also affected in locus coeruleus e.g. 17.33% loss at E14.5 KO (Fig. 5.8N, graph, see also in table 5.1), and 34.46% at E18.5 KO (Fig. 5.8O, graph, see also in table 5.1).
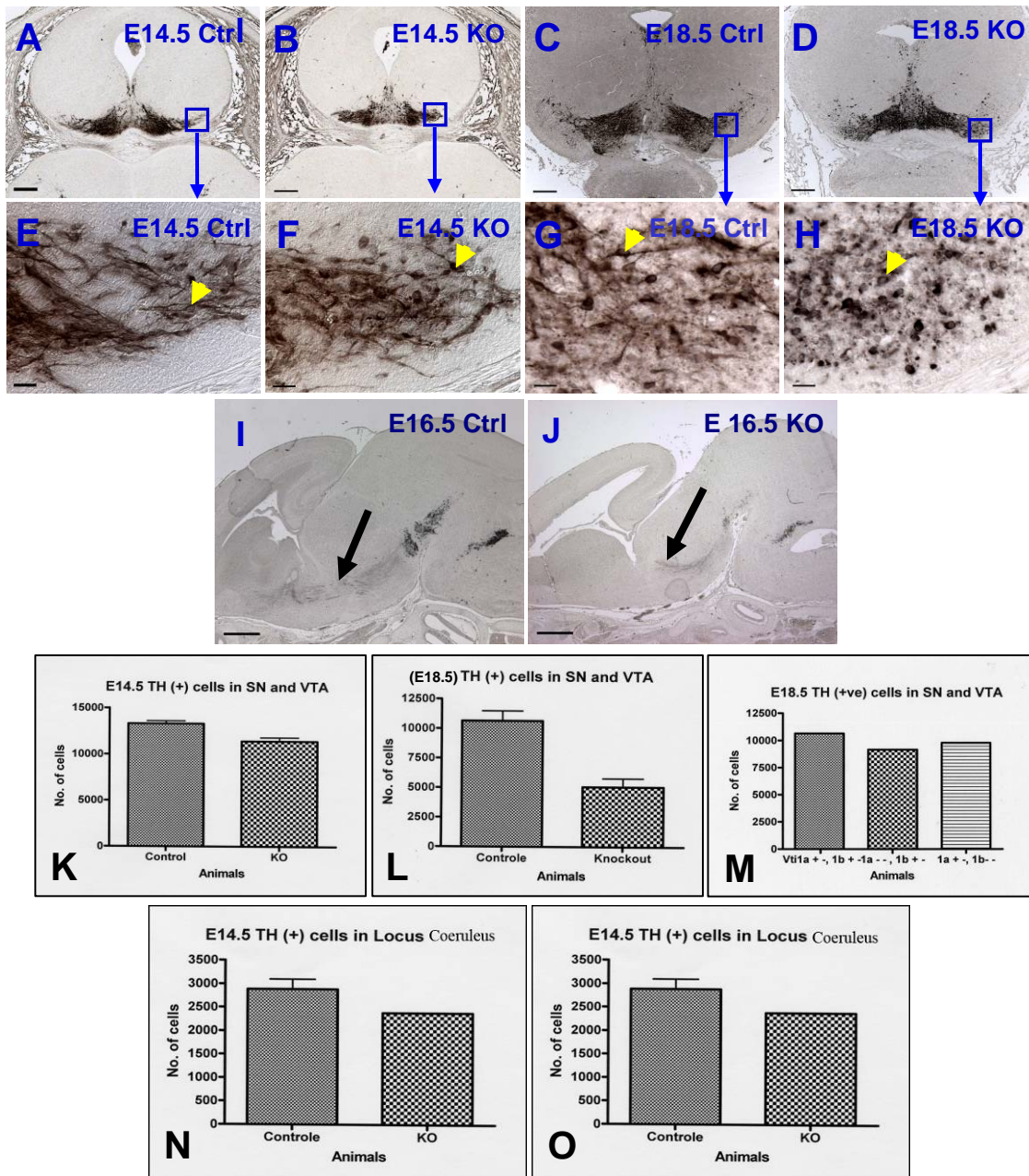
Fig. 5.8: Affected dopaminergic neurons in KO midbrain. Tyrosine hydroxylase (TH) positive cells in substantia nigra (SN) and ventral tegmental area (VTA) show no obvious difference in neurite outgrowth between control (E) and KO (F) at E14.5, whereas in E18.5 KO (D, H) the cells completely lack neurites. Nigro-striatal axons (arrows in I, J) do not reach their target in KO (J), instead they divert dorsally near the diencephalic-telencephalic border. There was also decrease in number of TH positive cells in SN plus VTA in E14.5 (14.30%, graph K) and E18.5 KO (52.40%, graph L). No marked difference in number of TH (+) cells between control and triallelic animals was seen at E18.5 (graph M). Locus coeruleus cells also showed decrease in number 17.33% at E14.5 and 34.46% at E18.5 as compared to controls (Graph N and O). Scale bar 200 µm (A-D), 20 µm (E-H), 500 µm (I, J).

5.9: Unusual inclusion bodies at E18.5 EM substantia nigra cells:

Substantia nigra was also investigated under the electron microscope at E18.5 stage. KO mice showed many more condensed, presumably dying cells (Fig. 5.9B, arrow) as compared to control showing normal immature neurons (Fig. 5.9A). Additionally in KO, processes contained many more unusual inclusion bodies, as shown at higher magnification in Fig. 5.9C. This was not seen in control animals.
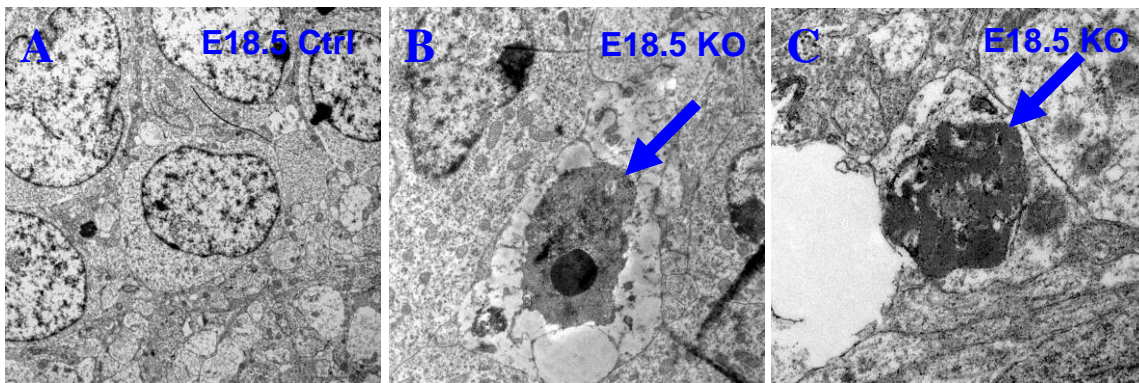
Fig. 5.9: Dopaminergic neuronal phenotype in KO at EM level. Electron microscopic pictures of neurons in substantia nigra show many dying cells at E18.5 (B, arrow) as well as unusual inclusion bodies (C, arrow) which were not seen in control (A). Magnification: 2156 x for (A) 3957 x for (B) and 16700 x for (C) compared to original magnification.

5.10: Loss of neurites in 5-HT' positive neurons in dorsal raphe at E18.5 KO:

The dorsal raphe nucleus is a part of the raphe nuclear complex and the largest source of serotonergic neurons. It provides a substantial portion of serotonin innervations to the forebrain. Serotonin positive neurons were labeled with anti 5-hydroxytryptamine antibody. At E14.5, 5-HT' positive neurons in dorsal raphe nucleus showed no marked difference in neurite outgrowth between control and KO (Fig. 5.10A, 5.10B) whereas at E18.5 KO, neurons showed significant reduction of processes (Fig. 5.10D, 5.10F, blue arrow). The corresponding controls at E18.5 stage are Fig 5.10C and 5.10E (blue arrow).
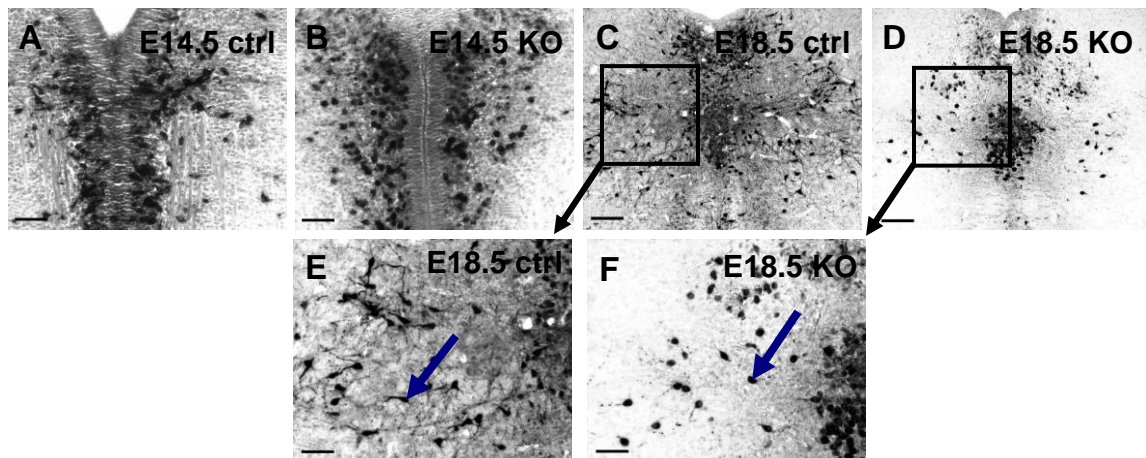
Fig. 5.10: Serotonergic neurons phenotype in KO brain. Comparable densities of 5-HT'-positive neurons were found in KO (B, D) and controls (A, B) at E14.5 and at E18.5, however, neuronal processes were largely reduced in E18.5 KO (D). Same is seen at higher magnification (F, arrow) when compared to controls (C, E). Scale bars 50µm (A, B, E, F) and 100µm (C, D).

5.11: Neurodegeneration at peripheral ganglia:

Ganglia contain accumulations of neurons in nervous system. One of the most exciting results of the vti1a/vti1b double knockout is neurodegeneration in peripheral ganglia. The peripheral ganglia show different degrees of neurodegeneration. Trigeminal (TG), nodose and petrosal, geniculate, and dorsal root ganglia (DRG) show severe neurodegeneration. Superior cervical ganglia (SCG) show moderate neurodegeneration where as vestibular and cochlear ganglia are least affected. In E14.5 KO, the reduction of total cell number in DRG was 84.30% (Fig. 5.11F, arrow), in nodose and petrosal 78.20%, and in geniculate ganglia 83.60% (Fig. 5.11J, arrow). At E18.5 they are reduced by 98.40% (Fig. 5.11H, arrow), 96.20%, 96.00% (Fig. 5.11L, arrow) respectively. When counted separately at E14.5, nodose ganglia were affected more than petrosal (nodose by 85.00%, petrosal by 67.20%, see also Table 5.1).

Superior cervical ganglia (SCG) at E14.5 didnot show much difference between control and KO (Fig. 5.11 M-N) but at E18.5, KO showed 54% reduction (Fig. 5.11P, arrow). Alternatively, DRGs when counted in triaalelic mice at E14.5 did not show significant difference from control (data not shown). Among least affected ganglia, vestibular and cochlear ganglia at E14.5 showed 18.10% (Fig. 5.11T) and 18.80% (Fig. 5.11X) whereas at E18.5 they showed 14.9% (Fig. 5.11V), 26% (Fig. 5.11Z) reduction respectively. On the other hand motor neurons at L2 level in E18.5, KO mice showed 61% (Fig. 5.11R) reduction (See details in table 5.1).

TG

DRG

Geniculate

SCG

Motor

Cochlear

Vestibular

A E14.5 Ctrl
B E14.5 KO
C E18.5 Ctrl
D E18.5 KO
E E14.5 Ctrl
F E14.5 KO
G E18.5 Ctrl
H E18.5 KO
I E14.5 Ctrl
J E14.5 KO
K E18.5 Ctrl
L E18.5 KO
M E14.5 Ctrl
N E14.5 KO
O E18.5 Ctrl
P E18.5 KO
Q E18.5 Ctrl
R E18.5 KO
S E14.5 Ctrl
T E14.5 KO
U E18.5 Ctrl
V E18.5 KO
W E14.5 Ctrl
X E14.5 KO
Y E18.5 Ctrl
Z E18.5 KO
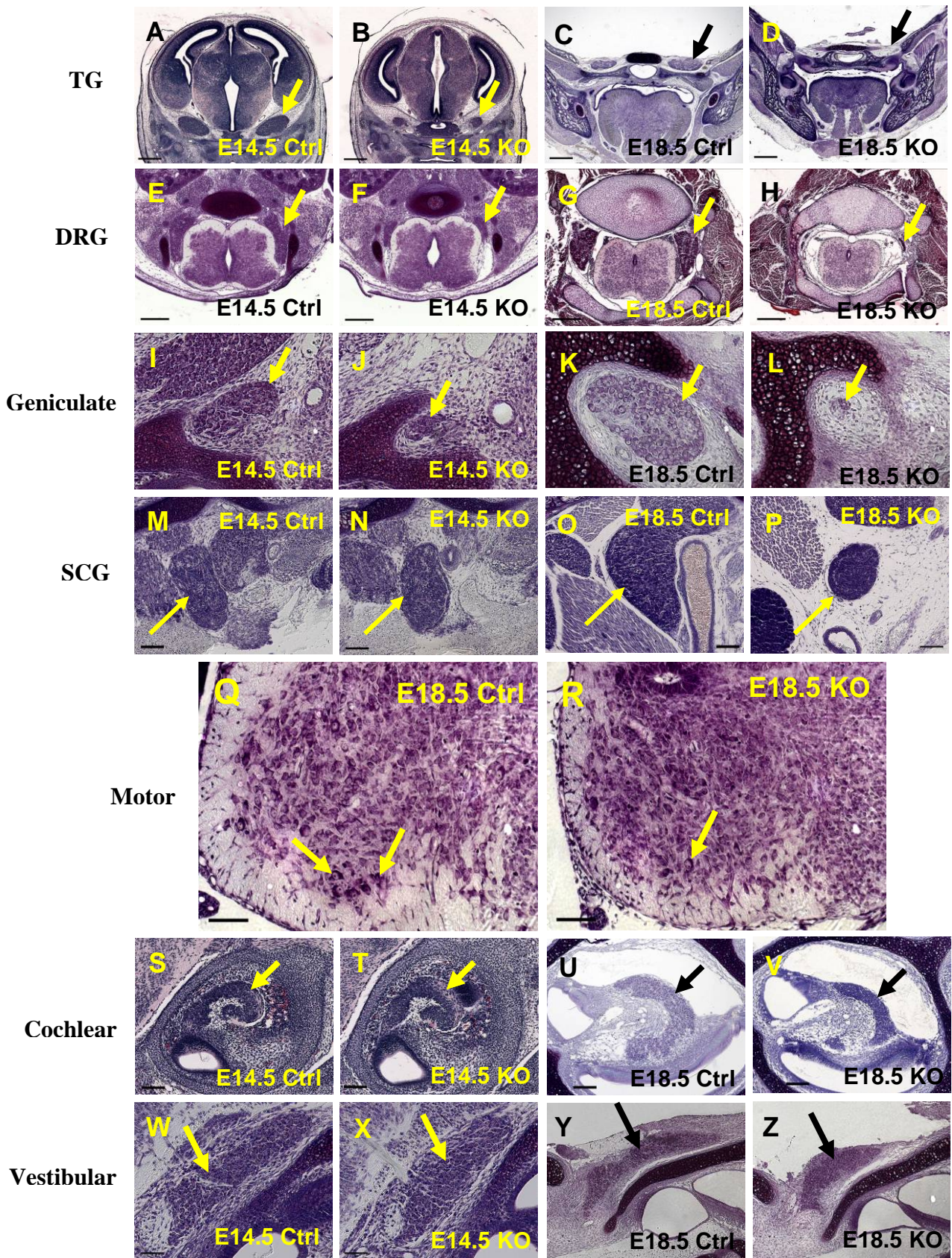
Table 5.1: Ganglia showing changes in cell numbers:

Ganglia	E14.5 Control	KO	% of Dec	E18.5 Control	KO	% of Dec
Nodose	8380±485	1258±217.5	**85.00**	NA	NA	
Petrosal	5133±792.5	1683±197.5	**67.20**	NA	NA	
Nod+ Pet	13510±1278	2940±20	**78.20**	12976	492	**96.20**
Geniculate	1248±12	205±10	**83.60**	1884	72	**96.00**
DRG	9210±170	1449±281	**84.30**	6896	108	**98.40**
SCG	NA	NA		33124	15224	**54.00**
Motor at L2	NA	NA		3750	1460	**61.00**
TH at SN &VTA	13310±290	11410±390	**14.30**	10650±833	5065±718	**52.40**
TH at LC	2885±215	2385±5	**17.30**	4645±362	3045±255.9	**34.46**
Vestibular	6755±50	5535±80	**18.10**	6288	5348	**14.90**
Cochlear	9103±412.5	7393±402.5	**18.80**	8496	6272	**26.00**

Table 5.2: Ganglia showing changes in volume:

Volume change per cubic µm						
Ganglia	E14.5 Control	KO	% of Dec	E18.5 Control	KO	% of Dec
Trigeminal	108200000±2333000	14870000±623100	**86.30**	126800000±38680000	2750000±35330	**97.80**
Nodose	14670000±114600	1949000±166200	**86.70**	*NA*	*NA*	
Petrosal	9533000±996500	2342000±101200	**75.40**	*NA*	*NA*	
Nod+Pet	24210000±881900	4291000±267300	**82.30**	*NA*	*NA*	
SCG	15330000±3265000	15740000±244700	**2.74 % increase**	*NA*	*NA*	
Vestibular	9579000±119400	7983000±379900	**16.70**	*NA*	*NA*	

Abbreviations: Nod = Nodose, Pet = Petrosal, DRG = Dorsal Root ganglion, L2 = Lumbar 2, SCG = Superior cervical ganglion, TH = Tyroxine hydroxylase, SN = Substantia nigra, LC = Locus coeruleus, *NA* = Not available, Dec = Decrease

Fig. 5.11: Neurodegeneration at peripheral ganglia in KO mice. Peripheral ganglia show different levels of neurodegeneration in KO. Trigeminal ganglia (arrows in A-D), dorsal root (arrows in E-H), nodose-petrosal and geniculate ganglia (I-L) are severely affected. Superior cervical ganglia (M-P) and spinal motor neurons (Q, R) are intermediately reduced. The least affected ones are cochlear (S-V) and vestibular ganglia (W-Z) either by volume or by total number of cells count. At E14.5 severely affected ganglia have a reduction by almost 80-85% in number neurons (table 5.1) and in volume (table 5.2), where as they show 98% reduction at E18.5. On the other hand, least affected ganglia are reduced by 18% (E14.5) and 15 to 25% (E18.5). Scale bar; 500µm (A-D), 200µm (E-H), 100 µm (M-P, S-Z) and 50µm (I-L, Q, R).

Not only a number of cells but also volume, showed similar reduction. Trigeminal ganglia (TG) were shrunken by 86.3% at E14.5 and 97.8% at E18.5 (Table 5.2). The other ganglia also showed a similar reducion in volume as they did in cell number (Table 5.1, 5.2).

5.12: Trigeminal ganglia at E12.5 stage and TUNNEL assay:

Above results suggest that neurone in KO trigeminal ganglia are formed normally and show neurodegenaration after certain developmental period or that they do not differentiate completely and degenerate. Therefore we investigated in developmental period at E12.5. HE staining of E12.5 KO ganglia (Fig. 5.12E, arrow) confirms that they are reduced approximately to half of size of control (Fig. 5.12E). Neuronal death was assessed by TUNNEL assay, which is a reliable maker of apoptotic cell death. Tunnel stained trigeminal ganglia clearly showed ahigher number of apoptotic neurons in KO (Fig. 5.12F, 5.12H) than in control (Fig. 5.12B, 5.12D).
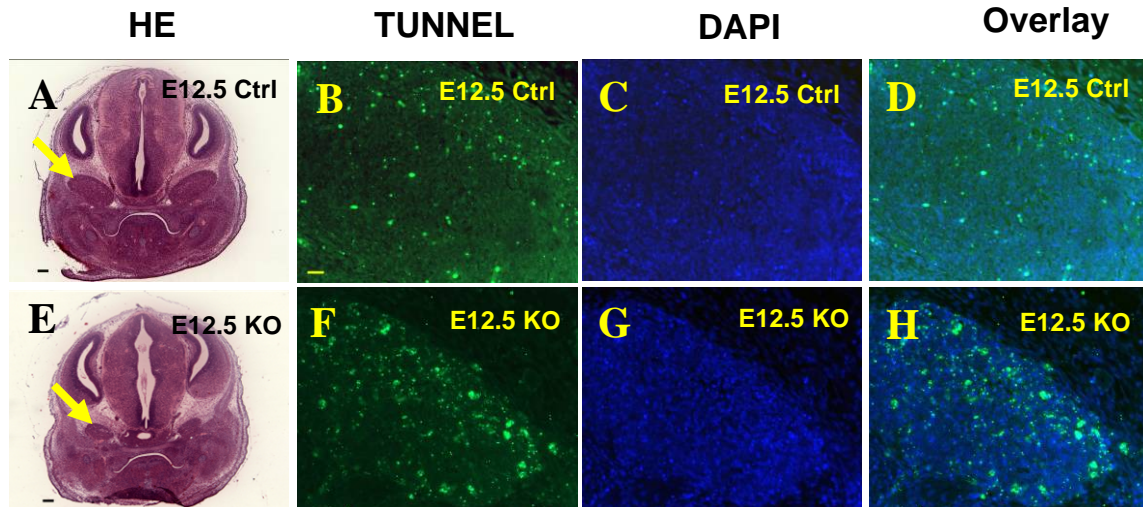
Fig. 5.12: Higher apoptotoic cells in KO TG. Neurodegeneration in peripheral ganglia e.g. trigeminal ganglion starts as early as at E12.5. In E12.5 KO (Fig.12E, arrow), its size is less than half of the control (Fig. 12A, arrow). Note TUNNEL positive apoptotic neurons are increased in E12.5 KO (Fig.12F, 12H) when compared to controls (Fig.12B, 12D). Scale bar 250µm (A, E), 50µm (B-D, F-H).

5.13: Expression of vti1a and vti1b in ganglia:

Above result showed that neurodegeneration in certian ganglia (e.g., TG, DRG) were more and for vestibular and cochlear ganglia it was minimum. We also looked into the possibility that whether vestibular and cochlear ganglia do not express vti1a and vti1b and therefore show low level of neurodegeneration. At E14.5, vti1a and vti1b immunohistochemistry in wild type mice (BL-6 and NMRI background) clearly showed that both proteins are expressed in vestibular as well as trigemnal ganglia (Fig. 5.13A-D). They are also expressed during E16.5 and E18.5 stages and other ganglia showed similar results (data not shown). We also checked vti1a and vti1b mRNA level in E18.5 wild type TG and vestibular ganglia. First heads were collected and cryoprotected and then TG and vestibular ganglia were disected by laser disection. Total mRNA were extracted from sections of ganglia. RT-PCR experiment showed that both vti1a and vti1b mRNAs were expressed in TG (Fig. 5.13F) and vestibular ganglia neurons (Fig. 5.13E).
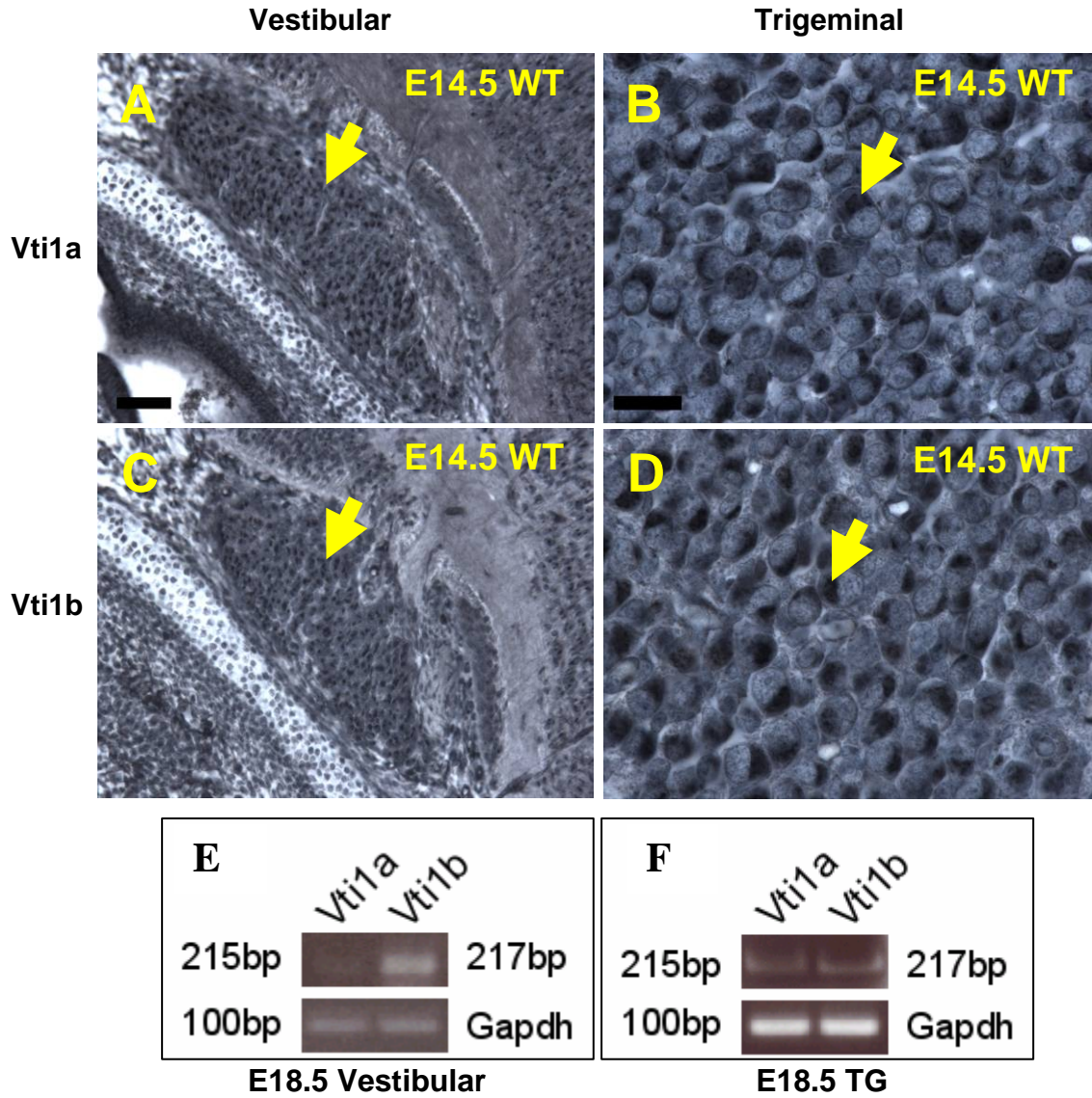
Fig: 5.13: Vti1a and vti1b mRNA and proteins are expressed in wildtype TG and vestibular ganglia. Both vti1a and vti1b proteins were expressed in neurons of E14.5 vestibular (A, C) and E14.5 trigeminal ganglia (B, D). Other ganglia also showed similar results (data not shown). Note vti1a and vti1b mRNA were also expressed (E, F) in vestibular and trigeminal ganglia (Scale car; 50μm (A, C), 20μm (B, D).

5.14: Loss of neuroendocrine cells in KO gut:

The neuroendocrine system is regarded as combination of both endocrine as well as nervous system. It acts like endocrine system using hormones as biochemical messengers or nervous system via electrical impulses, to regulate physiological events. Enterochromaffin (EC) cells or Kulchitsky cells are a type of neuroendocrine cell which are normally found in epithelial lining of the gastrointestinal tract. Neuro-endocrine cells or enterochromaffin cells in gut tissue were labelled with two different antibodies, one directed against chromogranin A+B, the other against neurofilament (rabbit polyclonal). Both antibodies showed that, at E18.5 the KO gut epithelium has clearly reduced number of neuroendocrine cells (Fig. 5.14B, 5.14D) as compared to controls (Fig. 5.14A and 5.14C) respectively.
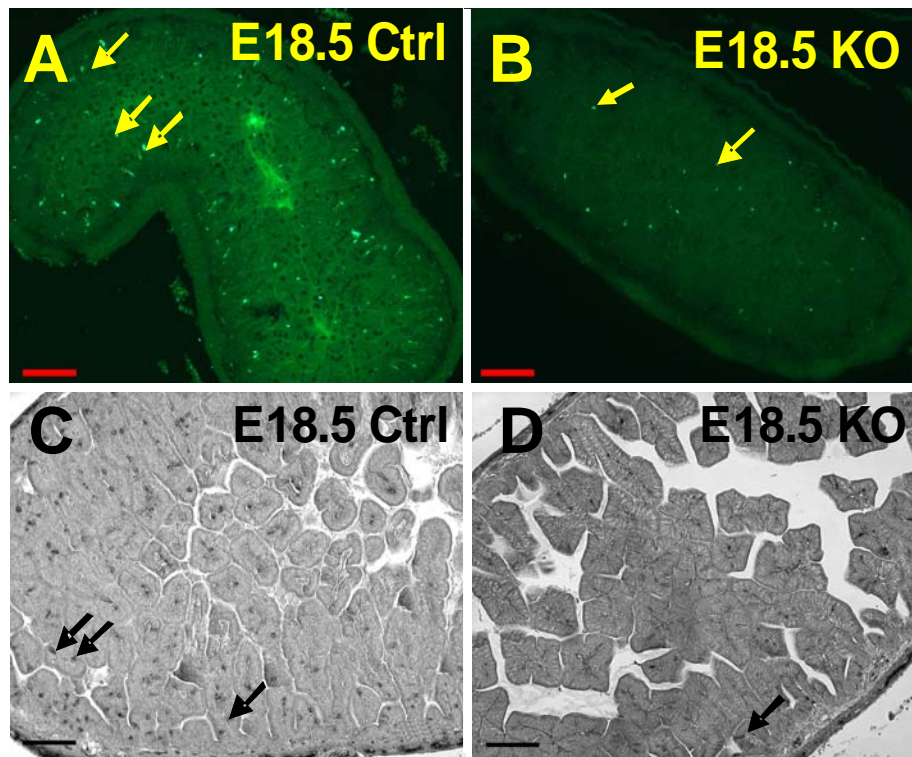
Fig. 5.14: Decreased neuroendocrine cells in KO gut epithelium. Neuroendocrine cells are decreased in E18.5 KO small intestine as seen by chromogranin A + B (B, arrow) and neurofilament (D, arrow) immunohistochemistry as compared to controls A and C respectively. Scale bar; 100 μm (A-D).

5.15: Loss of TH positive fibres in mandibular gland:

As shown earlier, there was 50% loss of superior cervical ganglia (SCG) cells in E18.5 KO. To determine whether the remaining neurons were able to reach their targets, we investigated mandibular gland, where sympathetic fibres can be labelled with anti tyrosine hydroxylase antibody. TH immunohistochemistry of E18.5 KO mandibular gland was unable to detect any fibres (Fig. 5.15D, 5.15F) whereas in control they can be seen normal density. (Fig. 5.15A, 5.15C).
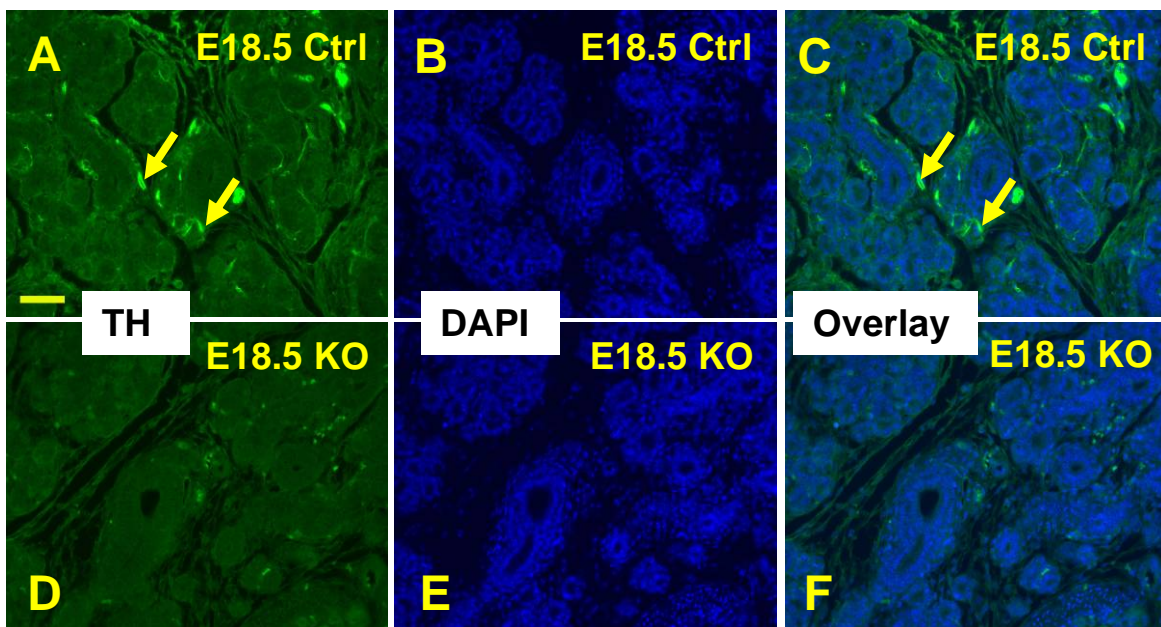

Fig. 5.15: Absence of TH immunoreactive fibers in KO mandibular gland. TH positive fibers are absent in E18.5 KO mandibular gland (D-F), which is a target organ for superior cervical ganglion (SCG). Note SCG has 50% reduction in number of neurons at E18.5 KO suggesting the fibers from SCG do not reach to the target organ and die before reaching to its target. Scale bar; 50µm (A-F)

5.16: Chromaffin cell phenotype:

Chromaffin cells are neuroendocrine cells which are normally found in adrenal medulla. They are neural crest derivatives, become innervated by preganglionic sympathetic axons and secrete epinephrine, norepinephrine, and enkephalin into the bloodstream. Chromaffin cells can be effectively labeled with anti-tyrosine kinase antibody. At E14.5, morphology as well as numbers of TH positive chromaffin cells did not differ among all four possible genotypes. (Fig.5.16A-D, graph 5.16K). At E16.5, total number of TH and PNMT immunolabeled chromaffin cells in double knockouts started to decrease (Fig. 5.16L, graph). E18.5 chromaffin cells could not be counted because cells were completely shrunken and there was not enough cytoplasmic staining around nucleus (Fig.5.16J) to identify individual cells.
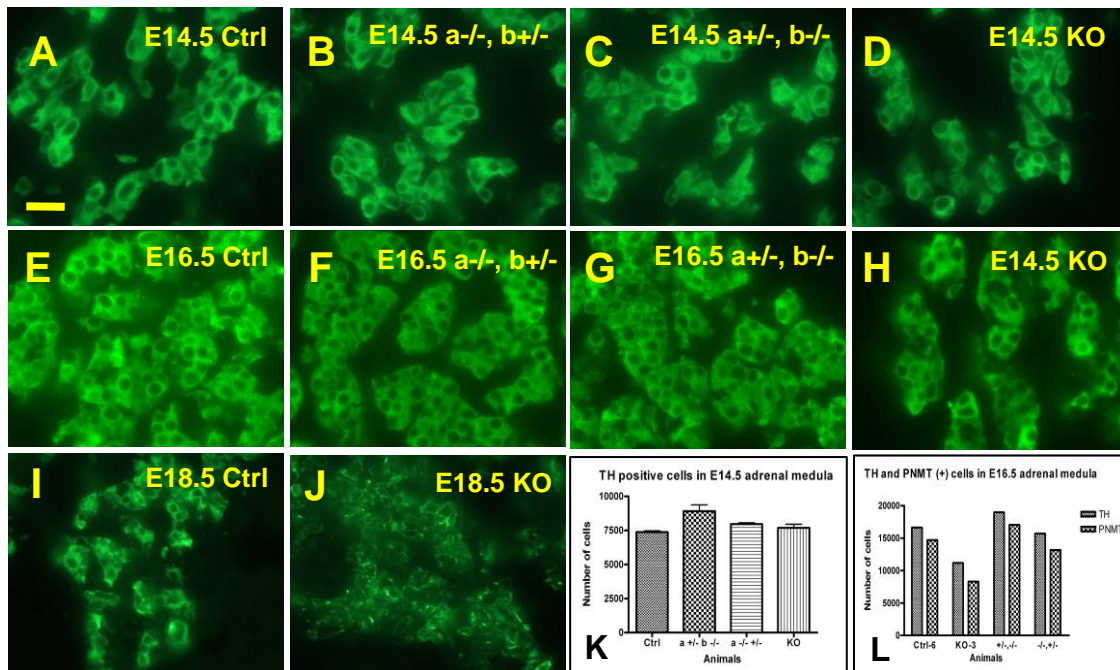
Fig. 5.16: Chromaffin cells are affected with increasing developmental period in KO mice. At E14.5, there was no marked difference in chromaffin cells structure (A-D) and numbers (Graph K) in all four genotypes at E14.5 where as the KO chromaffin cell numbers starts to decrease at E16.5 (Graph L) when counted after labelling with TH and PNMT antibodies. Structurally there was little difference in TH positive cells at E16.5 (E-H). In E18.5 KO, chromaffin cells could not be counted because cells were completely shrunken and there were very little cytoplasmic staining seen around nucleus (J) compared to control (I). Scale bar; 20μm (A-J).

5.17: Electron microscopy of chromaffin cells:

Chromaffin cells contain numerous dense core vesicles (DCVs) by which they are suitable model to study trafficking events such as vesicle exocytosis, endocytosis and/or recycling. Ultrastructurally chromaffin cells contain two distinct types of dense core vesicles, a smaller and a larger one [Grabner et al., 2005]. In this study, we counted total number of dense core vesicles regardless of subtypes in randomly selected sections at E16.5 and E18.5. In E16.5 KO, the total number of DCVs showed only 3.6% loss (Fig. 5.17B, graph 5.17E) whereas at E18.5 KO, the number of DCVs were reduced by 39.2% (Fig. 5.17D, graph 5.17F). On the other hand, the distribution of rough endoplasmic reticulum at E16.5 appears normal in both control and KO (Fig, 5.17A, 5.17B, yellow arrows) but in E18.5 KO, it was reduced by 39.5%. The extent of rough endoplasmic reticulum was measured using a stereological method (by drawing parallel horizontal lines at equal distances and superimposed over the picture. Then each time when rough endoplasmic reticulum crossed that parallel lines was counted and calculated in both controls and knockouts).
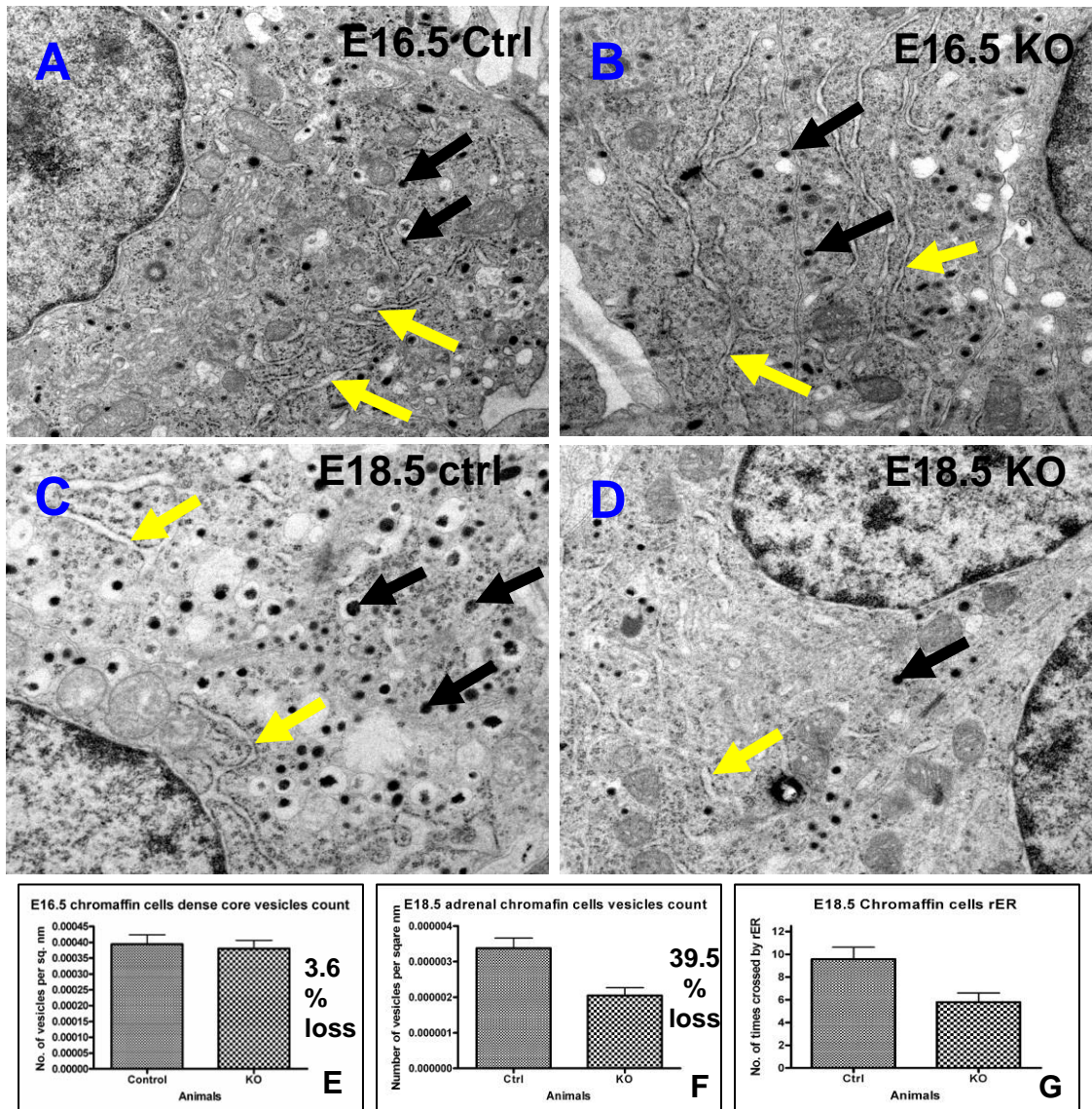
Fig. 5.17: Dense core vesicles are decreased in E18.5 KO chromaffin cells. Electron microscopy of E16.5 chromaffin cells shows a moderate loss of (3.6%) dense core vesicles in KO (black arrows in B) as compared controls (A, black arrows). At E18.5 dense core vesicles were reduced by almost half (D, black arrow) as compared to control (C, black arrows). Rough endoplasmic reticulum (rER) was similarly decreased in E18.5 KO chromaffin cells (D, yellow arrow) which were quantified by the number of crossings between rER and an over laid pattern of regular parallel lines.

5.18: Chromaffin cells at E12.5 trunk region:

The neural crest cells have diverse derivatives and play a classic role when studying molecular cues that underlie the determination of neural cell fate. Sympathoadrenal cells represent a major lineage of neural crest derivatives. Sympathoadrenal cells can give rise to diverse varieties of cells ranging from sympathetic neurons, chromaffin cells of the adrenal medulla, extra-adrenal chromaffin cells, and the intermediate small intensely fluorescent cells of sympathetic paraganglia [Anderson, 1993; Unsicker, 1993]. The sympathoadrenal lineage in the trunk region develops from neural crest cells that aggregate around the dorsal aorta to form the primary sympathetic anlagen [Le Douarin and Kalcheim, 1999]. In response to various signalling molecules like bone morphogenetic proteins (BMPs) produced by cells in the wall of the dorsal aorta [Reissmann et al., 1996; Schneider et al., 1999; Shah et al., 1996], the neural crest cells differentiate into catecholaminergic, tyrosine hydroxylase (TH)-positive neuronal sympathoadrenal progenitor cells.

Since we have 50% reduction in superior cervical ganglion cells and strong phenotype in adrenal chromaffin cells in E18.5 KO, we investigated whether the distribution of sympathoadrenal cells in trunk region was affected during early developmental period. We compared TH positive cells around aorta in both control and knockout at E12.5. There was no difference in TH positive cells between control and KO at rostral (adrenal medulla, Fig. 5.18A, 5.18B) and caudal levels around the aorta (Fig. 5.18C, 5.18D) suggesting that there no was difference in sympathoadrenal lineage differentiation and migration.
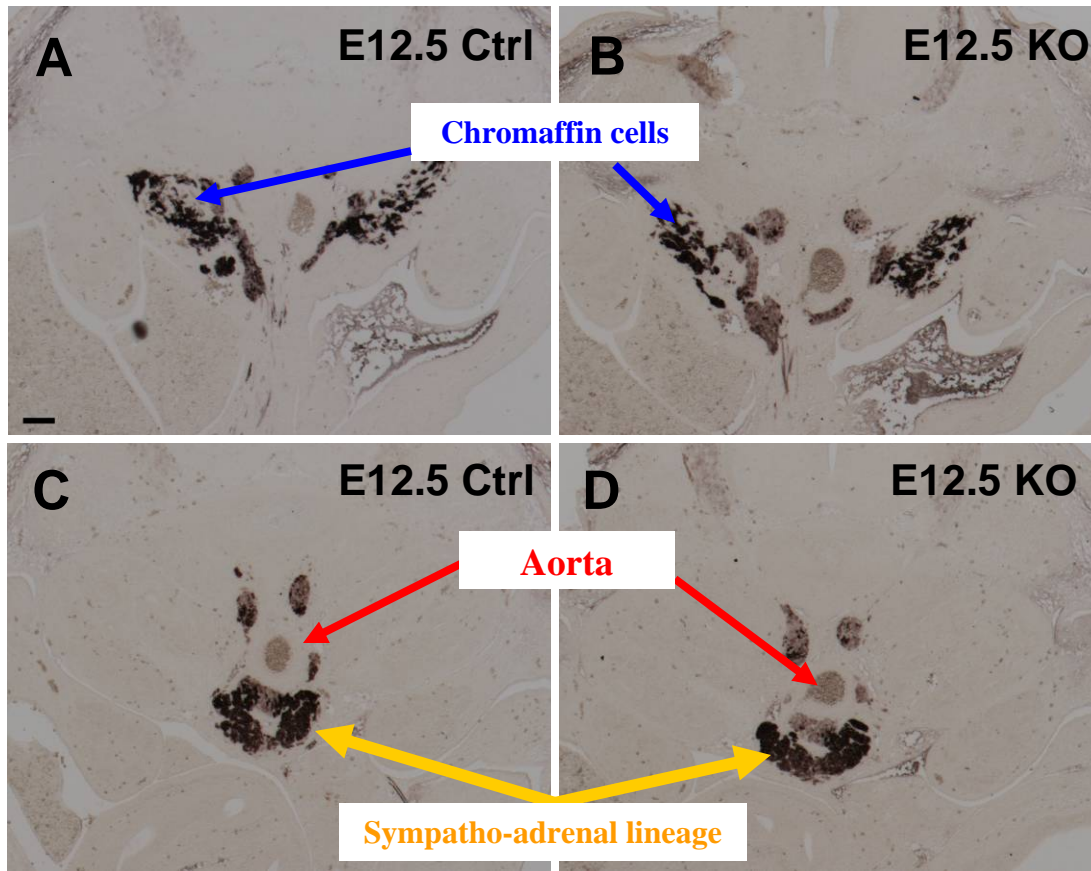
Fig. 5.18: Normal sympathoadrenal lineage in control and KO at E12.5 mice. TH immunohistochemistry at E12.5 showed that chromaffin cells in adrenal medulla seem normal in both control and KO (Fig. A, B). Chromaffin cells are derived from neural crest cells. Caudal to adrenal gland, around aorta (C, D, black arrows), from where they starts to migrate, neural crest derived sympathoadrenal precursor cells showed similar pattern (C, D, yellow arrows). This suggests that migration and early differentiation of chromaffin cells are not impaired in KO. Scale bar; 200µm (A-D)

5.19: Expression of vti1a and vti1b in chromaffin cells:

Both vti1a and vti1b proteins were expressed in all cortical and meduallary cell types of adrenal gland in pure wild type tissue (BL-6 as well as NMRI background). Double immuno labelling, using mouse anti-TH antibody for chromaffin cells and rabbit polyclonal antibodies against vti1a and vti1b for the two proteins, were applied to show expressions of the vti1a and vti1b in chromaffin cells. At E16.5, both proteins show normal expression (Fig. 5.19 A-F). They are also expressed at earlier stages (E14.5 data not shown). The normal endogenous expression of vti1a/1b protein in all developmental stages and strong phenotype at E18.5 KO chromaffin cells suggest that vti1a/1b related endosomal function might be crucial for their survival.
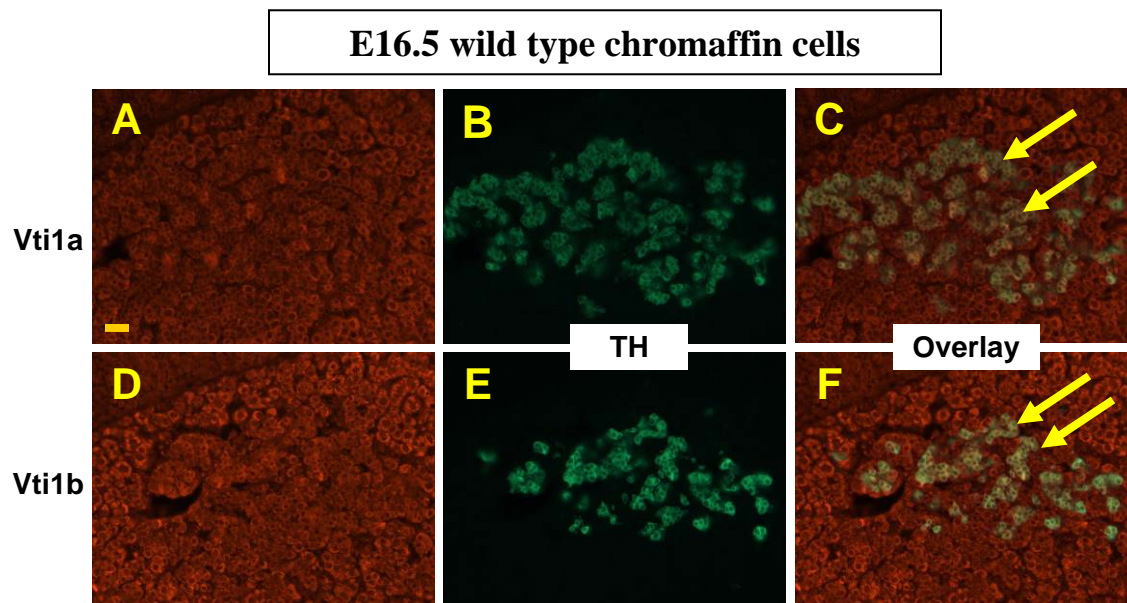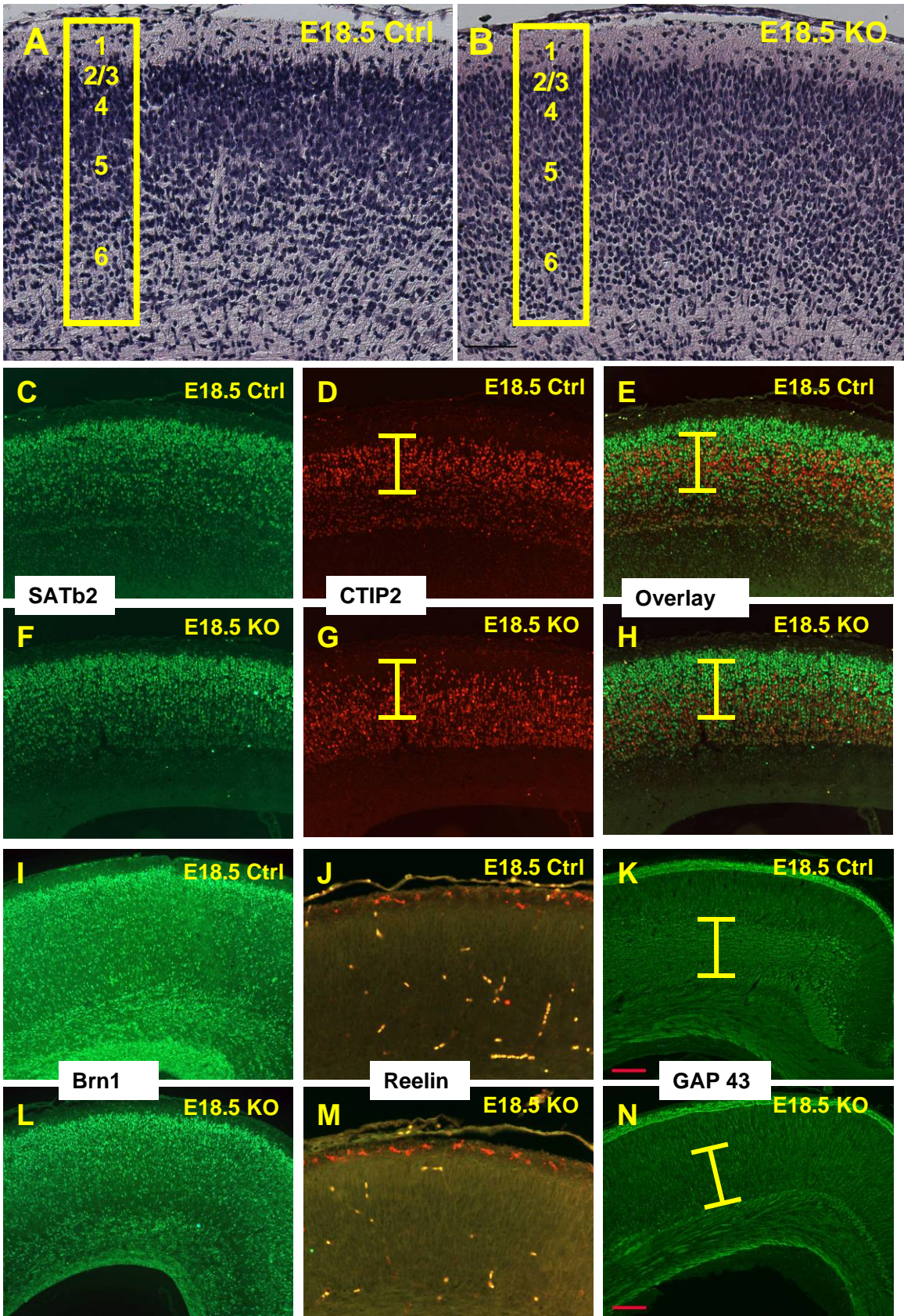

Fig. 5.19: Both vti1a and vti1b are expressed in control and KO chromaffin cells. Double immunolabeling, using TH (green)/vti1a (red) or TH (green)/vti1b (red) antibodies, showed that both vti1a and vti1b were expressed in E16.5 wild type chromaffin cells. Scale bar; 50μm (A-F).
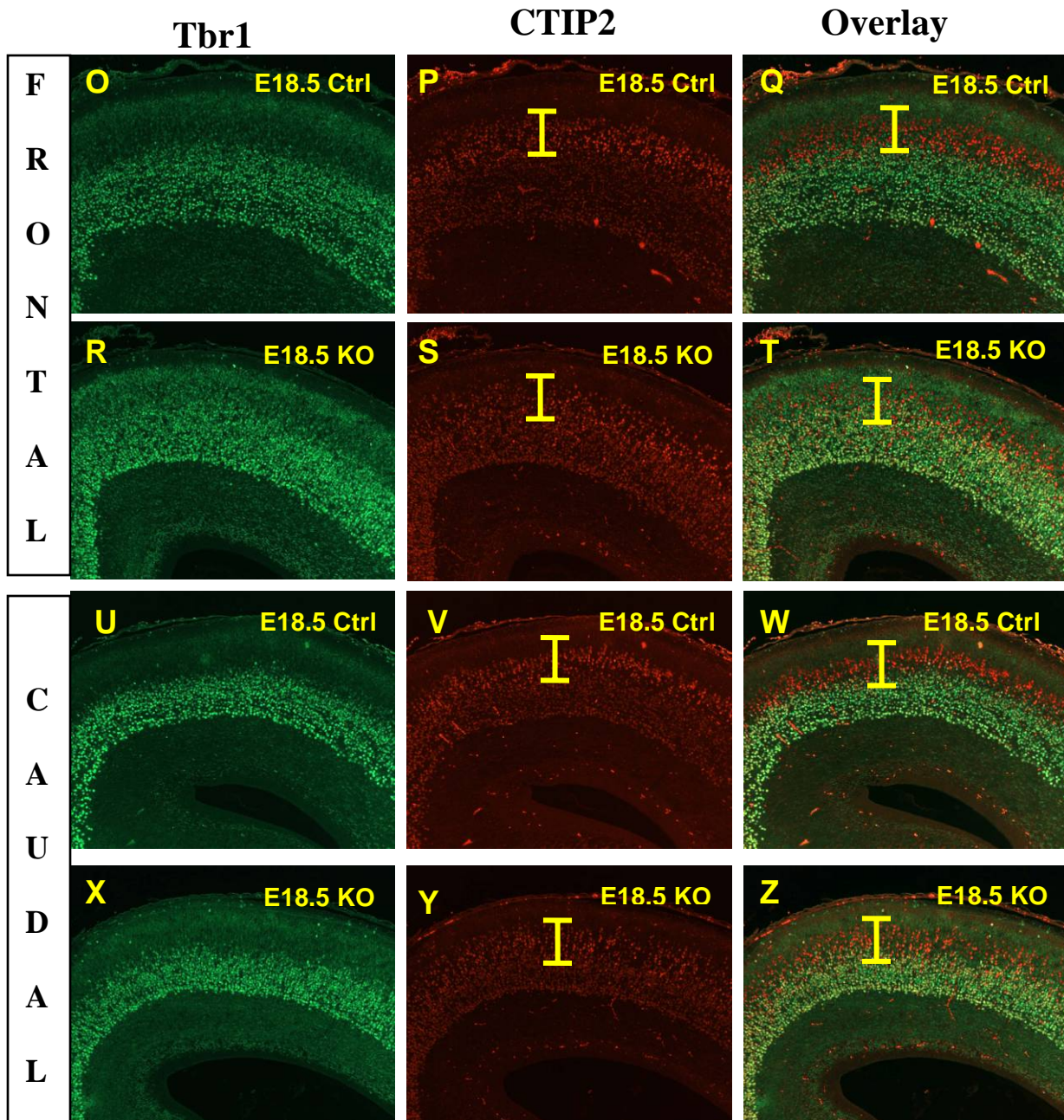
5.20: Cortical phenotype:

A dramatic phenotype was seen in the layering pattern of cerebral cortex. Haematoxylin and Eosin stained E18.5 cortex showed higher of neurons in deep layers of cortex. Since neocortex contains six distinct layers counted from superficial (upper) to deep (lower), different layer specific markers were used to label different layers of cortex. SATb2 which labels upper layers neurons [Britanova et al., 2005] showed in E18.5 control and knockout (Fig. 5.20 C-H) similar expression pattern suggesting there is no difference in upper layer neuronal fate. This was confirmed with Brn1, another upper layer marker [Sugitani et al., 2002] (Fig. 5.20I, 5.20L).

Since reelin is an important molecule which can affect the whole layering pattern if disturbed. When using antibody against reelin to label layer one neurons, no obvious change in its expression between control and knockout (Fig. 5.20J, 5.20M) was seen. On the other hand growth associated protein-43 (GAP-43) which is located in axonal growth cones and newly formed axons was dramatically reduced in KO (Fig. 5.20N) as compared to control (Fig 5.20K). Tbr1 antibody which labels layer 6 cells showed a higher number of neurons in E18.5 KO (Fig. E5.20R, 5.20T, 5.20X, 5.20Z) as compared to controls (Fig. 5.20O, 5.20Q, 5.20U, 5.20W). An antibody against chicken ovalbumin upstream promoter transcription factor-interacting protein 2 (CTIP2), also known as Bcl11b was used to label layer 5 neurons [Arlotta et al., 2005]. This antibody labels predominantly layer 5 (bright red cells) and also a small portion of layer 6 (dim red). The band of brihgt red cells was missing in E18.5 KO (Fig. 5.20G, 5.20H in sagggittal view and 5.20S, 5.20T in coronal view) as compared to control animals (Fig. 5.20D, 5.20E, saggittal view) and (Fig. 5.20P, 5.20Q coronal view). This phenotye was most prominant in frontal cortex. Note that a small band of cells can be detected in KO (Fig. 5.20Y, 5.20Z), however, it was clearly less prominant than in corresponding controls (Fig. 5.20V, 5.20W).

A — E18.5 Ctrl: 1, 2/3, 4, 5, 6

B — E18.5 KO: 1, 2/3, 4, 5, 6

C — E18.5 Ctrl — SATb2

D — E18.5 Ctrl — CTIP2

E — E18.5 Ctrl — Overlay

F — E18.5 KO

G — E18.5 KO

H — E18.5 KO

I — E18.5 Ctrl — Brn1

J — E18.5 Ctrl — Reelin

K — E18.5 Ctrl — GAP 43

L — E18.5 KO

M — E18.5 KO

N — E18.5 KO

Fig. 5.20: Deep layer neurons are affected in E18.5 KO cortex. E18.5 HE stained cortex shows more neurons in deep layer (B) as compared to control (A). Layer specific markers were used to label the different layer of cortex. There was no obvious change in upper layers in both control (C) and KO (F) as labelled by SATb2 (C, F, E, H) and Brn1 (I, L). Layer 5 was completely absent from frontal sections in KO (G, H, S, T) as labelled by CTIP2. In caudal sections however, there was small band of layer 5 in KO (Y, Z) which was still smaller than corresponding control (V, W). On the other hand, layer 6 showed more dense number of neurons in KO (R, T, X, Z) when compared to controls (O, Q, U, W) as shown by Tbr1 immunohistochemistry. Reelin stained cells in Layer 1 showed no obvious difference between KO (M) and control (J). GAP-43 positive axons were almost absent in KO cortex (N) as compared to control (K). Scale bar; 50µm (A, B, J, M) and 100 µm (C-I, K, L, N-Z).

5.20.1: Radial glia cells in knockout mice:

Radial glia cells are important cell type of the developing central nervous system. It has a role in several key developmental processes, ranging from patterning and neuronal migration to neurogenesis [Weissman et al., 2003]. Their processes extend from ventricular zone (VZ) to the pial surface and act as scaffold for migrating neurons. Two antibodies nestin and brain lipid binding protein (Blbp) were used to label radial glia cells during development. There was no difference in nestin immunoreactive radial glia cells between control (Fig. 5.21A, insert) and KO (Fig. 5.21B, insert) at E14.5 but density of radial glia cells seemed slightly reduced in E18.5 KO (Fig. 5.21D, 5.22E, also in insert) as compared to controls (Fig. 5.21C, 5.22B). Blbp staining at E18.5 however showed difference in its localization pattern but not density. There was unusual "honey comb" like appearance in E18.5 (Fig. 5.22D, also in insert) when compared to control which showed tubular or longitudinal pattern (Fig. 5.22A).
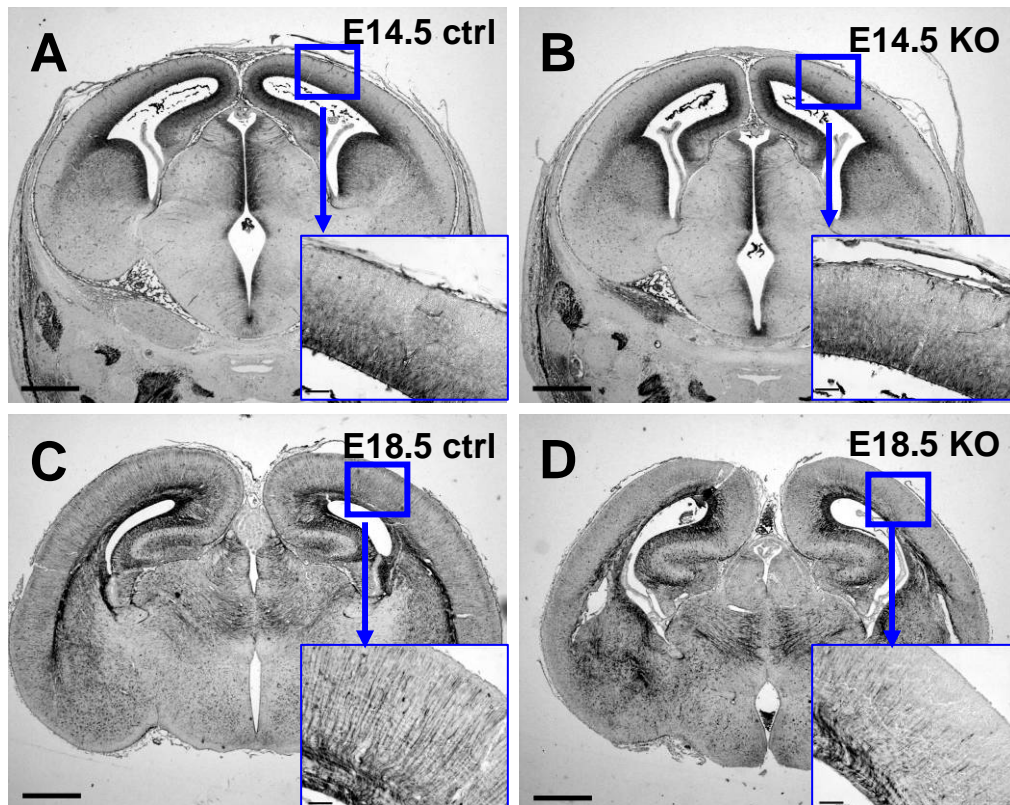
Fig: 5.21: Nestin positive radial glia cells are reduced in E18.5 KO cortex. Nestin immunoreactive radial glia cells were normal in between control (A, blue boxed insert) and KO (B, blue boxed insert) at E14.5, but were reduced in E18.5 KO (D, blue boxed insert) as compared to control (C, blue boxed insert). Scale bar; 250μm (A, D).
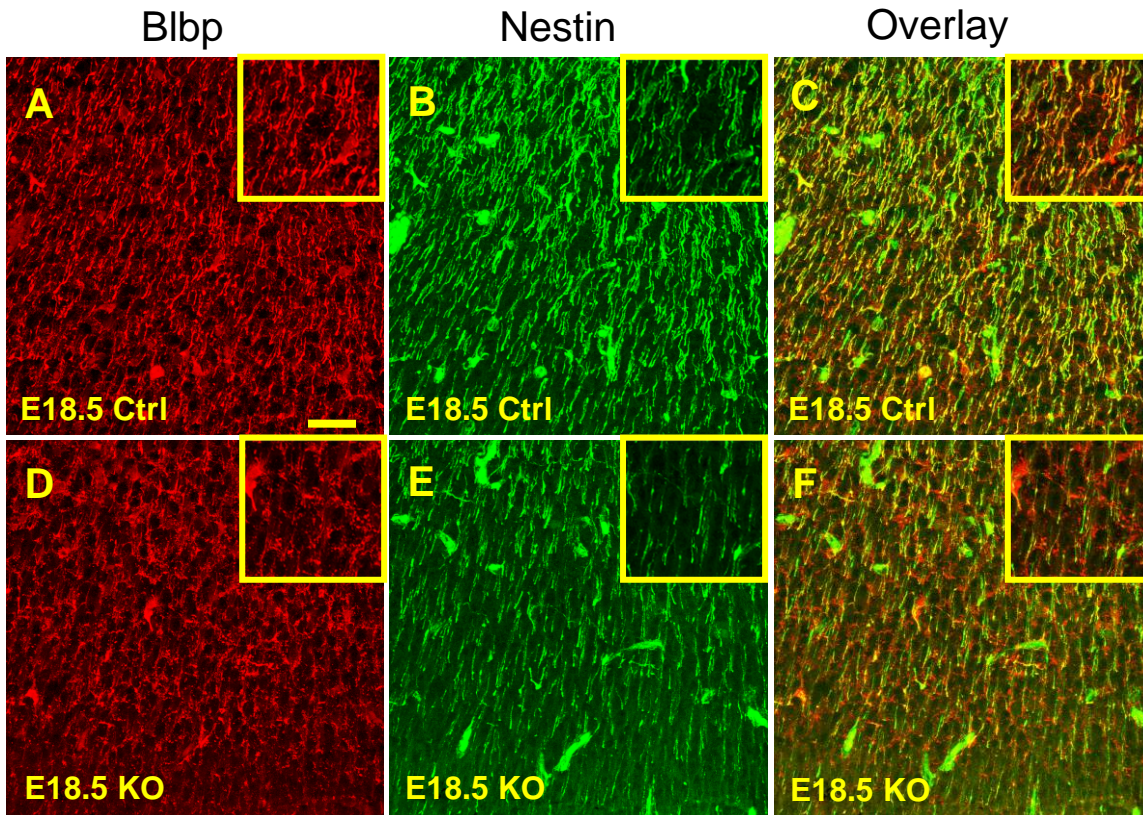
Fig. 5.22: Altered morphology of Blbp positive radial glia cells in KO cortex. Radial glial cells were labelled by brain lipid binding protein (Blbp) or nestin antibodies. Blbp staining pattern was different in KO in frontal section showing honey comb like appearance (D, also seen in higher magnification, yellow insert) which was completely different from corresponding control showing a rod like pattern (A, also seen in higher magnification, yellow insert). On the other hand, nestin labelling did not show difference in staining pattern in both control and KO (B, E) but the density of nestin positive fibers was reduced in KO (E, also in yellow insert). Scale bar; 20μm (A-F).

5.20.2: Depletion of progenitor cells in KO cortex:

The adult cortex contains six layer neurons which are born during developmental period from E11 to E17. These neurons are generated by progenitor cells that occupy the ventricular zone of the developing cerebral wall. Progenitor cells can be labelled by antibody against proliferating cell nuclear antigen (PCNA). PCNA immunoreactive cells at E14.5 did not show difference between controls (Fig. 5.23A) and KO (Fig. 5.23B) where as their numbers were clearly reduced in E18.5 (Fig. 5.23D, blue boxed insert) as compared to control (Fig. 5.23C, blue boxed insert). This suggests that progenitor cells in KO cortex are depleted from early to late developmental period.
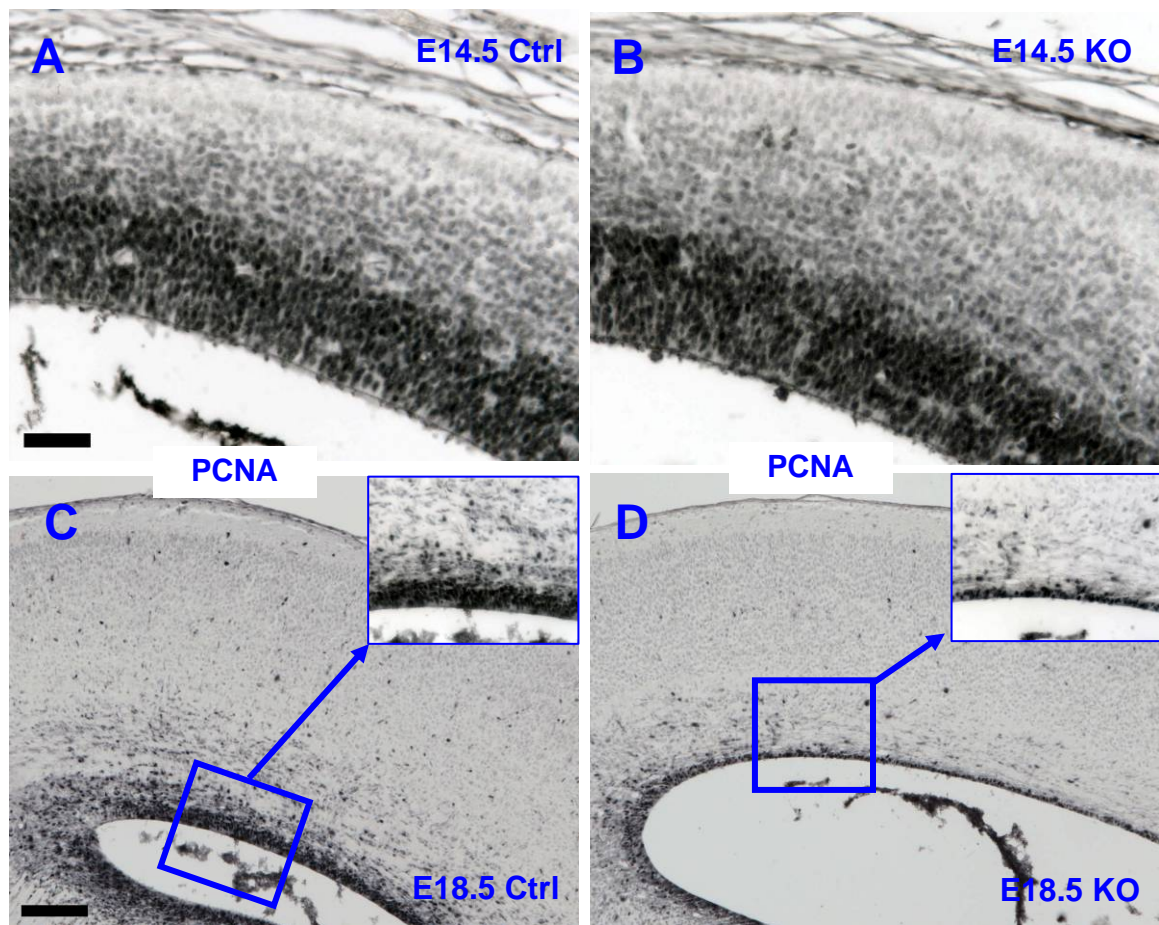
Fig. 5.23: Progenitor cells are decreased in E18.5 KO cortex. PCNA positive neural progenitor cells were normal between control (A) and KO (B) at E14.5 but were reduced in E18.5 KO (D, also in blue boxes) as compared to control (C, also in blue boxes). Scale bar; 50μm (A, B), 100μm (C, D).

5.20.3: LAMP-1 staining in E18.5 forebrain:

Lysosomal associated membrane protein-1 (LAMP-1) is localized in lysosomal membrane and late endosome. Antibody against LAMP-1 was used to find above-average labelled LAMP-1 positive neurons. A higher number of LAMP-1 immunoreactive neurons in KO were seen especially in thalamus (Fig. 5.24G), dorsal cortex (Fig. 5.24F) and lateral part of cortex (Fig. 5.24H) close to the huge gap (Fig. 5.24E, yellow box). The corresponding controls were Fig. 5.24C, 5.24B and 5.24D respectively.
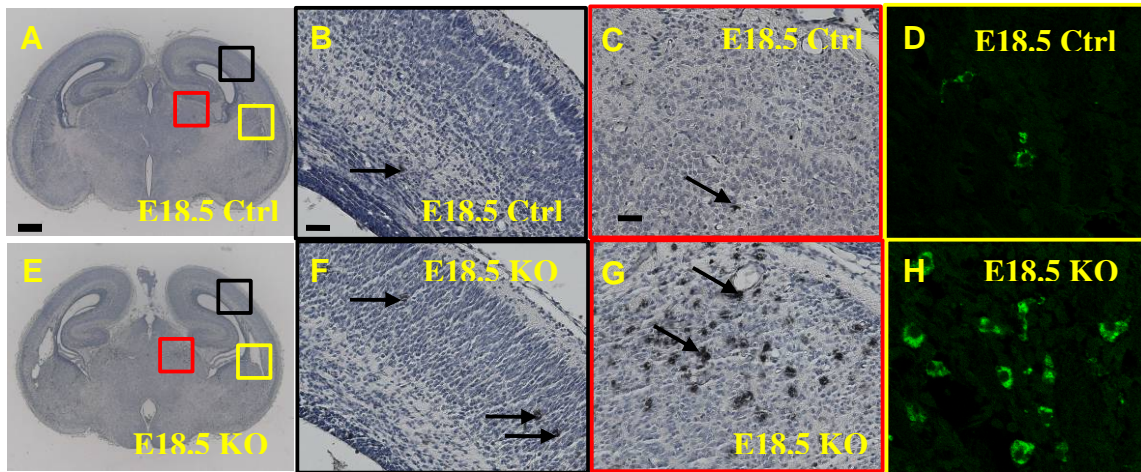
Fig. 5.24: LAMP-1 positive cells are increased in KO forebrain. More strongly LAMP-1 positive cells (arrows) were observed in KO cortex (F, arrows), thalamus (G, arrows) and at the pallial-subpallial border (H); approximate position outlined by black, red and yellow boxes in E; corresponding controls in B, C, D, A. The gap seen in the yellow box of E was a constant feature of the KO pallial-subpallial border. LAMP-2, another lysosomal marker also showed same result (data not shown). Scale bar; 250µm (A, E), 50 µm (B, C, F, G).

5.20.4: Reduced synaptophysin expression in KO forebrain:

Synaptophysin is an apparently much conserved protein of small synaptic vesicles. It can be found in all synapses of the central and peripheral nervous system [Navone et al., 1986; Wiedenmann and Franke, 1985]. Similarly synapsin I, an integral protein of synaptic vesicles is the collective name for two splice variants, synapsin Ia and Ib [Sudhof et al., 1989]. Antibody against synaptophysin and synapsin were used to label these proteins in different parts of the brain tissue. Synaptophysin staining at E18.5 KO cortex (Fig. 5.25B), entorhinal cortex (Fig. 5.25D), hippocampal proper (Fig. 5.25F) and habenulla (Fig. 5.25H) showed substantially less expression than controls (Fig. 5.25A, C, E, and G). Synapsin labelling confirmed this difference (data not shown).
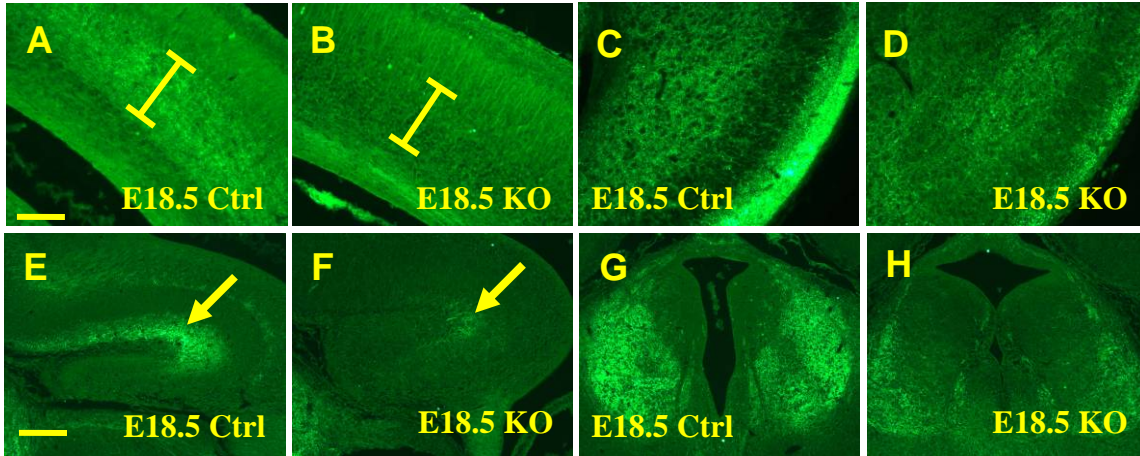
Fig. 5.25: Synaptophysin expression was decreased in KO forebrain. E18.5 KO showed complete loss of synaptophysin expression in cortex (B), reduced level of expression in entorhinal cortex (D), hippocampus (F) and habenulla (H). Respective controls shown in A, C, E and G. Scale bar; 50µm in A-D and 100µm in E-H.

5.20.5: Early appearance in GFAP positive cells in E18.5 KO mice:

Glial fibrilary acidic protein (GFAP) is an intermediate filament (IF) protein that is found in glial cells such as astrocytes. First described in 1971, GFAP is a type III intermediate filament protein that maps, in humans, to 17q21. Like the other IF-protein family members vimentin, desmin and peripherin, it is involved in structure and function of the cell's cytoskeleton. GFAP helps to maintain astrocyte mechanical strength, as well as the shape of cells [Fuchs and Weber, 1994]. GFAP is expressed in the central nervous system in astroglial cells. In general, glial cells start to appear either on late embryonic or early postnatal developmental period. At E18.5, there were more GFAP immunoreactive cells in KO entorhinal cortex (Fig. 5.26B) than control (Fig. 5.26A) whereas in other regions, like in hippocampus, there was no change. (Fig. 5.26 C, D). This suggests that glial cells are generated earlier in KO entorhinal cortex as compared to control.
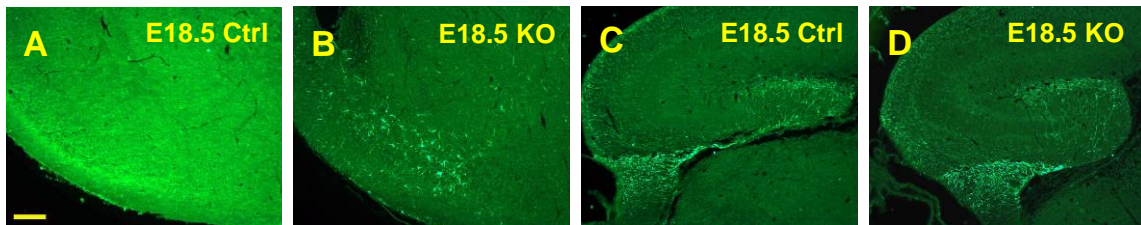
Fig. 5.26: GFAP positive cells are generated earlier in KO entorhinal cortex. More GFAP positive cells are seen in entorhinal cortex of E18.5 KO (B) as compared to control (A) whereas hippocampus showed similar staining pattern in control and KO (C, D). This suggests that astroglial cells in KO entorhinal cortex have been prematurely generated from radial glial cells. Scale bar; 100 μm (A-D)

Table 5.3: Summary of results:

Phenotype	Structure affected	Remarks (in KO)
Cortex	Cortex	Layer 5 neurons are absent, layer 6 is expanded, Early loss of progenitor cells at ventricular zone, Radial glia morphology slightly differed, GAP-43 staining is clearly reduced. Lamp-1 (+) cells are increased, Synaptophysin expression are absent, GFAP (+) cells are increased in entorhinal cortex
Tracts affected	Anterior commisure	Absent
	Corpus callosum	Thin in the middle, anteroposterior length is reduced
	Hippocampal commisure	Absent
	Thalamocortical axons	Cannot cross to PSPB border and stop within internal capsule region
	Corticothalamic axons	Only few corticothalamic axons can reach to thalamus
	Corticospinal tract	Absent
	Pyramidal tract	Absent
	Spinotrigeminal tract	Absent
	Tracts of Lissauer	Absent
	Nigrostriatal tract	Cannot reach striatum, slightly diverted dorsally at thalamostriatal border
	Mammilothaamic tract	Absent
	Optic Tract & Optic chiasma	Slightly thin
	At Striatum	Fibers are absent in medial side and few unusual fibers are found on lateral side
Neuro-degeneration	TG, DRG, Geniculate, Nodose-petrosal	Severely degenerated (about 98%), more TUNNEL positive cells in E12.5 TG
	SCG, Motor at L2	Moderately degenerated (50-60%)
	Vestibular, Cochlear	Least affected (14-26%)
Dopaminergic neurons	VTA and SN neurons	52% degeneration with loss of neurites. EM picture shows numerous dead cells at SN region.
	Locus Coeruleus	34% degeneration
Serotonergic neurons	Dorsal raphe	Loss of neurites
Others	Cerebrum	Gap in either side of cerebrum at external capsule region
	Mandibular gland	TH positive fibers are absent in mandibular gland
	Ventricles	Enlarged

	Pontine nuclei	Absent
	Gut	Neurofilament or Chromogranin A+B positive neuroendocrine cells are decreased
	Adrenal Chromaffin cells	Dense core vesicles are reduced, morphology of cells is greatly impaired and sympathoadrenal lineage around dorsal aorta is barely affected.
	Hippocampus	Dentate gyrus is enlarged, Absence of neurofilament positive fibers at hippocampus proper, Synaptophysin expression are reduced (see also tracts affected)

6: Discussion:

Vti1a and vti1b belong to the SNARE family of proteins thought to be involved in early and late endosome fusion. The fact that gene ablation of single genes did not lead to obvious phenotypes was interpreted as functional compensation of one for the other. Along this line mice lacking both vti1a as well as vti1b suffer from a broad range of developmental defects – summarized in Table 5.3 – leading to perinatal lethality.

Discussing the role of SNARE proteins involved in early and late endosome fusion affected cellular events may include

- lack of membrane reorganization leading to a asymmetric distribution of proteins required for asymmetric cell division, or more general leading to impaired axon growth or cell migration
- lack of sensing guidance cues due to ineffective retrograde signaling from the growth cone leading to impaired axon guidance
- lack of retrograde neurotrophic signaling leading to impaired neuronal survival and neuron degeneration.

These events may be apparent during neurogenesis, neuronal differentiation and target innervations and will be discussed in the context of development and degeneration of the peripheral nervous system, cortex development and impaired fiber projections.

6.1: Neurodegeneration in peripheral ganglia:

Vti1a/1b KO shows various degrees of neurodegeneration at peripheral ganglia. Ganglia like trigeminal, dorsal root ganglion, nodose-petrosal and geniculate are severely affected showing almost 98% reductions in number when seen at E18.5. Superior cervical ganglia, motor neurons at spinal cord show almost 50% reductions whereas vestibular and cochlear ganglia show 15-25% reduction (Fig. 5.11, Table 5.1 and 5.2). The reason why some ganglia show high degree of neurodegeneration and some little was really surprising. This could probably be explained by their neurotrophin dependency and modes of signal propagation from axon terminal towards cell body. Peripheral ganglia neurons differ from that of neurons at central nervous system in many ways. They do not

have similar extracellular matrix environment like in central nervous system and are almost completely dependent on survival factors coming from their target. During development of peripheral ganglia, neurons are generated and approximately 50% neurons who can make connection with target organ can survive and others will die. According to neurotrophic factor hypothesis, those surviving neurons require target-derived soluble factors for their survival and neurotrophins account the central factors among them [Ernfors et al., 1995; Yuen et al., 1996]. Among neurotrophins, most sensory neurons depend on NGF for their survival, or in case of trigeminal ganglion, they switch from BDNF- to NGF-dependency from early to late embryonic period [Huang et al., 1999]. Similarly, 70-80% of DRG neurons require NGF for their survival during development [Silos-Santiago et al., 1995]. On the other hand, vestibular ganglia neurons are exclusively dependent on BDNF and cochlear ganglia neurons are dependent upon NT3 [Ernfors et al., 1995]. Various mechanisms have been proposed on how neurotrophins bind with their receptors and propagate its signal transduction from axonal terminal to cell body. Wave propagation model, retrograde effecter model and signalling endosome model [Bronfman et al., 2007] have been proposed. Among them, signalling endosome model has gained a lot attention. For example using compartmentalized cultures of sympathetic and sensory neurons, studies have shown that both kinase activity and internalization of Trks are required for retrogradely transmitted nuclear responses [Heerssen et al., 2004; Riccio et al., 1997; Watson et al., 2001]. This internalization process occurs via early endosome and signalling endosome [Grimes et al., 1997; Grimes et al., 1996]. Moreover, it has recently been shown that endocytosis of growth factor receptors is important for their signalling because growth factors continue to signal from endosomes [Bronfman et al., 2007]. Apart from clathrin-coated vesicles and early endosomes, late endosomes containing internalized tracers were shown to localize to the cell body. These authors also found that MVBs predominantly mediate the retrograde axonal transport of endocytosed markers between nerve terminals and the neuronal cell body. In DRG, when NGF binds to its receptor TrkA, it is internalized and travels via signalling endosomes with the characteristics of early endosomes from target region to cell bodies [Delcroix et al., 2003]. Overall data illustrates that NGF-TrkA internalization is a well portrayed step involving early or late endosomes, it is likely that most sensory

neurons which depend on NGF die in Vti1a/1b KO suggesting endosomal pathway are important for their survival. On the other hand, BDNF and NT3 dependent neurons are less affected possibly because they do not require an endosomal fusion step. Instead, after binding to their corresponding receptors activate other survival signalling pathways e.g. PI3-Akt kinase or MAPK/ERK.

However, it should be mentioned that degeneration of peripheral neurons observed in the vti1a/1b double knockout starts prior to the known periods on ontogenetic cell death, and second the extent of cell death does not correlate with that described for distinct neurotrophic factors. This raised the question of whether earlier events in neuron development like proceeding neurotrophic support prior to target innervation or possibly impaired axon growth along with the inability to reach the target may actually account for their degeneration. This hypothesis would group the ganglia of the peripheral nervous system as neurons with short axons (cochlear ganglia) that may be not affected and long axons (sensory neurons of the TG or DRG) that may be much more affected.

We also tested the hypothesis whether lack of neurodegeneration at different ganglia (vestibular, cochlear) could simply be due to the absence of endogenous vti1a and vti1b. For that we tested expression of vti1a and vti1b at protein and mRNA level. Laser dissection of trigeminal and vestibular ganglia and RT-PCR experiment at E18.5 wild type showed that both TG and vestibular ganglia express mRNA expression of vti1a and vti1b (Fig. 5.13E, 5.13F). Immunohistochemistry using antibodies against vti1a and vti1b showed that they are present in all analyzed ganglia as early as E14.5 (Fig. 5.13A-D) suggesting that changes in neurodegeneration pattern were not due to its endogenous expression level.

6.2: Development of cortex:

The mammalian neocortex is a highly specialized structure which consists of a large variety of neurons. These neurons are organized into 6 layers from superficial to deep regions of the cortex and are arranged roughly parallel to the cortical surface. During restricted period of neurogenesis which in mice ranges between E11.5 to E17.5 (Fig. 6) [Angevine and Sidman, 1961; Caviness and Takahashi, 1995]. These neurons are generated by progenitor cells that occupy the ventricular zone (innermost layer) of the developing cerebral wall (telencephalic neuroepithelium). The earliest born neurons appear around E10.5 in the mouse and form layered structure called the preplate. Preplate is a layer of differentiated neurons superficial to the proliferative cells of ventricular zone and later splits into the more superficial marginal zone and the subplate. The cortical plate starts to develop in between these two zones [Bayer and Altman, 1991]. The cortical plate grows in an "inside-out" order, from layer 6 containing the earliest-born cortical plate neurons, to layer 2 comprising the latest-born neurons [Angevine and Sidman, 1961; Caviness, 1982].
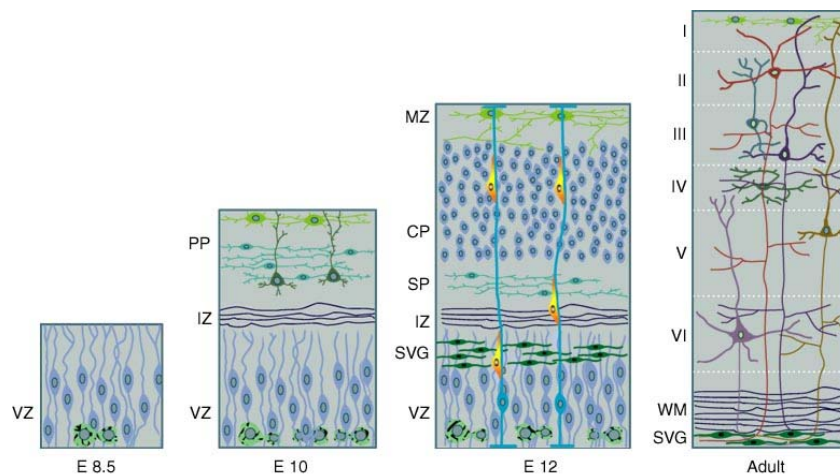
Fig. 6: Development of cortical layers in mice. At first ventricular zone gives rise to neural progenitor cells. After number of cell division, cortex form preplate. As neurogenesis starts after E10.5 post mitotic neurons migrate and forms cortical plate splitting preplate into marginal zone and subplate. Cortical plate is further expanded by continuous production of neurons and all six layers are formed by E17 establishing the foundation for adult structure by inside out growth pattern.

In vti1a/1b KO mice, HE stained E18.5 cortex showed more number of neurons in deep layers. Tbr1 immunolabeling, which labels the layer 6 neurons showed increase in numbers of neurons (Fig. 5.20R) as compared to controls (Fig. 5.20O). Surprisingly CTIP2, a marker for layer 5 neurons, showed complete absence in most parts of KO cortex (Fig. 5.20G, 5.20S). This phenotype was less apparent in caudal portion of the cortex where a small band of CTIP2 positive cells were seen in KO (Fig. 5.20Y). Nevertheless, it was still less conspicuous than corresponding control (Fig. 5.20V). On the other hand, no apparent difference was seen in upper layers as shown by two layer specific antibodies SAT b2 (Fig. 5.20C, 5.20F) and Brn1 (Fig. 5.20I, 5.20L).

To address a question why there is an alteration in layering pattern in KO cortex, we looked into Cajal Retzius cell in layer one. Cajal-Retzius cells express reelin and in reelin homozygous (reeler) mice, cortical neurons are oriented obliquely and layering pattern is almost inverted [Jossin et al., 2003]. Reelin antibody staining in vti1a/1b KO cortex showed no obvious changes in between controls and knockouts (Fig. 5.20J, 5.20M). Although, the distribution pattern of reelin positive cells were slightly different between control and KOs, there was no obvious difference in increase or decrease of whole layer thickness as reported in reeler mice. This suggests that changes in deep layer of neurons in vti1a/1b KO mice were not due to defective reelin signaling.

We also looked into radial glia cells morphology whose role in neuron production and migration has been well reported [Weissman et al., 2003]. Blbp stained radial glia cells in E18.5 KO mice cortex showed an unusual honey comb like appearance (Fig. 5.22D) which was completely different architecture than normal longitudinal appearance in control mice (Fig. 5.22A). This difference in KO could be due to abnormal distribution of Blbp with in a single cell, probably a potential role of trafficking protein vti1a/1b. This honey comb phenotype was prominent in frontal cortex and there was no apparent difference in caudal part of cortex (data not shown). In contrast, Nestin labeled radial glia showed no difference in morphology but density of radial glia cells seem reduced (Fig. 5.22B, 5.22E). However, the differences in expression pattern of two radial glia markers were not surprising because previous report have also shown similar results. In reeler mice cortex, RC2 immunolabeled radial glia showed no difference in its expression but

Blbp staining was reduced compared to control [Hartfuss et al., 2003]. Based on the known role of radial glia, we might expect some changes in migration pattern in vti1a/1b knockout mice. However this possibility seems less likely because only early born deep layers were affected in vti1a/1b KO cortex but not in late born upper layers. If migration could have played important role, we would also expect changes in upper layer but this was not the case in our KO mice. Moreover migration experiment can be confirmed by injecting BrDU at certain time (e.g. E12, E13, E14) and allowed to migrate for a while and analyze at it later (e.g. E16 or E18), which we intend to do in near future. Therefore, involvement of partial role of migration can not be ruled out completely in this stage.

The other known role of radial glia in neurons production could however play a role in vti1a/1b KO mice. Compared to decrease density in Nestin immunoreactivity at E18.5 stage at vti1a/1b KO (Fig. 5.21D, 5.22E), no changes were seen at E14.5 stage between both controls and KO (Fig. 5.21A, 5.21B). This suggests that depletion of radial glia cells occurs between E14.5 and E18.5. Above results could also be supported by depletion of other major type of proliferative cells seen in E18.5 KO ventricular zone (VZ) as labeled by PCNA immunohistochemistry. At E18.5, a remarkable reduction of PCNA positive cells in VZ proriferative cells in vti1a/1b KO (Fig. 5.23C, 5.23D) was identified but no apparent difference was seen at E14.5 stage (Fig. 5.23A, 5.23B).

To date, the molecular mechanism causing continuous depletion of progenitor cells remains to be identified? This could be correlated with symmetric versus asymmetric division of neural progenitors at ventricular zone and possible role of trafficking in neurogenesis. During early stages of neurogenesis, neural progenitor cells (NPC) at ventricular zone divides symmetrically giving rise to two daughter NPCs. After several rounds of such events following many asymmetric divisions that giving rise to one NPC and one non-stem-cell progenitors or neuron. Non-stem-cell progenitors later on undergo symmetric differentiating divisions, generating two post-mitotic neurons [Gotz and Huttner, 2005]. The neural progenitor cells (neuroepithelial) are highly polarized cells and soluble factors which are probably needed to maintain as NPC are located at apical surface. If it divides, symmetrically apical proteins are divided equally between apical and basolateral domain and are able to maintain as progenitor fate. But when it divides

asymmetrically, apical proteins are distributed to one side which then gives rise to one progenitor cell. The other will develop as a neuron because it doesn't get sufficient factor to establish as NPC. Therefore, if trafficking is disturbed, the cell polarity will also be disturbed resulting early generation of neurons. This was seen in hydrocephalic hop gait (hyh) mutant mice where trafficking protein α-SNAP is mutated. As a result, the cell polarity is completely disturbed leading higher numbers of neurons [Chae et al., 2004]. Therefore similar role of trafficking proteins like vti1a/1b in similar events can be expected.

Still ambiguity remains if there is continuous depletion in progenitor cells, we would expect uniform increase in most of the layers of cortex including upper layers, which is not the case in vti1a/1b KO. Instead vti1a/1b KO mice show complete absence of layer 5, increase in layer 6 and no significant changes in upper layers suggesting failure in fate specification for deeper layers. Transcription factors like Fezl knockout mice has shown similar phenotype where layer-5 neurons were missing, layer-6 was increased with altered molecular properties and hence unable to deliver subcerebral projections. On the other hand upper layers were normal [Molyneaux et al., 2005].

At this stage we are not sure whether the phenotype seen in vti1a/1b null cortex was due to alteration in symmetric/asymmetric division, failure in early decisions regarding lineage-specific differentiation from neural progenitors or any changes in signaling molecules (e.g. Wnt-Frizzeled pathway which has been shown its role in corticofugal pathway). More experiments are needed to dissect the underlying molecular mechanism.

6.3: Impaired fiber tracts in KO mice:

6.3.1: Impairment in projection fibers (thalamocortical and corticofugal axons)

Vti1a/1b KO shows various abnormalities in major projection fibers especially thalamocortical axons (TCA) and corticofugal axons (CFA). The term corticofugal here refers to cortico-thalamic, corticopontine and corticospinal fibers. At E14.5, the TCA of KO mice do not cross pallio-subpallial (PSPB) border (Fig. 5.5B) and at E18.5, they lie with in internal capsule area (Fig. 5.5D). TCA was labeled by neurofilament immunohistochemistry and it was further conformed by DiI labeling (Fig. 5.5F). Not only TCA, CFA also show impairment in its distribution. DiI labeling at E16.5 KO mice cortex showed only a few corticothalamic axons could reach thalamus (Fig. 5.5H). Now the question arises why thalamocortical axons can not cross PSPB border at E14.5 KO stage where as control mice do? This could be explained by "handshake hypothesis". The *'handshake hypothesis'* states that during early embryonic days (E13-14) in mice, the TCA and corticofugal fibers advances through their route and meets at pallio-subpallial border and uses each other as guidance scaffolds along the rest of their future courses [Blakemore and Molnar, 1990; Molnar and Blakemore, 1995]. If one type of fibers develops unusually then other could be affected in its further developments and this was supported by a number of studies. Defects in corticothalamic and thalamocortical pathway were found in mice with mutations in transcription factor genes that are expressed in the cortex (*Tbr1*), thalamus (*Gbx2*) or in both (*Pax6*) [Hevner et al., 2002; Jones et al., 2002; Stoykova and Gruss, 1994]. In these mutants, both thalamic and corticofugal connections are abnormal and do not arrive at their final targets which supports the notion that thalamic axons must have an intimate relationship with the preplate (corticofugal) axons. Moreover, CFA also show abnormality in vti1a/1b double knockout mice. Only a few fibers can reach to internal capsule and thalamus at E16.5 as shown in DiI labeled tissue. Therefore the failure of thalamocortical axons crossing through the PSPB border in KO could be due to absence of adequate support from corticofugal fibers coming from cortex.

Indeed, corticofugal and thalamocortical axons are also influenced by genes expressed regions they grow through during development. Transcription factors Pax6, Tbr1, Ngn2, Emx2 and Otx2 or absence of Emx1 in the ventral pallial region have modulatory potential for molecular patterning at the PSPB and axonal path finding [Molnar et al., 2003]. Similarly abnormal development of axonal connections in absence of Pax6 function appear to be related with ultrastructural defects along PSPB as failure of axonal guidance molecule expression including Sema3C, Sema5A, and possibly Netrin-1 [Jones et al., 2002]. Membrane bound or diffusible factors like limbic associated membrane protein (LAMP), cadherins, ephrins and Eph receptors, neurotrophins, netrin 1 and semaphorins [Lopez-Bendito and Molnar, 2003] have shown their influence on thalamocortical axons. However the null mutant mice for these genes show subtle effect suggesting that these molecules have either minor roles or they work together [Price et al., 2006]. Dcx and Dclk and Slits and their receptors robo1 and robo2 have also shown their role in development of both TCA and CFA [Deuel et al., 2006; Lopez-Bendito et al., 2007].

Similarly Wnt/Frizzled signaling pathway has also shown to have a role in development of reciprocal connection between cortex and subcortical area. In Frizzled 3 (Fzd3) mutant mice, thalamic axons fail to reach their target areas in the cortex. CFA pause and degenerate in the intermediate zone and future white matter. They show a complete loss of the thalamocortical, corticothalamic, and nigrostriatal tracts and of the anterior commisure, and have variable loss of the corpus callosum. However, peripheral nerve fibers and major axon tracts in the more caudal regions of the CNS are mostly or completely unaffected which is not in case of vti1a/1b.

Since vti1a/1b KO mice have only few corticofugal axons reaching to the thalamus, the development of corticofugal axons on the other hand also depend upon coordinated development of layer 5 and layer 6 neurons in the cortex. Vti1a/1b KO lacks layer 5 neurons in frontal regions (Fig. 5.20S) and caudal region show presence of few layer 5 neurons. Layer 5 neurons which give rise to corticopontine and corticospinal axons were labeled by CTIP2 antibody. Moreover layer 6 in cortex gives rise to corticothalamic axons and vti1a/1b KO mice showed increase in layer 6 neurons (Fig. 5.20R). However,

an increase in number of layer 6 neurons could not generate increase in corticothalamic axons. Instead, only fractions of fibers can reach to the thalamus suggesting layer 6 neurons in KO do not differentiate sufficiently. Similarly, corticopontine and corticospinal axons were remarkably reduced in KO and did not form thick cerebral peduncle at the lateral side ventral thalamus. Although HE staining and neurofilament immunohistochemistry did show rudimentary cerebral peduncle (Fig. 5.6D, 5.6F), DiI labeling failed to label it (Fig. 5.6E). This could be either the cerebral peduncle in KO was too small and therefore, we did not get the right labeled section in all analyzed KO or no fibers from cortex could reach there. The second possibility is more likely because pyramidal axons were also absent in KO when seen at the level of medulla (Fig. 5.6H, 5.6J). In normal case, pyramidal axons are the continuation of cerebral peduncle and after crossing at the meduallary discussion in medulla, they form corticospinal axons.

Interestingly, transcription factor forebrain embryonic zinc finger-like *Fezl* (also known as Zfp312, Fez1, and Fez), have been shown its important role in development of corticospinal motor neuron (CSMN). In fezl$^{-/-}$ mice CSMN are absent leading to absence of corticospinal axons and other subcerebral fiber tracts [Molyneaux et al., 2005].

Nevertheless, the axonal as well as dendritic growth also depends upon behavior of growth cone dynamics. If there is impairment in vesicular activities in growth cones, it can not form long fiber tracts adequately. Growth associated proteins-43 (GAP-43) antibody, which stains newly formed axonal growth cones, also showed remarkable reduction in its expression in KO inner cortex (Fig. 5.20N). This is in line with predicted role of vti1a/1b during growth cone development. Growth cone formation and extension of plasma membrane during axonal growth need tremendous amounts of vesicle recycling and possibly endosomal fusion steps, vti1a could be important during these activities.

Preliminary result in KO chromaffin cells by measuring vesicular activities with capacitance and amperometry (from our collaborators, J. Sorensen, Max plank institute, biophysical chemistry, Goettingen, Germany, unpublished data) suggest that there are no adequate vesicular activities going on in KO cells. The exocytosis coupled with endocytic

cycle was greatly impaired in vti1a/1b KO chromaffin cells. This might support the idea that at first defective growth cone formation and plasma membrane extension in cortex lead to abnormal formation of corticofugal fibers which then cannot act as scaffold for incoming thalamocortical fibers (Handshake mechanism), finally leading to stoppage of TCA at PSPB border.

6.3.2: Absence/impairment in commissural axons:

The two mammalian cortical hemispheres need to communicate with each other to share information and for effective processing. This is achieved by coordinate activity between two hemispheres and the two hemispheres are connected via commissural axons. Principally, three are three commissural axons the corpus callosum (CC), hippocampal commisure (HC) and anterior commisure (AC). Vti1a/1b knockout mice completely lack the anterior commisure (Fig. 5.1$_a$B) and the hippocampal commisure (Fig. 5.1$_a$B) and show variable loss of corpus callosum (Fig. 5.1$_b$H). However, the defect seen in commissural system was not a generalized effect because the posterior commisure and the habenullar commisure were present in vti1a/1b knockout mice (data not shown). The anterior corpus callosum in KO is comparable to control but in the middle, its thickness is noticeably reduced (Fig. 5.1$_b$H). Similar to other major tracts in brain, they are also influenced by a complex interplay of long-range and short-range guidance cues. Any disorder in guidance cues can cause defective development. Such abnormalities could be due to intrinsic defects in receptor expression and signaling at the growth cone, or from absence of an extracellular environment which is appropriate for navigation [Lindwall et al., 2007]. Classical guidance factors like the Slits, Netrins, and their receptors have shown important role in axon guidance. For example various knockout studies have shown roles of Slit2 in CC [Bagri et al., 2002], Robo1 in CC and HC [Andrews et al., 2006], Netrin1 and doublecortin and doublecortin like kinase (Dcx and Dclk) in all three commisures [Deuel et al., 2006; Serafini et al., 1996]. Moreover, novel guidance factors such as members of the Wnt family Frizzeled-3 [Wang et al., 2006], and extracellular matrix components such as heparin sulfate proteoglycans [Inatani et al., 2003], have been shown to be involved in formation of mammalian brain commisures. Additionally, a role for FGF signaling has been reported in the formation of midline glial structures which

coincides with commissural defects [Lindwall et al., 2007; Smith et al., 2006]. Short range guidance molecules like semaphorins Sema3b, Sema3f [Falk et al., 2005; Sahay et al., 2003] for anterior commisure and Ephrins and Eph receptors e.g. Ephrinb1 and EphrinB3 [Mendes et al., 2006] have also shown for their role in commissural formation for corpus callosum development.

The difference between vti1a/1b KO and Netrin 1 is that Netrin-1 KO shows equal effect in all three commissures whereas vti1a/1b KO lack completely AC and HC and show partial effect on CC. The other similarities between the two knockouts are both KO mice show complete absence of pontine nuclei. On the other hand, in Frizzeled-3 KO mice, CC and AC are absent and HC is partially affected. Moreover, they also lack other major fiber tracts like thalamocortical, corticothalamic, and nigrostriatal tracts which are similar to vti1a/1b KO mice. Dcx and Dclk double knockout mice lack all major commissures and also display abnormal neuronal lamination in cortex, as well as abnormal dendritic morphology and axon elongation in vitro [Deuel et al., 2006]. Similar to role of vti1a/1b in endosomal transport, it might be important to notice that Dcx and Dclk are involved in regulating microtubule-based vesicle transport, which is important for migration and axonal outgrowth. Despite having variable data showing number of molecules involved in formation of all three commissural axons, the reason for selective difference in these commisure, complete absence (agenesis) in AC and HC and partial defect (dysgenesis) in CC, remains unknown. However it is inevitable that vti1a/1b related endosomal function is required for formation of these commissural axons. The endosomal function may be needed during local, anterograde or retrograde signaling events and propagating their signal towards nucleus by multiple signaling factors. On the other hand endosomal function and recycling of vesicles could also be needed during extension of plasma membrane and axonal growth cone development.

6.3.3: Other affected tracts related to degeneration of ganglia:

Tracts of Lissauer (dorsolateral) was completely absent in E14.5 vti1a/1b KO mice (Fig. 5.7B) when compared to control (Fig. 5.7A). This absence of Lissauer tract was not surprising because dorsal root ganglia neurons were also reduced by 80% in KO mice (Fig. 5.11F). Since more than two-thirds of the axons in the tract of Lissauer at mid-

thoracic and lumbosacral levels of the rodent spinal cord are primary afferent fibers arrive via DRG, and rest arise from intrinsic fibers [Chung et al., 1979], the absence of Lissauer tract could be secondary to neurodegeneration seen at dorsal root ganglia. Similarly absence of neurofilament labelled spinotrigeminal tract in E16.5 vti1a/1b KO mice (Fig. 5.7D) was also due to secondary effect of severe degeneration seen in trigeminal ganglia.

6.3.4: Synaptophysin expression in Forebrain:

Synaptophysin and synapsin expression were almost absent in E18.5 KO cortex, hippocampus and dramatically reduced in entorhinal cortex and habenulla (Fig. 5.25 A-H). The absence of synapsin and synaptophysin in cortex and in hippocampus could be secondary to absence of afferent and efferent cortical projection fibers. If there are no incoming and outgoing fibers, we would certainly expect no synapses. The reduction in habenulla and entorhinal cortex could also be partly due to secondary effects because they also receive fibers from various part of cortex and in absence of so, they show reduction in synapsin and synaptophysin expression. However, reduction in synaptic vesicle markers synaptophysin and synapsin expressions could also be partly due to reduction in synaptic vesicle reserve pool possibly resulted from insufficient synaptic vesicle recycling and retrieval after exocytosis.

6.3.5: Fibers at striatum:

At striatum, E18.5 vti1a/1b KO mice lack fiber bundles in medial part of striatum as shown by HE staining (Fig. 5.4E blue arrows). This was also shown by neurofilament immunolabeling (Fig. 5.4F blue arrows). In contrast, there are unusual few aberrant bundles of fibers in lateral part of striatum lying near to corticostriatal border in KO (Fig. 5.4E, yellow arrows). These aberrant fiber bundles were neurofilament positive (Fig. 5.4F, yellow arrows) and nestin negative (Fig. 5.4G). Now two important questions arise here. Firstly, where do these aberrant fibers bundle (in lateral side of KO) originate from? Secondly, why fibers on medial side of striatum in KO are absent (Fig. 5.4E, yellow arrows) which are normally present in control (Fig. 5.4A, yellow arrows). To find this

answer, we injected DiI either in cortex or in dorsal thalamus which are the main sources of striatal fibers. In normal case, the striatal fibers predominantly originate either from ipsilateral thalamus or from ipsilateral cortex. A few fibers may originate from contralateral cortex. We used DiI in both cortex and both thalamus one at a time assuming that both hemisphere behave the same. When DiI was applied in thalamus, no DiI labeled fibers were seen in KO striatum compared to normal presence of fibers in control. This proved that KO thalamus cannot send fibers in striatum. At the same time, it also proved that aberrant fibers in KO do not arrive from thalamus. Similarly, when DiI was applied in cortex, no DiI positive fibers were seen in medial part of striatum of KO mice suggesting KO cortex also can not send fibers in striatum (medial). In contrast, a few DiI positive fibers were seen in lateral part of KO striatum suggesting the unusual aberrant bundle were originated from cortex.

On the other hand we also looked into another possibility where these aberrant striatal fibers in KO might arrive from the external capsule fibers. The KO external capsule fibers were impaired in caudal part of forebrain, slightly posterior to the internal capsule region, leaving a huge gap that was not seen in case of control (Fig. 5.3B). Normally, external capsule fibers divides cortex (pallium) with subpallial part of forebrain and are nestin positive at embryonic stage 18.5 (Fig. 5.3A arrow). However such idea of turning out of external capsule anteriorly and forming aberrant bundle in striatum was avoided because the aberrant striatal fibers in KO (lateral part) was nestin negative.

7. Summary:

Endocytosis is considered a highly important aspect in cellular signaling. Endocytosis is part of the vesicle cycling at the plasma membrane. Docking, fusion and retraction of vesicles is regulated by specific proteins, including the SNARE proteins. Vti1a and vti1b are members of the SNARE family proteins sharing 30% of their amino acid sequences and are involved in early and late endosome fusion. To study the biological relevance of vti1a and vti1b, mice lacking these genes were generated by Prof. G. Fischer von Mollard (Göttingen/Bielefeld). Mice lacking both vti1a and vti1b died perinatally; however, ablation of single genes did not lead to obvious phenotypes suggesting their compensatory role for one another. To address the question which developmental events depend on vti1a/1b function, double mutant mice were analyzed in great detail during the period of embryonic day 12 to 18. Numerous developmental defects could be observed. They include degeneration of many ganglia of the peripheral nervous system, malformation of the cerebral cortex as well as lack of numerous projections within the central nervous system.

In PNS, KO mice showed various degrees of neurodegeneration in different ganglia. Trigeminal (TG), dorsal root (DRG), nodose-petrosal (nod-pet) ganglia showed severe neurodegeneration. Superior cervical ganglia (SCG) showed moderate level and vestibular and cochlear ganglia were the least affected ones. At E14.5, TG, DRG, nod-pet ganglia were reduced by 80% and at E18.5 by 98%. SCG neurons were not affected at E14.5 but they were reduced by 54% at E18.5. Vestibular and cochlear ganglia at E14.5 showed 18% reduction and at E18.5, they were reduced by 15-25%. This neurodegeneration may arise due to a lack of retrograde trafficking support during development of these ganglia or due to lack of delivering efficient plasma membrane required during axonal growth cone formation. Disparity in neurodegeneration among these ganglia could be due to the distance between the ganglia and their target. Unlike TG and DRG, vestibular and cochlear ganglia have less distant targets which may explain better survival.

In cortex the normal topography of layering pattern was severely disturbed. Ctip2 immunoreactive layer 5 neurons were apparently missing and Tbr1 positive layer 6 neurons were expanded. In contrast, Satb2 and Brn1 positive upper layer neurons were barely affected. At E14.5, nestin positive radial glial cells were not affected but their density was reduced at E18.5. Alternatively, Blbp immunoreactive radial glial cells showed an unusual honey comb appearance in frontal sections compared to normal rod like structure in control mice. Moreover, PCNA positive neural progenitors cells in ventricular zone were greatly reduced in KO cortex suggesting their early depletion. This whole cortical phenotype could be caused by altered productivity in the ventricular zone during cortical layer development. The altered productivity may arise due to disturbances in cell polarity, failure in early decisions regarding lineage-specific differentiation from neural progenitors or any changes in signalling molecules that could cause such consequences. More experiments are needed to find out the mechanism. Especially experiments like Brdu injection should be focused to show role of vti1a/1b in migration or differentiation. Experiments regarding asymmetric distribution of proteins leading to enhanced neurogenesis can be another priority.

In CNS, double KO mice lack several commissural as well as projection fiber tracts. Among commissural axons, anterior commisure and hippocampal commisure were completely absent and corpus callosum was thin in the middle. Among projection fiber tracts, thalamocortical axons could not cross pallio-subpallial border at E14.5 and stopped within the internal capsule area by E18.5. On the other hand, DiI labelled corticothalamic axons showed only a few axons reaching the thalamus at E18.5. Corticospinal and pyramidal tracts were missing in E18.5 KO. This phenotype suggests endosomal trafficking events are essential for axonal growth and early topographic arrangement. Earlier studies in SNAP null mutant mice, where regulated neuroexocytosis is completely abolished, had shown normal topography of both early thalamocortical and corticofugal projections. This suggested that the formation of major axonal tracts do not rely on activity-dependent mechanisms required during evoked neurotransmitter release [Molnar et al., 2002]. However, in vti1a/vti1b double KO mice, imbalance between endocytosis and exocytosis could have affected intercellular communication mediated by

constitutive secretion of neurotransmitters or growth factors. On the other hand, recycling and delivery of new plasma membrane during axonal growth cone formation could be greatly compromised and hence leading to such severe phenotype.

The present doctoral thesis has demonstrated the vital role of vt1a and vti1b related early and late endosomal functions during mouse development. Numerous deficits and malformations in nervous system development were identified possibly leading to perinatal lethality. Further experiments are required to elucidate the precise molecular and cell biological mechanisms by which lack of vti1a/1b leads to the described phenotypes.

8. References:

Adams JC. 1977. Technical considerations on the use of horseradish peroxidase as a neuronal marker. Neuroscience 2:141-5.

Advani RJ, Bae HR, Bock JB, Chao DS, Doung YC, Prekeris R, Yoo JS, Scheller RH. 1998. Seven novel mammalian SNARE proteins localize to distinct membrane compartments. J Biol Chem 273:10317-24.

Advani RJ, Yang B, Prekeris R, Lee KC, Klumperman J, Scheller RH. 1999. VAMP-7 mediates vesicular transport from endosomes to lysosomes. J Cell Biol 146:765-76.

Alberts B, Bray D, Lewis J, Raff M, Roberts K, Watson, JD. 1994. Molecular Biology of the cell. New York, NY, USA, and London, UK: Garland Publishing, Inc., 600-626.

Anderson DJ. 1993. Molecular control of cell fate in the neural crest: the sympathoadrenal lineage. Annu Rev Neurosci 16:129-58.

Andrews W, Liapi A, Plachez C, Camurri L, Zhang J, Mori S, Murakami F, Parnavelas JG, Sundaresan V, Richards LJ. 2006. Robo1 regulates the development of major axon tracts and interneuron migration in the forebrain. Development 133:2243-52.

Angevine JB, Jr., Sidman RL. 1961. Autoradiographic study of cell migration during histogenesis of cerebral cortex in the mouse. Nature 192:766-8.

Antonin W, Fasshauer D, Becker S, Jahn R, Schneider TR. 2002. Crystal structure of the endosomal SNARE complex reveals common structural principles of all SNAREs. Nat Struct Biol 9:107-11.

Antonin W, Holroyd C, Fasshauer D, Pabst S, Von Mollard GF, Jahn R. 2000a. A SNARE complex mediating fusion of late endosomes defines conserved properties of SNARE structure and function. Embo J 19:6453-64.

Antonin W, Holroyd C, Tikkanen R, Honing S, Jahn R. 2000b. The R-SNARE endobrevin/VAMP-8 mediates homotypic fusion of early endosomes and late endosomes. Mol Biol Cell 11:3289-98.

Antonin W, Riedel D, von Mollard GF. 2000c. The SNARE Vti1a-beta is localized to small synaptic vesicles and participates in a novel SNARE complex. J Neurosci 20:5724-32.

Atlashkin V, Kreykenbohm V, Eskelinen EL, Wenzel D, Fayyazi A, Fischer von Mollard G. 2003. Deletion of the SNARE vti1b in mice results in the loss of a single SNARE partner, syntaxin 8. Mol Cell Biol. 15:5198-207.

Atlachkine, Vadim (PhD thesis, 2002). Characterisation of Vti1b and Vti1a proteins and generation of knock-out mice.

Arlotta P, Molyneaux BJ, Chen J, Inoue J, Kominami R, Macklis JD. 2005. Neuronal subtype-specific genes that control corticospinal motor neuron development in vivo. Neuron 45:207-21.

Atlashkin V, Kreykenbohm V, Eskelinen EL, Wenzel D, Fayyazi A, Fischer von Mollard G. 2003. Deletion of the SNARE vti1b in mice results in the loss of a single SNARE partner, syntaxin 8. Mol Cell Biol 23:5198-207.

Bayer SA and Altman J. 1991. NeocorticalDevelopment. 255, Raven, New York.

Bagri A, Marin O, Plump AS, Mak J, Pleasure SJ, Rubenstein JL, Tessier-Lavigne M. 2002. Slit proteins prevent midline crossing and determine the dorsoventral position of major axonal pathways in the mammalian forebrain. Neuron 33:233-48.

Bennett MK, Calakos N, Scheller RH. 1992. Syntaxin: a synaptic protein implicated in docking of synaptic vesicles at presynaptic active zones. Science 257:255-9.

Blakemore C, Molnar Z. 1990. Factors involved in the establishment of specific interconnections between thalamus and cerebral cortex. Cold Spring Harb Symp Quant Biol 55:491-504.

Blott EJ, Griffiths GM. 2002. Secretory lysosomes. Nat Rev Mol Cell Biol 3:122-31.

Bock JB, Klumperman J, Davanger S, Scheller RH. 1997. Syntaxin 6 functions in trans-Golgi network vesicle trafficking. Mol Biol Cell 8:1261-71.

Brandhorst D, Zwilling D, Rizzoli SO, Lippert U, Lang T, Jahn R. 2006. Homotypic fusion of early endosomes: SNAREs do not determine fusion specificity. Proc Natl Acad Sci U S A 103:2701-6.

Breckenridge LJ, Almers W. 1987. Currents through the fusion pore that forms during exocytosis of a secretory vesicle. Nature 328:814-7.

Bright NA, Reaves BJ, Mullock BM, Luzio JP. 1997. Dense core lysosomes can fuse with late endosomes and are re-formed from the resultant hybrid organelles. J Cell Sci 110 (Pt 17):2027-40.

Britanova O, Akopov S, Lukyanov S, Gruss P, Tarabykin V. 2005. Novel transcription factor Satb2 interacts with matrix attachment region DNA elements in a tissue-specific manner and demonstrates cell-type-dependent expression in the developing mouse CNS. Eur J Neurosci 21:658-68.

Broadie K, Prokop A, Bellen HJ, O'Kane CJ, Schulze KL, Sweeney ST. 1995. Syntaxin and synaptobrevin function downstream of vesicle docking in Drosophila. Neuron 15:663-73.

Bronfman FC, Escudero CA, Weis J, Kruttgen A. 2007. Endosomal transport of neurotrophins: roles in signaling and neurodegenerative diseases. Dev Neurobiol 67:1183-203.

Burkhardt JK, Hester S, Lapham CK, Argon Y. 1990. The lytic granules of natural killer cells are dual-function organelles combining secretory and pre-lysosomal compartments. J Cell Biol 111:2327-40.

Caviness VS, Jr. 1982. Neocortical histogenesis in normal and reeler mice: a developmental study based upon [3H] thymidine autoradiography. Brain Res 256:293-302.

Caviness VS, Jr., Takahashi T. 1995. Proliferative events in the cerebral ventricular zone. Brain Dev 17:159-63.

Chae TH, Kim S, Marz KE, Hanson PI, Walsh CA. 2004. The hyh mutation uncovers roles for alpha Snap in apical protein localization and control of neural cell fate. Nat Genet 36:264-70.

Chandler DE, Heuser JE. 1980. Arrest of membrane fusion events in mast cells by quick-freezing. J Cell Biol 86:666-74.

Chen YA, Scheller RH. 2001. SNARE-mediated membrane fusion. Nat Rev Mol Cell Biol 2:98-106.

Chidgey MA. 1993. Protein targeting to dense-core secretory granules. Bioessays 15:317-21.

Chung K, Langford LA, Applebaum AE, Coggeshall RE. 1979. Primary afferent fibers in the tract of Lissauer in the rat. J Comp Neurol 184:587-98.

Deak F, Schoch S, Liu X, Sudhof TC, Kavalali ET. 2004. Synaptobrevin is essential for fast synaptic-vesicle endocytosis. Nat Cell Biol 6:1102-8.

Delcroix JD, Valletta JS, Wu C, Hunt SJ, Kowal AS, Mobley WC. 2003. NGF signaling in sensory neurons: evidence that early endosomes carry NGF retrograde signals. Neuron 39:69-84.

Deuel TA, Liu JS, Corbo JC, Yoo SY, Rorke-Adams LB, Walsh CA. 2006. Genetic interactions between doublecortin and doublecortin-like kinase in neuronal migration and axon outgrowth. Neuron 49:41-53.

Di Fiore PP, Gill GN. 1999. Endocytosis and mitogenic signaling. Curr Opin Cell Biol 11:483-8.

Dunn KW, McGraw TE, Maxfield FR. 1989. Iterative fractionation of recycling receptors from lysosomally destined ligands in an early sorting endosome. J Cell Biol 109:3303-14.

Ernfors P, Van De Water T, Loring J, Jaenisch R. 1995. Complementary roles of BDNF and NT-3 in vestibular and auditory development. Neuron 14:1153-64.

Falk J, Bechara A, Fiore R, Nawabi H, Zhou H, Hoyo-Becerra C, Bozon M, Rougon G, Grumet M, Puschel AW, Sanes JR, Castellani V. 2005. Dual functional activity of semaphorin 3B is required for positioning the anterior commissure. Neuron 48:63-75.

Fasshauer D. 2003. Structural insights into the SNARE mechanism. Biochim Biophys Acta 1641:87-97.

Fasshauer D, Antonin W, Margittai M, Pabst S, Jahn R. 1999. Mixed and non-cognate SNARE complexes. Characterization of assembly and biophysical properties. J Biol Chem 274:15440-6.

Felder S, Miller K, Moehren G, Ullrich A, Schlessinger J, Hopkins CR. 1990. Kinase activity controls the sorting of the epidermal growth factor receptor within the multivesicular body. Cell 61:623-34.

Fischer von Mollard G, Stevens TH. 1998. A human homolog can functionally replace the yeast vesicle-associated SNARE Vti1p in two vesicle transport pathways. J Biol Chem 273:2624-30.

Fuchs E, Weber K. 1994. Intermediate filaments: structure, dynamics, function, and disease. Annu Rev Biochem 63:345-82.

Ghosh RN, Gelman DL, Maxfield FR. 1994. Quantification of low density lipoprotein and transferrin endocytic sorting HEp2 cells using confocal microscopy. J Cell Sci 107 (Pt 8):2177-89.

Gotz M, Huttner WB. 2005. The cell biology of neurogenesis. Nat Rev Mol Cell Biol 6:777-88.

Grabner CP, Price SD, Lysakowski A, Fox AP. 2005. Mouse chromaffin cells have two populations of dense core vesicles. J Neurophysiol 94:2093-104.

Griffiths G. 2002. What's special about secretory lysosomes? Semin Cell Dev Biol 13:279-84.

Grimes ML, Beattie E, Mobley WC. 1997. A signaling organelle containing the nerve growth factor-activated receptor tyrosine kinase, TrkA. Proc Natl Acad Sci U S A 94:9909-14.

Grimes ML, Zhou J, Beattie EC, Yuen EC, Hall DE, Valletta JS, Topp KS, LaVail JH, Bunnett NW, Mobley WC. 1996. Endocytosis of activated TrkA: evidence that nerve growth factor induces formation of signaling endosomes. J Neurosci 16:7950-64.

Gruenberg J, Howell KE. 1989. Membrane traffic in endocytosis: insights from cell-free assays. Annu Rev Cell Biol 5:453-81.

Hammond C, Helenius A. 1995. Quality control in the secretory pathway. Curr Opin Cell Biol 7:523-9.

Hartfuss E, Forster E, Bock HH, Hack MA, Leprince P, Luque JM, Herz J, Frotscher M, Gotz M. 2003. Reelin signaling directly affects radial glia morphology and biochemical maturation. Development 130:4597-609.

Hayashi T, McMahon H, Yamasaki S, Binz T, Hata Y, Sudhof TC, Niemann H. 1994. Synaptic vesicle membrane fusion complex: action of clostridial neurotoxins on assembly. EMBO J 13:5051-61.

Hayat, MA. 1970. Staining, Principles and Techniques of Electron Microscopy. 1, pp. 241–319. Van Nostrand Reinhold Company, New York.

Heerssen HM, Pazyra MF, Segal RA. 2004. Dynein motors transport activated Trks to promote survival of target-dependent neurons. Nat Neurosci 7:596-604.

Hevner RF, Miyashita-Lin E, Rubenstein JL. 2002. Cortical and thalamic axon pathfinding defects in Tbr1, Gbx2, and Pax6 mutant mice: evidence that cortical and thalamic axons interact and guide each other. J Comp Neurol 447:8-17.

Hirling H, Steiner P, Chaperon C, Marsault R, Regazzi R, Catsicas S. 2000. Syntaxin 13 is a developmentally regulated SNARE involved in neurite outgrowth and endosomal trafficking. Eur J Neurosci 12:1913-23.

Hohl TM, Parlati F, Wimmer C, Rothman JE, Sollner TH, Engelhardt H. 1998. Arrangement of subunits in 20 S particles consisting of NSF, SNAPs, and SNARE complexes. Mol Cell 2:539-48.

Hopkins CR. 1983. Intracellular routing of transferrin and transferrin receptors in epidermoid carcinoma A431 cells. Cell 35:321-30.

Huang EJ, Zang K, Schmidt A, Saulys A, Xiang M, Reichardt LF. 1999. POU domain factor Brn-3a controls the differentiation and survival of trigeminal neurons by regulating Trk receptor expression. Development 126:2869-82.

Hunt JM, Bommert K, Charlton MP, Kistner A, Habermann E, Augustine GJ, Betz H. 1994. A post-docking role for synaptobrevin in synaptic vesicle fusion. Neuron 12:1269-79.

Inatani M, Irie F, Plump AS, Tessier-Lavigne M, Yamaguchi Y. 2003. Mammalian brain morphogenesis and midline axon guidance require heparan sulfate. Science 302:1044-6.

Jahn R, Scheller RH. 2006. SNAREs--engines for membrane fusion. Nat Rev Mol Cell Biol 7:631-43.

Jahn R, Sudhof TC. 1999. Membrane fusion and exocytosis. Annu Rev Biochem 68:863-911.

Jones L, Lopez-Bendito G, Gruss P, Stoykova A, Molnar Z. 2002. Pax6 is required for the normal development of the forebrain axonal connections. Development 129:5041-52.

Jossin Y, Bar I, Ignatova N, Tissir F, De Rouvroit CL, Goffinet AM. 2003. The reelin signaling pathway: some recent developments. Cereb Cortex 13:627-33.

Kanwar, Namita (PhD Thesis, 2006). Analysis of mice deficient in late endosomal SNARE proteins VAMP8/endobrevin and Vti1b.

Katzmann DJ, Odorizzi G, Emr SD. 2002. Receptor downregulation and multivesicular-body sorting. Nat Rev Mol Cell Biol 3:893-905.

Kirchhausen T. 2000. Clathrin. Annu Rev Biochem 69:699-727.

Kornfeld S, Mellman I. 1989. The biogenesis of lysosomes. Annu Rev Cell Biol 5:483-525.

Kreykenbohm V, Wenzel D, Antonin W, Atlachkine V, von Mollard GF. 2002. The SNAREs vti1a and vti1b have distinct localization and SNARE complex partners. Eur J Cell Biol 81:273-80.

Le Douarin NM and Kalcheim C. 1999. The Neural Crest, 2nd edn. Cambridge: Cambridge University Press.

Lindwall C, Fothergill T, Richards LJ. 2007. Commissure formation in the mammalian forebrain. Curr Opin Neurobiol 17:3-14.

Lodish H., Berk A., Zipursky S.L., Matsudaira P., Baltimore D., and Darnell J.E. (2001). Protein sorting: organelle biogenesis and protein secretion. 4th:691-743.

Lopez-Bendito G, Flames N, Ma L, Fouquet C, Di Meglio T, Chedotal A, Tessier-Lavigne M, Marin O. 2007. Robo1 and Robo2 cooperate to control the guidance of major axonal tracts in the mammalian forebrain. J Neurosci 27:3395-407.

Lopez-Bendito G, Molnar Z. 2003. Thalamocortical development: how are we going to get there? Nat Rev Neurosci 4:276-89.

Low SH, Roche PA, Anderson HA, van Ijzendoorn SC, Zhang M, Mostov KE, Weimbs T. 1998. Targeting of SNAP-23 and SNAP-25 in polarized epithelial cells. J Biol Chem 273:3422-30.

Lupashin VV, Pokrovskaya ID, McNew JA, Waters MG. 1997. Characterization of a novel yeast SNARE protein implicated in Golgi retrograde traffic. Mol Biol Cell 8:2659-76.

Mallard F, Tang BL, Galli T, Tenza D, Saint-Pol A, Yue X, Antony C, Hong W, Goud B, Johannes L. 2002. Early/recycling endosomes-to-TGN transport involves two SNARE complexes and a Rab6 isoform. J Cell Biol 156:653-64.

Marsh EW, Leopold PL, Jones NL, Maxfield FR. 1995. Oligomerized transferrin receptors are selectively retained by a lumenal sorting signal in a long-lived endocytic recycling compartment. J Cell Biol 129:1509-22.

Mayer A, Wickner W, Haas A. 1996. Sec18p (NSF)-driven release of Sec17p (alpha-SNAP) can precede docking and fusion of yeast vacuoles. Cell 85:83-94.

Mayor S, Presley JF, Maxfield FR. 1993. Sorting of membrane components from endosomes and subsequent recycling to the cell surface occurs by a bulk flow process. J Cell Biol 121:1257-69.

McBride HM, Rybin V, Murphy C, Giner A, Teasdale R, Zerial M. 1999. Oligomeric complexes link Rab5 effectors with NSF and drive membrane fusion via interactions between EEA1 and syntaxin 13. Cell 98:377-86.

McCracken AA, Brodsky JL. 1996. Assembly of ER-associated protein degradation in vitro: dependence on cytosol, calnexin, and ATP. J Cell Biol 132:291-8.

Mellman I. 1996. Endocytosis and molecular sorting. Annu Rev Cell Dev Biol 12:575-625.

Mendes SW, Henkemeyer M, Liebl DJ. 2006. Multiple Eph receptors and B-class ephrins regulate midline crossing of corpus callosum fibers in the developing mouse forebrain. J Neurosci 26:882-92.

Mills IG, Urbe S, Clague MJ. 2001. Relationships between EEA1 binding partners and their role in endosome fusion. J Cell Sci 114:1959-65.

Molnar Z, Blakemore C. 1995. How do thalamic axons find their way to the cortex? Trends Neurosci 18:389-97.

Molnar Z, Higashi S, Lopez-Bendito G. 2003. Choreography of early thalamocortical development. Cereb Cortex 13:661-9.

Molnar Z, Lopez-Bendito G, Small J, Partridge LD, Blakemore C, Wilson MC. 2002. Normal development of embryonic thalamocortical connectivity in the absence of evoked synaptic activity. J Neurosci 22:10313-23.

Molyneaux BJ, Arlotta P, Hirata T, Hibi M, Macklis JD. 2005. Fezl is required for the birth and specification of corticospinal motor neurons. Neuron 47:817-31.

Monck JR, Fernandez JM. 1996. The fusion pore and mechanisms of biological membrane fusion. Curr Opin Cell Biol 8:524-33.

Mukherjee S, Ghosh RN, Maxfield FR. 1997. Endocytosis. Physiol Rev 77:759-803.

Mullis KB, Faloona FA. 1987. Specific synthesis of DNA in vitro via a polymerase-catalyzed chain reaction. Methods Enzymol 155:335-50.

Mullock BM, Smith CW, Ihrke G, Bright NA, Lindsay M, Parkinson EJ, Brooks DA, Parton RG, James DE, Luzio JP, Piper RC. 2000. Syntaxin 7 is localized to late endosome compartments, associates with Vamp 8, and Is required for late endosome-lysosome fusion. Mol Biol Cell 11:3137-53.

Nakamura N, Yamamoto A, Wada Y, Futai M. 2000. Syntaxin 7 mediates endocytic trafficking to late endosomes. J Biol Chem 275:6523-9.

Navone F, Jahn R, Di Gioia G, Stukenbrok H, Greengard P, De Camilli P. 1986. Protein p38: an integral membrane protein specific for small vesicles of neurons and neuroendocrine cells. J Cell Biol 103:2511-27.

Oyler GA, Higgins GA, Hart RA, Battenberg E, Billingsley M, Bloom FE, Wilson MC. 1989. The identification of a novel synaptosomal-associated protein, SNAP-25, differentially expressed by neuronal subpopulations. J Cell Biol 109:3039-52.

Peden AA, Park GY, Scheller RH. 2001. The Di-leucine motif of vesicle-associated membrane protein 4 is required for its localization and AP-1 binding. J Biol Chem 276:49183-7.

Prekeris R, Klumperman J, Chen YA, Scheller RH. 1998. Syntaxin 13 mediates cycling of plasma membrane proteins via tubulovesicular recycling endosomes. J Cell Biol 143:957-71.

Prekeris R, Yang B, Oorschot V, Klumperman J, Scheller RH. 1999. Differential roles of syntaxin 7 and syntaxin 8 in endosomal trafficking. Mol Biol Cell 10:3891-908.

Price DJ, Kennedy H, Dehay C, Zhou L, Mercier M, Jossin Y, Goffinet AM, Tissir F, Blakey D, Molnar Z. 2006. The development of cortical connections. Eur J Neurosci 23:910-20.

Reissmann E, Ernsberger U, Francis-West PH, Rueger D, Brickell PM, Rohrer H. 1996. Involvement of bone morphogenetic protein-4 and bone morphogenetic protein-7 in the differentiation of the adrenergic phenotype in developing sympathetic neurons. Development 122:2079-88.

Riccio A, Pierchala BA, Ciarallo CL, Ginty DD. 1997. An NGF-TrkA-mediated retrograde signal to transcription factor CREB in sympathetic neurons. Science 277:1097-100.

Rossi V, Banfield DK, Vacca M, Dietrich LE, Ungermann C, D'Esposito M, Galli T, Filippini F. 2004. Longins and their longin domains: regulated SNAREs and multifunctional SNARE regulators. Trends Biochem Sci 29:682-8.

Sahay A, Molliver ME, Ginty DD, Kolodkin AL. 2003. Semaphorin 3F is critical for development of limbic system circuitry and is required in neurons for selective CNS axon guidance events. J Neurosci 23:6671-80.

Schneider C, Wicht H, Enderich J, Wegner M, Rohrer H. 1999. Bone morphogenetic proteins are required in vivo for the generation of sympathetic neurons. Neuron 24:861-70.

Schoch S, Deak F, Konigstorfer A, Mozhayeva M, Sara Y, Sudhof TC, Kavalali ET. 2001. SNARE function analyzed in synaptobrevin/VAMP knockout mice. Science 294:1117-22.

Schulze KL, Broadie K, Perin MS, Bellen HJ. 1995. Genetic and electrophysiological studies of Drosophila syntaxin-1A demonstrate its role in nonneuronal secretion and neurotransmission. Cell 80:311-20.

Serafini T, Colamarino SA, Leonardo ED, Wang H, Beddington R, Skarnes WC, Tessier-Lavigne M. 1996. Netrin-1 is required for commissural axon guidance in the developing vertebrate nervous system. Cell 87:1001-14.

Shah NM, Groves AK, Anderson DJ. 1996. Alternative neural crest cell fates are instructively promoted by TGFbeta superfamily members. Cell 85:331-43.

Silos-Santiago I, Molliver DC, Ozaki S, Smeyne RJ, Fagan AM, Barbacid M, Snider WD. 1995. Non-TrkA-expressing small DRG neurons are lost in TrkA deficient mice. J Neurosci 15:5929-42.

Simonsen A, Gaullier JM, D'Arrigo A, Stenmark H. 1999. The Rab5 effector EEA1 interacts directly with syntaxin-6. J Biol Chem 274:28857-60.

Smith KM, Ohkubo Y, Maragnoli ME, Rasin MR, Schwartz ML, Sestan N, Vaccarino FM. 2006. Midline radial glia translocation and corpus callosum formation require FGF signaling. Nat Neurosci 9:787-97.

Steegmaier M, Klumperman J, Foletti DL, Yoo JS, Scheller RH. 1999. Vesicle-associated membrane protein 4 is implicated in trans-Golgi network vesicle trafficking. Mol Biol Cell 10:1957-72.

Steegmaier M, Lee KC, Prekeris R, Scheller RH. 2000. SNARE protein trafficking in polarized MDCK cells. Traffic 1:553-60.

Stow JL, Manderson AP, Murray RZ. 2006. SNAREing immunity: the role of SNAREs in the immune system. Nat Rev Immunol 6:919-29.

Stoykova A, Gruss P. 1994. Roles of Pax-genes in developing and adult brain as suggested by expression patterns. J Neurosci 14:1395-412.

Subramaniam VN, Loh E, Horstmann H, Habermann A, Xu Y, Coe J, Griffiths G, Hong W. 2000. Preferential association of syntaxin 8 with the early endosome. J Cell Sci 113 (Pt 6):997-1008.

Sudhof TC. 2004. The synaptic vesicle cycle. Annu Rev Neurosci 27:509-47.

Sudhof TC, Czernik AJ, Kao HT, Takei K, Johnston PA, Horiuchi A, Kanazir SD, Wagner MA, Perin MS, De Camilli P, et al. 1989. Synapsins: mosaics of shared and individual domains in a family of synaptic vesicle phosphoproteins. Science 245:1474-80.

Sugitani Y, Nakai S, Minowa O, Nishi M, Jishage K, Kawano H, Mori K, Ogawa M, Noda T. 2002. Brn-1 and Brn-2 share crucial roles in the production and positioning of mouse neocortical neurons. Genes Dev 16:1760-5.

Sun W, Yan Q, Vida TA, Bean AJ. 2003. Hrs regulates early endosome fusion by inhibiting formation of an endosomal SNARE complex. J Cell Biol 162:125-37.

Sutton RB, Fasshauer D, Jahn R, Brunger AT. 1998. Crystal structure of a SNARE complex involved in synaptic exocytosis at 2.4 A resolution. Nature 395:347-53.

Tang BL, Low DY, Tan AE, Hong W. 1998. Syntaxin 10: a member of the syntaxin family localized to the trans-Golgi network. Biochem Biophys Res Commun 242:345-50.

Trimble WS, Cowan DM, Scheller RH. 1988. VAMP-1: a synaptic vesicle-associated integral membrane protein. Proc Natl Acad Sci U S A 85:4538-42.

Unsicker K. 1993. The chromaffin cell: paradigm in cell, developmental and growth factor biology. J Anat 183 (Pt 2):207-21.

Valdez AC, Cabaniols JP, Brown MJ, Roche PA. 1999. Syntaxin 11 is associated with SNAP-23 on late endosomes and the trans-Golgi network. J Cell Sci 112 (Pt 6):845-54.
van Deurs B, Holm PK, Kayser L, Sandvig K, Hansen SH. 1993. Multivesicular bodies in HEp-2 cells are maturing endosomes. Eur J Cell Biol 61:208-24.

von Mollard GF, Nothwehr SF, Stevens TH. 1997. The yeast v-SNARE Vti1p mediates two vesicle transport pathways through interactions with the t-SNAREs Sed5p and Pep12p. J Cell Biol 137:1511-24.

Wang Y, Zhang J, Mori S, Nathans J. 2006. Axonal growth and guidance defects in Frizzled3 knock-out mice: a comparison of diffusion tensor magnetic resonance imaging, neurofilament staining, and genetically directed cell labeling. J Neurosci 26:355-64.

Ward DM, Pevsner J, Scullion MA, Vaughn M, Kaplan J. 2000. Syntaxin 7 and VAMP-7 are soluble N-ethylmaleimide-sensitive factor attachment protein receptors required for late endosome-lysosome and homotypic lysosome fusion in alveolar macrophages. Mol Biol Cell 11:2327-33.

Washbourne P, Cansino V, Mathews JR, Graham M, Burgoyne RD, Wilson MC. 2001. Cysteine residues of SNAP-25 are required for SNARE disassembly and exocytosis, but not for membrane targeting. Biochem J 357:625-34.

Watson FL, Heerssen HM, Bhattacharyya A, Klesse L, Lin MZ, Segal RA. 2001. Neurotrophins use the Erk5 pathway to mediate a retrograde survival response. Nat Neurosci 4:981-8.

Weissman T, Noctor SC, Clinton BK, Honig LS, Kriegstein AR. 2003. Neurogenic radial glial cells in reptile, rodent and human: from mitosis to migration. Cereb Cortex 13:550-9.

Wiedenmann B, Franke WW. 1985. Identification and localization of synaptophysin, an integral membrane glycoprotein of Mr 38,000 characteristic of presynaptic vesicles. Cell 41:1017-28.

Xu Y, Wong SH, Tang BL, Subramaniam VN, Zhang T, Hong W. 1998. A 29-kilodalton Golgi soluble N-ethylmaleimide-sensitive factor attachment protein receptor (Vti1-rp2) implicated in protein trafficking in the secretory pathway. J Biol Chem 273:21783-9.

Yamashiro DJ, Tycko B, Fluss SR, Maxfield FR. 1984. Segregation of transferrin to a mildly acidic (pH 6.5) para-Golgi compartment in the recycling pathway. Cell 37:789-800.

Yang B, Gonzalez L, Jr., Prekeris R, Steegmaier M, Advani RJ, Scheller RH. 1999. SNARE interactions are not selective. Implications for membrane fusion specificity. J Biol Chem 274:5649-53.

Yuen EC, Howe CL, Li Y, Holtzman DM, Mobley WC. 1996. Nerve growth factor and the neurotrophic factor hypothesis. Brain Dev 18:362-8.

Zerial M, McBride H. 2001. Rab proteins as membrane organizers. Nat Rev Mol Cell Biol 2:107-17.

Zimmerberg J, Vogel SS, Chernomordik LV. 1993. Mechanisms of membrane fusion. Annu Rev Biophys Biomol Struct 22:433-66.

Zwilling D, Cypionka A, Pohl WH, Fasshauer D, Walla PJ, Wahl MC, Jahn R. 2007. Early endosomal SNAREs form a structurally conserved SNARE complex and fuse liposomes with multiple topologies. EMBO J 26:9-18.

9.1: List of Figures:

9.2: List of Tables:

10. Curriculum Vitae:

Name:	**Ajaya Jang Kunwar**
	Born on 03.12.1975 in Morang (Nepal)
	Single
School:	
1981 - 1991	Janta Model secondary high school
	Biratnagar, Nepal
College:	
1992 - 1994	Intermediate in science (I. Sc., Biology)
	Mahendra Morang Adarsh Multiple Campus
	(Tribhuwan University), Biratnagar, Nepal
1994 - 1997:	Bachelor in science (B. Sc., Biology)
	Mahendra Morang Adarsh Multiple Campus
	(Tribhuwan University), Biratnagar, Nepal
.	
Dec 1999 - Dec 2002:	Master of Science in Human Anatomy,
	B. P. Koirala Institute of Heath Sciences, Dharan,
	Nepal
Promotion:	
Oct 2004 – Present:	Georg-August University Goettingen
	Dept. of Anatomy/Neuroanatomy
	Topic: "Functions of vti1a and vti1b in the development
	of the mouse nervous system: evidence from double
	knockout mice" (under Prof. Dr. Kerstin Krieglstein)
Career:	
Jan 2003 - March 2004:	Lecturer in Dept. of Anatomy
	Kathmandu Medical College, Kathmandu, Nepal